Investigation of Spatio-Temporal Effects of fMRI Visual Field Mapping Techniques on V1

John J. Janik
Marquette University

INVESTIGATION OF SPATIO-TEMPORAL EFFECTS OF FMRI VISUAL FIELD MAPPING TECHNIQUES ON V1

By

John J. Janik III

A Dissertation submitted to the Faculty of the Graduate School,
Marquette University,
in Partial Fullfillment of the Requirements for
the Degree of Doctor of Philosophy

Milwaukee, Wisconsin

December 2011

ABSTRACT
INVESTIGATION OF SPATIO-TEMPORAL EFFECTS OF FMRI VISUAL FIELD MAPPING TECHNIQUES ON V1

John Janik

Marquette University, 2011

Blood oxygenation level dependent functional magnetic resonance imaging has been used extensively for mapping the representation of the visual field within the human brain. Visual field mapping using fMRI has been used clinically to assess patients with cortical pathology and to plan surgical treatment impacting the visual system. The accuracy of fMRI-based visual field mapping methods needs to be better understood for clinical use. This accuracy can be important for presurgical mapping of brain function near a tumor resection site since inaccurate rendition of the underlying neural function could lead to inappropriate resection of viable brain tissue. The most widely used method for visual field mapping is temporal phase mapping. This dissertation investigates the accuracy of temporal phase mapping, specifically focused on the detection of polar angle visual field locations in primary visual cortex. Early studies show that polar angle positions are not uniformly distributed as suggested by animal studies. These non-uniformities are seen as relatively under-represented areas in the visual field maps used to display the fMRI data. This dissertation shows that temporal phase mapping is susceptible to hemodynamic distortions that lead to missassignment of visual field locations. Further analysis of the non-uniformity in the frequency distribution of voxels representing different angular position within the visual field shows an under-representation of locations near the vertical meridia in V1. These results led to the development of a new retinotopic mapping technique, code-based mapping. The main reason for developing a new retinotopic mapping technique was to reduce the under-representations of vertical meridia posed by using temporal phase mapping when assigning a stimulus location to a voxel. This dissertation shows that code-based mapping is a viable method for mapping visual field locations and produces a uniform distribution of voxels representing different angular positions within the visual field. Furthermore, the code-based mapping method is less susceptible to the hemodynamic biases than temporal phase mapping. With respect to clinical utility of fMRI mapping techniques, the code-based mapping shows a greater potential to accurately map a patient's visual field in the presence of a tumor or other malformations that can induce large noise effects in the fMRI voxel responses.

ACKNOWLEDGEMENTS

John J. Janik III

In particular order I would like to thank my wife, children, and parents for their support. I would also like to thank Kristina Ropella and Edgar DeYoe for guidance and mentorship. I would also like to thank Jon Weiser, and Jed Mathis for technical assistance. This study was supported by NIH grants EY13801, EB843 to E. DeYoe and a Department of Education GAANN Fellowship grant to K. Ropella, Anthony J and Rose E Bagozzi Medical Research Fellowship to K. Ropella.

TABLE OF CONTENTS

ACKNOWLEDGEMENTS……i
LIST OF FIGURES iv
Background 1
BOLD fMRI and Neuronal Activation 5
Methods to Map the Visual Field onto the Primary Visual Cortex using BOLD fMRI. 7
Functional Field Map (FFMap) 7
Temporal Phase Mapping 9
Random Stimulus Presentation Mapping..... 12
Visual Topography and Potential Non-uniformities in the visual space representation in the visual cortex 16
Visual field excitation and cortical representation in monkey V1 are generally uniform..... 16
Non-uniformities exist in detailed V1 topography and LGN 19
Non-fMRI Visual Field Mapping Techniques and Possible Uneven Distribution of Visual Field Function across V1..... 21
Assessment due to Injury..... 21
Direct Electric Measurement during Surgery 22
Back to Our Example..... 23
Specific Aims..... 24
Aim I: Determine if the voxel representations of polar angle, using temporal phase mapping, is biased by non-neuronal sources. 25
Aim Ia: Quantitatively investigate the impact of visual stimulus attributes and data processing techniques used in temporal phase mapped fMRI on the polar angle voxel distribution. 25
Aim Ib: Determine if the non-uniformity in the polar angle voxel distribution correlates to specific cortical locations in primary visual cortex..... 25
Aim II: Determine if random stimulus presentation eliminates non-neuronal biasing effects in the polar angle voxel distribution as compared to temporal phase mapping. 26
Aim IIa: Develop a method to present and analyze random stimulus presentation fMRI data. 26
Aim IIb: Compare code-based mapping to temporal phase mapping..... 27
Aim I: Determine if the voxel representations of polar angle, using temporal phase mapping, is biased by non-neuronal sources 29
Introduction..... 29

General Methods 33
Subjects 33
fMRI Experimental Parameters 33
Visual Stimulation - Retinotopic Mapping 34
Post-processing 36
Functional Field Maps 37
ROI Selection 39
Histogram Construction and Analysis 39
Results 40
Discussion 64
Conclusions 69
Aim II: Determine if random stimulus presentation eliminates non-neuronal biasing effects in the polar angle voxel distribution as compared to temporal phase mapping 71
Introduction 71
Experimental Methods 74
Subjects 74
Visual Stimulus 75
Retinotopic Mapping Methods 75
Code-based vs. temporal-phase based mapping 83
Results 84
Discussion 93
Conclusion 98
Conclusion 100
Relevance of Thesis to the Body of Research 100
Future of Code-based Mapping 101
Appendix A: Supplementary Figures for Aim I 108
References 110

LIST OF FIGURES

Figure 1: MRI System 5

Figure 2: BOLD Mechanism 7

Figure 3: Functional Field Mapping 9

Figure 4: Temporal Phase Mapping 10

Figure 5: Distinct Methods of Stimulus Presentation 14

Figure 6: Random Stimulus Presentation Concept 15

Figure 7: Cortical Representation of Visual Space 19

Figure 8: LGN Representation of Visual Space 20

Figure 9: Temporal Phase Mapping 36

Figure 10: Functional Field Mapping 39

Figure 11: Characterization of the Polar Angle Voxel Distribution 42

Figure 12: Polar Angle Maps 44

Figure 13: V1 ROI 46

Figure 14: Anatomically Fixed 48

Figure 15: Noise Effects in V1 50

Figure 16: NSR Method 51

Figure 17: Distribution of Noise in V1 53

Figure 18: Echo Sequences 55

Figure 19: Stimulus Rotation 56

Figure 20: Stimulus Contrast 57

Figure 21: Stimulus Size 59

Figure 22: Voxel Size Simulation 61

Figure 23: Noise Simulation I 63

Figure 24: Retinotopic Mapping Methods 76

Figure 25: Input Stimuli Comparison 79

Figure 26: Code-based Mapping Signal Detection 80

Figure 27: Polar Angle Maps 85

Figure 28: Number of Stimulus Location Maps 87

Figure 29: Polar Angle Voxel Distributions 89

Figure 30: Noise Simulation II 91

Figure 31: Mapping Method Detection Sensitivity 93

Background

Resection of brain tissue is a common treatment for numerous neurological disorders such as brain tumors. Due to the location of the tumor, the surgeon often desires an assessment of the patient's visual field to determine the following: (1) Is there a current visual field deficit as a result of the tumor? (2) How large is the deficit? (3) How sensitive is the deficit to stimulus intensity and spatial resolution of the stimulus presented? and (4) Is there a chance of creating new visual deficit once the tumor is removed? All of this information is relevant to determining how much neuronal tissue to remove at the boundary between viable neuronal tissue and the tumor. The physician at this point has several options: (1) perform a clinical visual field assessment, (2) have the patient undergo a Goldman's/Humphries visual field perimetry test, or (3) use a rather new visual field assessment technique using fMRI mapping.

The basic in-office clinical visual field assessment is typically performed in the doctor's office [70]. This test is a crude visual field test that can be performed by having the patient look straight ahead and count the fingers shown by the examiner as the fingers move from the patient's fovea to the far periphery of the patient's visual field. The patient is typically asked to cover one eye and focus on the examiner's nose while conducting the test. If an entire visual field must be tested, both eyes must be examined. The clinical visual field test suffers from lack of accuracy due to subjective reporting by the patient and the perception of the examiner, and lacks a reliable method of monitoring eye movement of the patient. While this method of visual field assessment is crude, the test does offer a quick (less than five minutes) examination of the patient's gross visual field.

In our example of brain surgery described above, this simple periphery technique would only be able to inform the physician of the presence of a visual field deficit and a general idea regarding the location of the deficit. This technique would not be able to provide information on intensity sensitivity or spatial resolution of the deficit's visual field effect or relate information regarding possible visual field deficit risk after removal of the brain tissue.

An alternative to the basic in-office clinical visual field assessment would be automated, computerized visual field assessment, otherwise known as visual field perimetry tests [36]. For these procedures, one eye is covered, and the patient places his or her chin in a bowl-shaped chin rest. Small diameter flashes of light of varying intensities are presented randomly about the visual field. When the patient sees a flash of light, he or she pushes a button. In all standardized testing, the right eye is tested first, followed by the left eye. This process produces a computerized map of the visual field as sensed by the subject tested. A more specific kind of visual field perimetry test that is tailored to testing patients with visual field deficits due to neuronal malformations is the Goldman's perimetry test [71]. The Goldman's perimetry presents moving light targets on the surface of a concave bowl that is 33 cm away from the patient's cornea. The speed of the target is typically 2-3° per second moving from the viewable area of the patient's visual field to the non-viewable area of the patient's visual field. The standard diameter of the flashing light target is 2.26 mm; however, the size of the target may vary with eccentricity (magnitude from the center of focus) depending on the functionality of the subject's vision. An increase or decrease in size is equivalent to a 5 dB relative shift in

brightness. The subject is asked to respond via button press when they see the target. The perimetry test is easy to administer and is a small time investment (~20-30 minutes).

The Goldman's Test will report on several factors regarding a patient's visual function: (1) fixation error, which is an indicator of fatigue or cooperation, (2) false positives (i.e. pushing the button when there are no lights present), (3) false negatives (i.e. not pushing the button when the light is present), (4) reliability index (overall how the patient performed), and (5) standard deviation of visual field location at each point measured. One of the main issues with a perimetry test is the sparse sampling grid over the field of view.

Although the sampling grid for the visual field is higher in resolution than the in-office clinical method described earlier and more consistent with respect to controlling the positions of the test stimulus and repeatability of the visual test stimulus, it is possible for any computerized visual perimetry test to miss a tumor encompassing 3°x5° of visual field near the fovea [37, 70]. Even though the computerized visual perimetry test is more reliable with respect to repeatability of the testing locations in the patient's visual space than the in-office clinical visual field assessment, the visual functional data collected regarding a patient still has no means to align the visual field to the patient's anatomy, specifically the primary visual cortex, V1.

The correlation between the computerized visual perimetry test to a human's cortical brain function is supported from monkey data [1-3,8-11, 12-18] and injury-based human data [24-35], all of which is discussed later in more detail with respect to fMRI mapping. Getting back to the issue of brain resection that involves visual areas of the brain, the Goldman's perimetry would be able to detect a visual deficit, the relative

sensitivity of the deficit, and the location in the visual field with the limitations stated above. However, the computerized visual perimetry test does not provide a direct connection or map from the visual deficit of the patient to their brain anatomy, which is crucial in the case of surgery where tissue removal may lead to loss of vision.

A novel technique under investigation for mapping a patient's visual field to the visual cortex of the brain uses functional magnetic resonance imaging (fMRI). In this method, a patient lays down in a MRI scanner and is fitted with special optics that allow the examiner to project visual images onto the subject's retina (Figure 1). Typically, a visual stimulus, such as a black and white checkerboard pattern, is projected into the MRI scanner via a fiber optic video system. This video system projects stimuli with specific eccentricity and polar angle coordinates to the patient's retina while the fMRI unit is collecting data. The data consists of MR signal that varies with changes in the blood oxygenation levels of the brain as the visual stimulus is presented to the subject [69]. Such fMRI is referred to as blood oxygenation level dependent (BOLD) fMRI. The collected data, which can be localized to specific locations in the brain, is then analyzed through a series of signal detection and filtering schemes to produce a functional field map (FFMap), which represents those locations of the visual field space that have produced BOLD signal in the visual cortex of the brain. The FFMap reports several factors regarding a patient's visual function: (1) fixation error (via eye tracking through the visual system), (2) the completeness of the patient's visual field (fMRI visual field coverage is 15^{o}x15^{o}), and (3) exact visual field locations as mapped to the visual cortex of the brain. Since this functional imaging technique is relatively new for mapping brain function, the surgeon has several questions regarding the FFMap: (1) Exactly how is

BOLD fMRI, a hemodynamic signal, linked to underlying neuronal activation, (2) What is an FFMap and how it is created, and (3) how accurate and reliable is the FFmap?

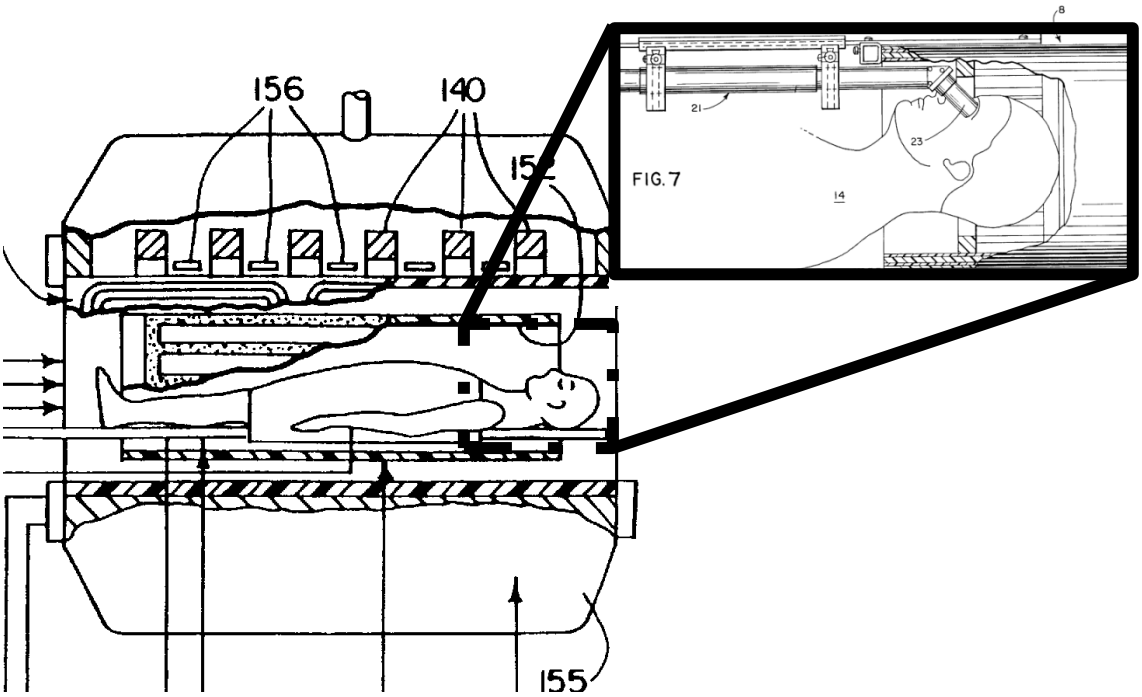

Figure 1: MRI System. Setup of a visual stimulus projection system in an fMRI unit. Adapted from US Patent 6430431, DeYoe. MRI System for Measuring Vision Capabilities. Pg. 11 [69].

BOLD fMRI and Neuronal Activation

When a visual stimulus is presented to the visual system, an increase in neuronal activity in the visual cortex leads to a change in oxygen use and demand in the local area of the active neurons. The change in oxygen demand leads to a compensatory change in blood flow and volume. This change in blood flow leads to a change in the ratio between deoxyhemoglobin (paramagnetic) and oxyhemoglobin (diamagnetic), which in turn translates to an increase in the percent change in the fMRI signal when measuring the T_2^* decay signal [40-42]. Studies have shown that the T_2^* decay signal is an indication of the

field inhomogeneity in the local area being sampled by BOLD fMRI [40-42]. In brain mapping using fMRI, the main question is what is the source of the BOLD signal?

The origin of the BOLD signal has been a subject of much debate and investigation. Oxyhemoglobin is weakly diamagnetic and produces minimal susceptibility changes in the magnetic field. On the other hand, deoxyhemoglobin is paramagnetic and introduces significant susceptibility changes (inhomogeneity) in the magnetic field. At a neuronal resting state (i.e. no neuronal firing) the ratio between oxyhemoglobin and deoxyhemoglobin is relatively constant (Figure 2, left). Therefore there is no change in the homogeneity of the magnetic field present. As neural activity increases (Figure 2, right) the blood flow to the neuronal tissue that is active increases. The increase in blood flow into the local capillary bed leads to an increase in oxyhemoglobin in the tissue area and a decrease in deoxyhemoglobin in the tissue area. As the more paramagnetic deoxyhemoglobin leaves the tissue area that is active, the induced magnetic field becomes more homogeneous and is measured as an increase in the BOLD signal [41].

A specific example related to this dissertation research is to examine when a visual stimulus elicits a neuronal response in V1. When there is an increase in neuronal activity due to visual stimulation in V1, blood flow to the region increases, changing the deoxyhemoglobin concentration and decreasing the paramagnetic properties of the local tissue (i.e. increasing the magnetic field's homogeneity), and therefore producing a change in the BOLD signal [43-45]. It is still controversial as to what exactly triggers the increase in blood flow. There are arguments for local neuronal interconnections and cortical neurons [46-51] and synaptic activity [52-56]. It is thought that the input to

excited neurons being measured by fMRI from other cortical neurons and intracortical connections are recorded from the local field potential (LFP) whereas the output at the synaptic level is recorded from multi-unit activity (MUA)[49, 50, 55]. Even with this controversy, the BOLD signal is known to correlate with neuronal activity through a cascade of metabolic events.

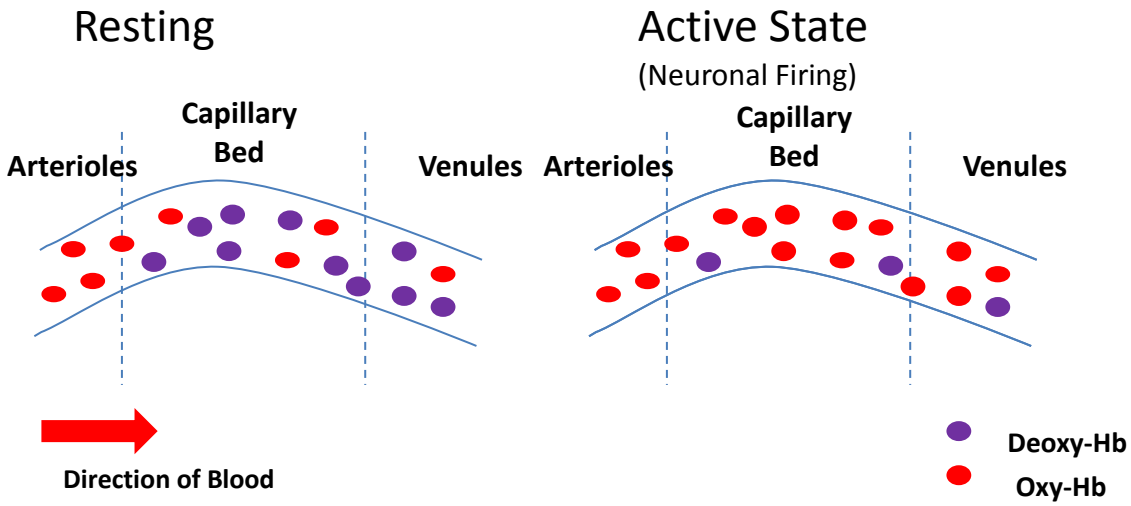

Figure 2: BOLD Mechanism. The resting state (left side) and active state (right side) of oxyhemoglobin and deoxyhemoglobin during no neuronal firing (resting state) and neuronal firing (active state).

Methods to Map the Visual Field onto the Primary Visual Cortex using BOLD fMRI

Functional Field Map (FFMap)

A Functional Field Map (FFMap) is a graphical representation of the subject's visual field showing the complete distribution of visual field locations that maximally activate voxels in the primary visual cortex (Figure 3A) [40]. The FFMap is created by using a wedge (polar angle) and annulus (eccentricity) retinotopic mapping stimuli and

subsequent fMRI data to identify the preferred stimulus position (angle and eccentricity) that maximally activates each voxel in primary visual cortex. This mapping process is called Temporal Phase Mapping. For each activated voxel, a circle symbol is placed on a diagram of the visual field at the preferred location and is colored black to indicate a valid fMRI response. The radius of the circles indicates the 70% confidence interval for the preferred location and is based on a separate analysis of the variance of the temporal delay of the BOLD signal for a set of responding voxels [16].

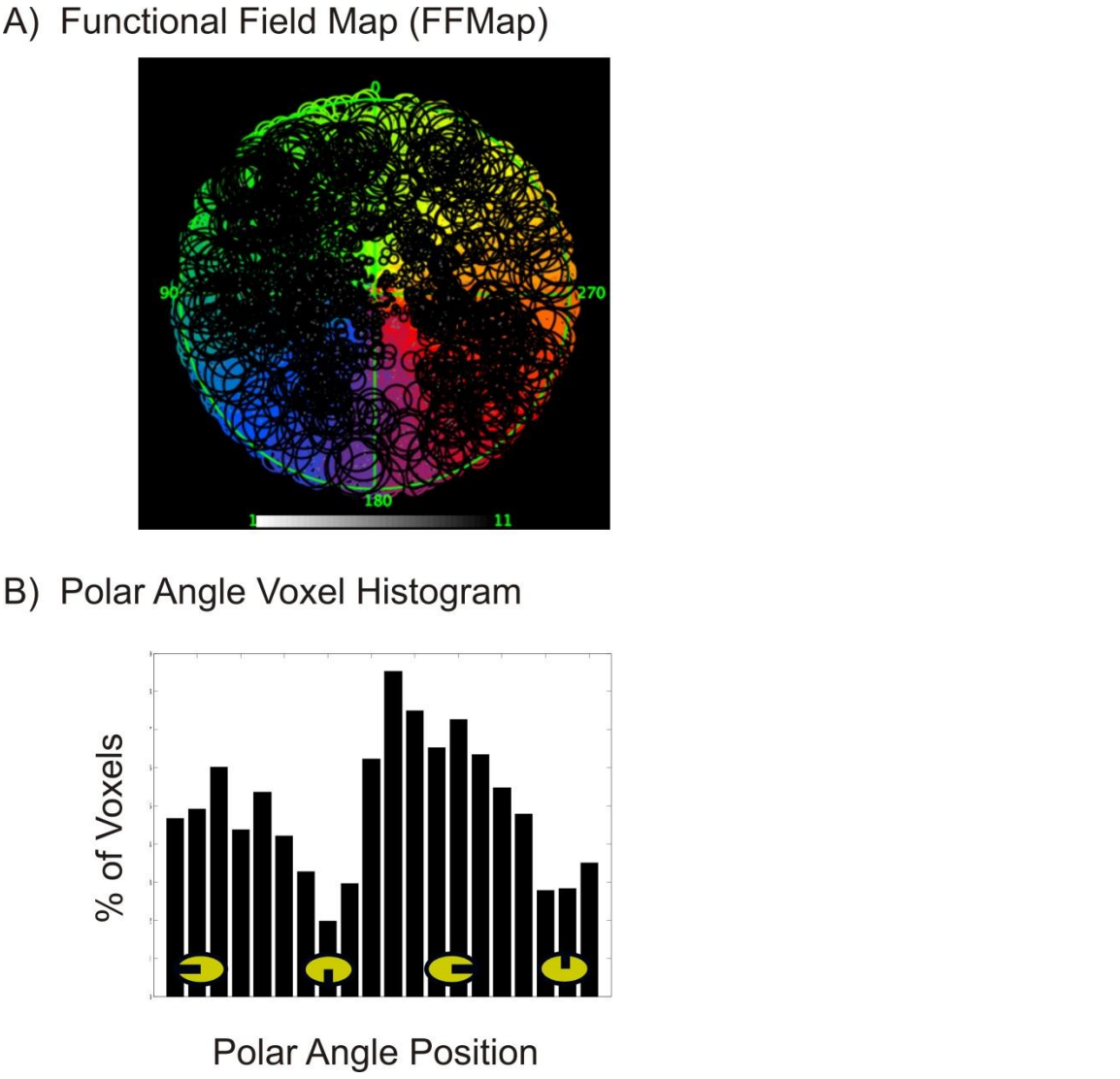

Figure 3: Functional Field Mapping. (A) Functional Field Map (FFMap) representative of a subject with normal vision. (B) The corresponding voxel histogram of all of the voxels with valid polar angle visual field coordinates from the FFMap (A).

Temporal Phase Mapping

Temporal phase mapping distinguishes between different sectors of the visual field by assigning different phases, or time delays, of the period BOLD response to each visual sector. Figure 4 outlines how the temporal phase analysis works. A flashing checkered wedge slowly rotates about the visual field over a period of 40 seconds back to the original starting position. This rotation sequence is repeated 5 times. This rotation

creates a delay in the starting time of the stimulus for each visual sector relative to the original starting position of the wedge. Consequently, the temporal phase of the fMRI response signal is used to associate the visual field polar angle with the position of the visual stimulus. Different colors can then be used to color the fMRI response signals (right) according to the optimal visual field polar angle (left).

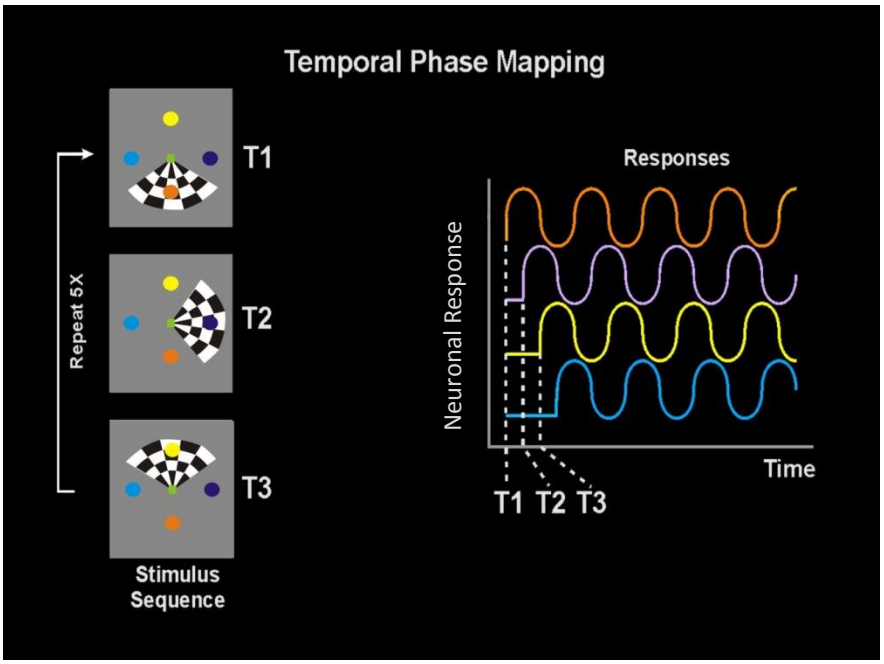

Figure 4: Temporal Phase mapping. On the left, one 120 degree black/white checkered wedge sequentially rotates about a central fixation point five times in a sequential fashion (clock-wise/counter clockwise). The corresponding time series for each colored dot and time point (T1, T2, and T3) in the visual field is shown (right).

Temporal phase mapping offers a novel method to quantitatively map the visual field to the visual cortex. These maps are called retinotopic maps because they represent the known organization of visual field orientation on primary visual cortex. Several studies have produced retinotopic maps expressing eccentricity or polar angle visual field locations in the visual cortex using temporal phase mapping [6, 22, 23, 59]. However, as this dissertation will demonstrate, temporal phase mapping does have limitations regarding consistently producing the expected voxel representation of a

subject's visual field. Figure 3A shows a typical FFMap from a subject with reported normal vision. The FFMap suggests the subject has two visual field deficits, a lesser deficit along the superior vertical meridian and another more distinct deficit along the inferior vertical meridian.

One method that has been developed in this dissertation to analyze the percent contribution of the orientation stimuli (eccentricity or polar angle) producing these deficits is to separate the respective orientation data. This is accomplished by creating two separate histograms of all of the voxels that respond to eccentricity and polar angle, respectively. The polar angle and eccentricity voxel histograms are generated from the FFMap data and contain all of the valid phase delays (cross correlation coefficient, $r^2 > 0.3$, $p < 0.05$) from voxels in the subject's primary visual cortex that assisted in generating the FFMap (Figure 3A). The eccentricity voxel histogram does not show signs of the deficits seen in the FFMap (Appendix A: Figure S1). The polar angle voxel histogram shows over/under representations of specific polar angle visual field locations across the primary visual cortex of this subject (Figure 3B), which is contradictory to the known literature [tootell]. The current literature in animals suggests that the distribution of cortical area in the polar angle orientation of the visual field is constant with respect to each visual field polar [1-4].

In order to understand if temporal phase mapping is producing the correct representation of the visual field onto the visual cortex, a thorough investigation of the retinotopic distribution of visual space onto the primary visual cortex must be done. Specifically, we examined the fMRI response of voxels in V1 when a subject was presented a visual field sector of a specific polar angle (also referred to as a wedge in our

specific use) and what level of statistical confidence exists in the fMRI response to the visual stimulus.

Random Stimulus Presentation Mapping

Given the observation described above that FFMaps of normal vision subjects can have areas of deficit and a nonuniform polar angle voxel histogram generated from temporal phase mapping [5], alternatives to producing the FFMap using sequential based stimuli was examined in this dissertation research. The goal was to determine whether or not there was a reasonable cause for using an alternative presentation stimuli other than the sequential-based temporal phase mapping to generate the FFMap.

Figure 5 illustrates the meaning of random stimulus presentation in this dissertation research. More specifically, for every visual stimulus location, shown as orange 18º wedges (Figure 5, Right corner), that is displayed; no single stimulus location will have a high correlation to any other stimulus location through the duration of presentation time. Whereas in temporal phase mapping (Figure 5, Left corner), multiple stimulus locations are highly correlated to other stimulus locations through the duration of presentation time.

In this research, an input visual stimulus was designed to minimize the error that occurs when assigning a voxel response to an input stimulus time series. The idea was to create unique input stimulus patterns for different sectors of visual space such that when a single voxel fMRI response was statistically compared with the input stimulus sequence for a spatially specific visual stimulus wedge, the comparison between the voxel response and the stimulus time series using a least squares method for each sector will be

minimized for one of the sectors with little to no overlap with stimulus time series of neighboring sectors.

An input stimulus function was created by randomly presenting a visual field polar angle numerous times over the duration of an fMRI scan. The visual field is divided into twenty equal polar angle segments. Each of the twenty visual field sectors is associated with one unique input stimulus function. Each input stimulus function can be viewed as a unique "code" for a specific visual field sector. For example, as an 18° wedge stimulates a specific polar angle sector (purple dot) in the visual field (Figure 6 – left) over time, that polar angle sector gets a unique stimulus presentation sequence over time (left purple time series) representing only that visual field sector.

To determine which visual field sector a voxel is responding to, the stimulus time series must first be convolved with a gamma variate function (simulated hemodynamic impulse response, HIR) and have pink noise added to the stimulus time series. This convolution will generate a simulated BOLD response for each stimulus time series. Thus, given a voxel's actual fMRI signal and the estimated fMRI signal, a "goodness of fit" can be calculated using a multiple linear regression to determine which visual field sector(s) a voxel optimally responds (explained in more detail in Chapter 3).

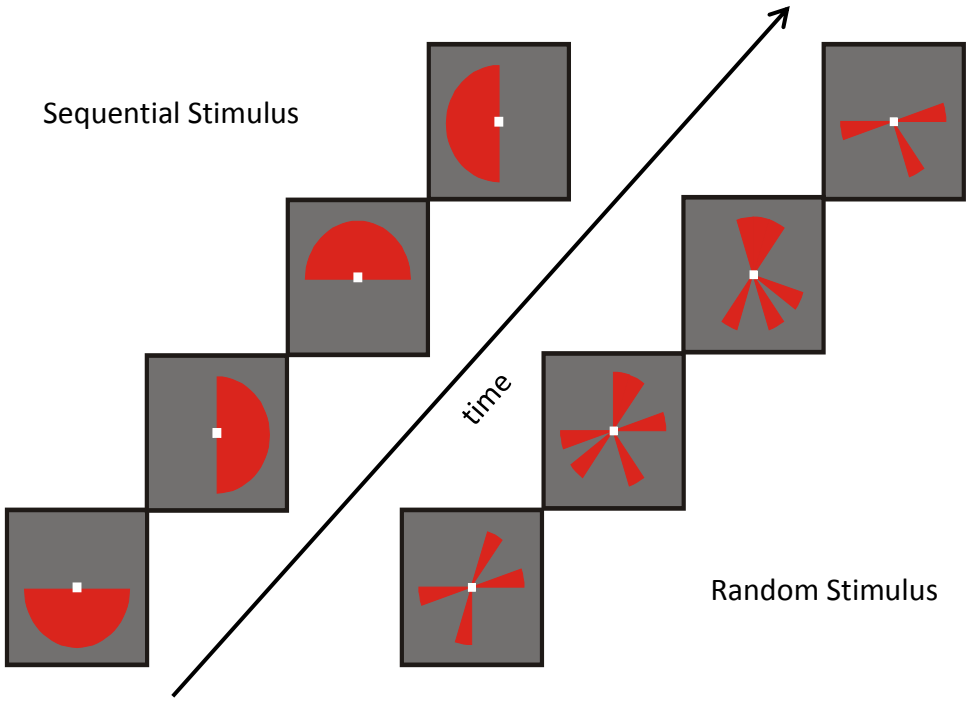

Figure 5: Distinct Methods of Stimulus Presentation. Two distinct methods of stimulating the visual field. The sequential stimulus (top) represents a typical method for presenting the temporal phase mapping technique for visual field mapping. The random stimulus (bottom) represents an implementation of the code based mapping technique discussed in the dissertation.

Previous mapping of visual cortex has been done using pseudo-random sequences to elicit fMRI responses in the visual cortex. Gallant et al. used polar angle sectors displayed in a pseudo-random sequence to examine the spatial linearity in the BOLD response in V1[60]. Linearity by spatial summation was assessed directly by comparing voxel responses to wedges and rings with sums of responses to component sectors[60]. Also, Biswal used a pseudo-random sequence to elicit fMRI responses from visual field sectors to create an assumption free fMRI analysis algorithm[61]. Biswal displayed a smaller visual stimulus that did not cover the entire visual field. The intent of this research was to determine if a stimulus could be detected using a specific algorithm that was not based on assumptions such as the multiple linear regression algorithms used in this dissertation. Other methods of measuring neuronal activity such as collected visually

evoked potentials (VEP) from EEG recordings have used pseudo-random sequences to map retinotopic responses [68] but these methods suffer from the limitations of lower spatial resolution to produce detailed retinotopic maps. To date, no one has attempted to use a random stimulus presentation technique to quantitatively map the primary visual cortex using fMRI with the purpose of investigating the expected voxel representations of the visual field in V1.

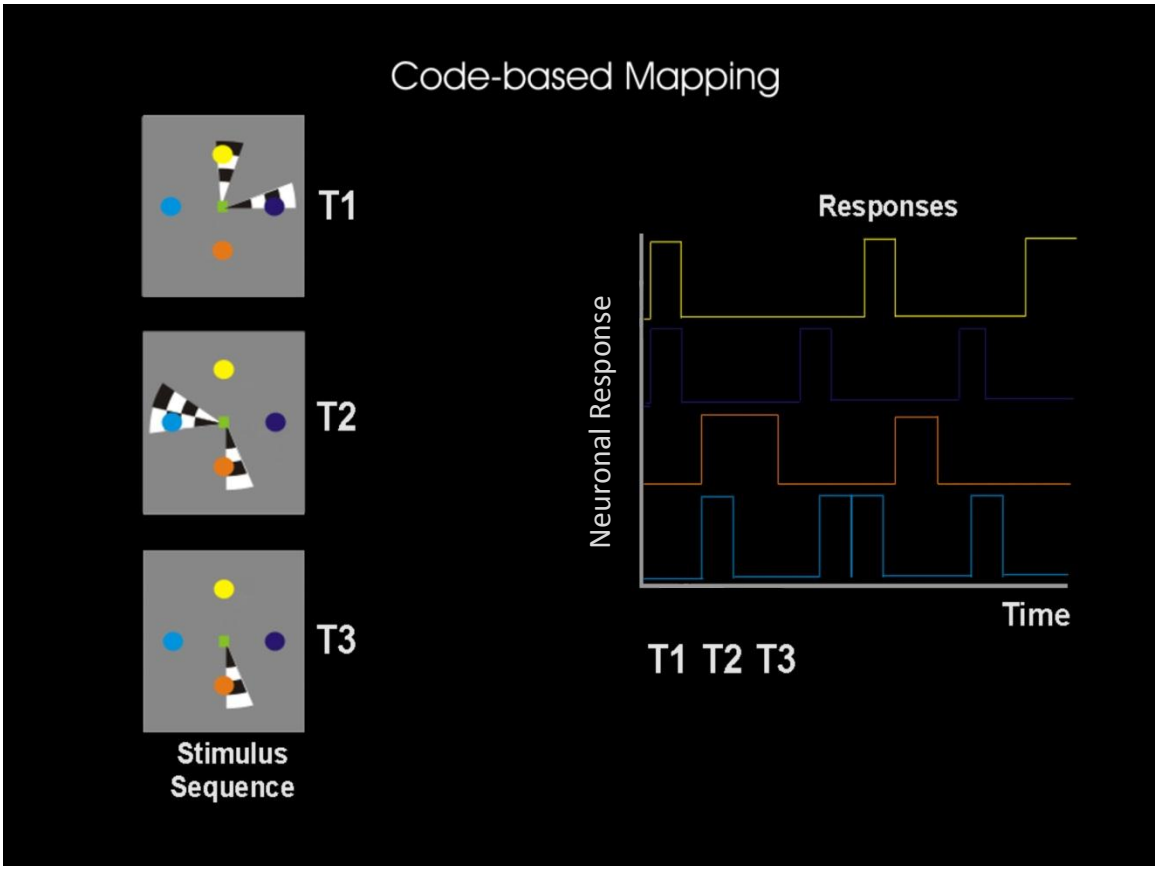

Figure 6: Random Presentation Concept. The twenty 18 degree polar angle locations are presented in an uncorrelated sequence relative to each other (left). The corresponding time series for each colored dot in the visual field is shown (right).

Visual Topography and Potential Non-uniformities in the visual space representation in the visual cortex

To construct spatially accurate cortical maps of visual function, we must have an understanding of the neural behavior of the primary visual cortex when the visual field is excited. The following section establishes the link between specific visual field excitation and cortical representation in monkey V1, the most analogous to the human visual field. The monkeys' and other animals' V1 topography and possible deficits in the representation of the visual field are examined in terms of previous literature. Findings in these species may provide insight into the behavior of human primary visual cortex relative to the visual field excitation used in fMRI mapping. We now examine various aspects of the visual system in the macaque monkey species and other animal models in searching for possible under/over representations in neuronal behavior across the visual cortex that may explain the observed deficits in the FFMap (Figure 3A) from the fMRI responses generated by the polar angle stimulus obtained in our experiments [5].

Visual field and cortical representation in monkey V1 are generally uniform

Since the 1960s, the monkey's visual anatomy and function have been researched extensively. In particular, the monkey's visual field representation in the visual cortex has been detailed [1-3,8-11, 12-14] using a number of techniques. Most of the early monkey data was gathered by measuring the extracellular potentials [13, 15-18], single unit recordings [14], or 2-deoxyglucose staining [1, 8] in the cortex. These techniques gave

researchers a method for directly correlating visual field activation and some form of cortical response.

The earliest extracellular recordings showed that stimulating a localized region of visual space excited a localized region of monkey primary visual cortex [13]. Hubel and Wiesel [10-12] were the first to show that the visual cortex received input from the lateral geniculate nucleus and that the primary visual cortex was anatomically organized to handle this input in a retinotopic manner [12-14]. They achieved this mapping of visual field to visual cortex by sequentially moving light bars across a screen and recording the electrical response in the animal's visual cortex. They found that the cortical response, as reflected in the extracellular recordings, also moved sequentially across the visual cortex, however, in the opposite direction of the moving light bar.

In a 2-deoxyglucose (2-DG) study, Tootell showed that the representation of the visual field within primary visual cortex of macaque monkeys completely covers the cortex [1]. The 2-DG method tags relative glucose utilization by neuronal cells. As the cell uses more glucose the non-metabolized 2-DG accumulates in the cell. The resultant accumulation of the 2-DG can be captured using autoradiography[1]. Tootell illustrated (Figure 7) that the 2-DG stain highlighted the primary visual cortex when the monkey was presented with a visual target that covered the entire visual field. The topography of V1 was then sectored into regions of eccentricity and polar angle (Figure 7 - left) that corresponded to regions of eccentricity and polar angle of the visual stimulus (Figure 7 - right). Tootell showed that the area of cortex in V1 representing a visual field sector of a specific polar angle was not significantly different from one polar angle degree to the next (arrow widths in Figure 7). Tootell supported Hubel and Wiesel's findings that the

V1 representation of the visual field is flipped and reversed (Colorbars on figure 7) with respect to the visual field.

Tootell reported that the area of the region of the V1 cortex responsible for responding to the vertical meridian of the visual field was not doubled or repeated [10, 19]. This was interesting because the vertical meridian represents the boundary between V1 and V2. These two visual cortical regions process visual information for different purposes but each used the single representation of the vertical meridian, not two distinct representations of the vertical meridian.

Tootell illustrated a cortical magnification phenomenon in V1 with eccentricity of the visual field. Cortical magnification is the phenomenon by which a larger cortical surface area is dedicated to the representation of the fovea relative to the cortical surface area dedicated to the peripheral visual field. To this point in the literature, there has been no neurophysiological evidence to suggest that the polar angle sectors are associated with any sort of "magnification" across the cortex. A deeper investigation into the literature must be done to understand if the deficits observed in the FFMap are potentially non-uniformities in polar angle activation across V1.

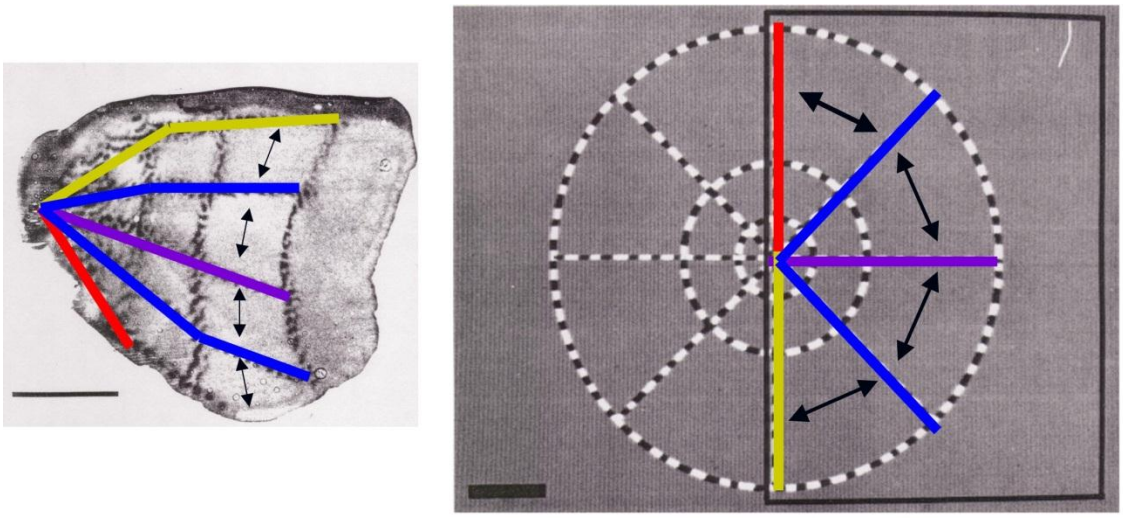

Figure 7: "Cortical representation of visual space" adapted from Tootell et al. J Nsci. 8:1531-1568 (1998). Illustrates the correlation between the stimulation of half of the visual field (right) and the response via 2-DG staining in the contralateral monkey primary visual cortex (left).

Non-uniformities exist in detailed V1 topography and LGN

The anatomy and function of the lateral geniculate nucleus (LGN) suggests that in non-human primates the difference in LGN surface area responsive to the visual field along the vertical meridian versus the horizontal meridian is approximately 1.4:1 (horizontal: vertical meridian). Van Essen and Connolly [21] show that four equal polar angle sectors (wedges) in the visual field are represented unequally, in terms of surface area in LGN layer 6 (Figure 8). The two sectors of layer 6 representing the horizontal meridian (sectors (2) and (3) in Figure 8) stimulate 31% and 26% of the LGN layer 6 surface area, respectively. The sectors neighboring the vertical meridian, sectors (1) and (4), each stimulate 21% of the surface area in LGN layer 6. A 1.4:1 difference in the LGN surface areas of stimulated layer 6 is found by taking the ratio of total surface area

representing the horizontal meridian (sector 2 + sector 3) and total surface area representing the vertical meridian (sector 1 + sector 4).

Recent reports in human LGN using BOLD fMRI signals have shown a 2:1 ratio in the number of voxels in LGN (horizontal: vertical meridian) when presenting temporal phase mapping stimuli [64]. It is conceivable that these distortions in polar angle could be translated to V1. In preliminary studies using temporal phase mapped fMRI of human V1, it has been observed that significantly disparate over/under representations of specific visual field polar angle locations exist when mapping normal vision subjects [5]. These preliminary results suggest that the difference in active voxels between the vertical meridian and horizontal meridian is at least 3.5:1.

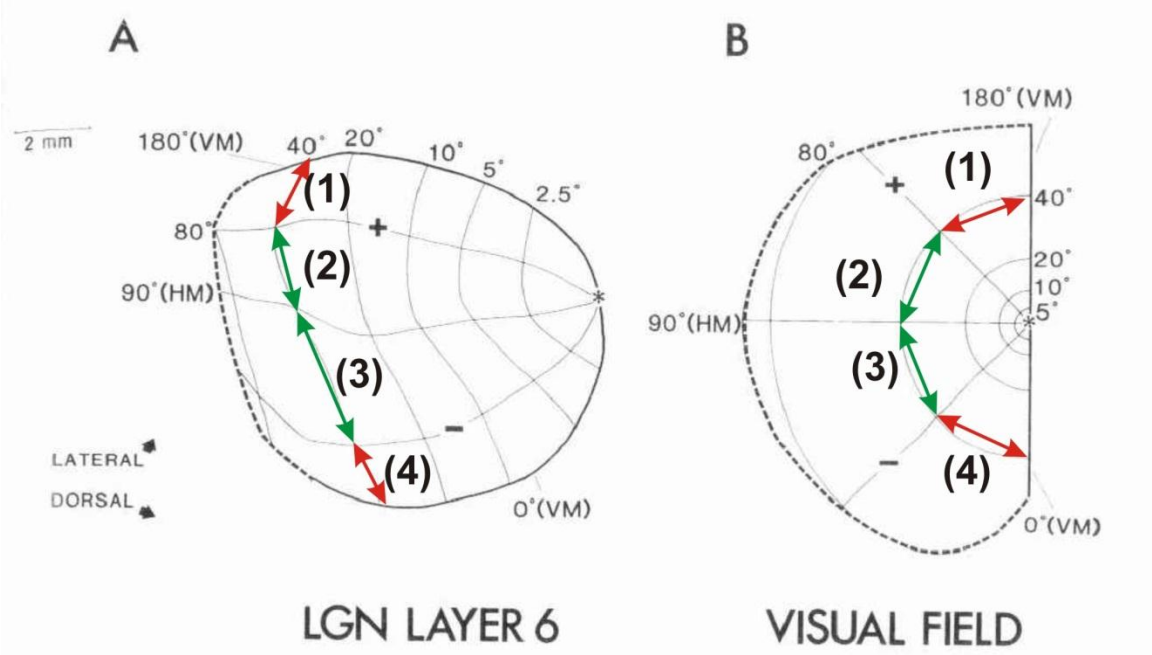

Figure 8: LGN Representation of Visual Space. (A) Macaque Monkey LGN Layer 6 representation of Left hemi visual space. (B) Left hemi visual space for (A). Adapted from Van Essen D, J Comp Neurol. 226:544-564 (1984).

Other species give a different insight into V1 representation of the visual field. A distinct double representation of the vertical meridian near the V1/V2 boundary in electrophysiological recordings [2] exists in ferret and some monkey species [10]. This phenomenon causes approximately 3-5° of polar angle next to the vertical meridian to have an overlapped representation on the V1/V2 cortical border.

Visual field data from various animal species has provided some insight into the possible under/over representations of visual field locations that may occur when mapping the human visual field. However, none of the data explains the deficits seen the in the FFMap produced by the polar angle stimulus previously described using temporal phase mapping fMRI [5].

Non-fMRI Visual Field Mapping Techniques and Possible Uneven Distribution of Visual Field Function across V1

In determining whether the true visual field representation in V1 is evenly represented across V1, it would be helpful if data measured directly from human neurons during visual field excitation existed. This is not the case; however there are alternatives to examine the extent of evenly distributed visual field orientation data across V1 cortical area in the human visual field.

Assessment due to Injury

The first accounts in modern history of direct correlation between visual field stimulation and human cortical response were observed in subjects treated for bullet wounds in World War I and World War II. Tatsuji Inouye [24], a Japanese

ophthalmologist, reported that head injuries to different regions of the brain caused different perceptual and sensory deficits. Specifically, Inouye published that injuries to specific locations in the occipital lobe affected specific characteristics of visual perception. He further observed that when certain areas in the occipital lobe were damaged, only portions of the visual field were lost. Since then, many surgeons have performed cortical stimulation during surgery to map visual function before tumor resection [25-35]. Unfortunately, none of the reported studies gave insight into how the perception of the visual field was distributed across the visual cortex.

Direct Electric Measurement during Surgery

Most traditional methods used during surgery to identify areas of cortex responsive to visual field location rely on cortical stimulation. Cortical stimulation has been used to map motor, language, somatosensory and visual function of the patient prior to surgery. For visual function, the mappings are performed during surgery to assess the functionality of the perception of the visual field and how the neurological pathology affects the patient's visual function. This method does provide real-time data regarding the patient's medical state at the moment of the procedure; however, the intraoperative recordings are time consuming, which increases the patient's time under anesthesia and subsequent recovery time. In addition, cortical recordings are performed on people with severe neurological issues that necessitate an opening of the patient's skull, thus it is difficult to study visual function in a normal, healthy brain.

Assessment of a visual field in an injured brain leads to explaining how that particular patient's visual field is functioning and does not provide insight into the functionality of the normal population of humans. Therefore, the data discussed does not provide general evidence regarding the behavior of visual field orientation across V1 or any other visual field in the human visual system. The data presented do give confidence that once a visual field deficit is present in a patients methods do exist to confirm the existence of these visual field deficits. This information will assist in providing a gold standard of measurement for visual field deficits to compare against fMRI visual field mapping once we have gained clarity on the interactions of the fMRI mapping methods and the human brain response to the stimulation being presented.

Back to Our Example

Returning to our example, suppose now that the surgeon has been given the opportunity to use the FFMap analysis as more information to use during pre-surgical planning for the patient's tumor resection. What did our surgeon decide to do with additional information about visual function provided by the FFmap? The surgeon decides to use the FFMap test primarily due to the link from the visual field location to the patient's visual cortex. This piece of information will tell the surgeon where specific regions of the visual field lie with respect to the tumor. Even though the temporal phase mapping technique leaves uncertainties regarding the reliability of the connection between visual field and visual cortex, the surgeon believes that the information will be of value in terms of defining regions of concern in resection. The surgeon will still opt for the patient to get a Goldman's test because it is accepted as a clinically reliable standard

for assessing visual field reception. Even though the FFMap test can detect a visual deficit, provide the location of the deficit in the visual field, and establish the map between the visual field location and the patient's visual cortex, the surgeon is still hesitant to completely rely on the FFMap test as the gold standard.

The reason the surgeon is hesitant to adopt the FFMap analysis as a tool in presurgical planning for tumor resection is that the reliability of the FFMap with respect to accurately correlating a section of cortical tissue to the visual stimulus location is still not at an acceptable statistical level. This dissertation research examines the first step in proving the correlation between visual field stimulus presentation and V1 BOLD responses. Specifically this research focuses on determining if temporal phase mapping produces true representations of visual field locations as measured by fMRI given that early investigations suggests that polar angle visual field locations have a systematic bias in the distribution of voxels in V1. This dissertation research will develop a method of stimulus presentation; hence eventually visual field mapping that is not sensitive to systematic biases when measuring retinotopy with BOLD fMRI.

Specific Aims

This dissertation research is focused on producing the true voxel representation of the human visual field onto the visual cortex using fMRI-based mapping techniques with the polar angle coordinate system. More specifically, early investigations of the voxel distributions associated with temporal phase mapping method using polar angles showed unexpected non-uniformities in the distribution as one moved across polar angles. These non-uniformities can lead to incorrect assignment of visual field locations in an FFMap to

regions of the visual cortex. Such possible misassignments lead to false positives in the FFMap and thus assessment of a patient's visual field representation. In order for FFMaps to be used as a clinical tool, these false positives in the polar angle coordinate and their cause must be understood. If their origin cannot be understood completely, an alternative approach to mapping the visual system must be developed. Specifically this research aims to:

Aim I: Determine if the voxel representations of polar angle, using temporal phase mapping, is biased by non-neuronal sources.

Aim Ia: Quantitatively investigate the impact of visual stimulus attributes and data processing techniques used in temporal phase mapped fMRI on the polar angle voxel distribution.

We have observed that the voxel representation of the polar angle coordinate is not uniformly distributed as suggested by previous electrophysiology studies [1]. We hypothesized that the source of this non-uniformity in mapping polar angle may lie in the attributes of stimulus presentation, namely the temporal and spatial attributes of the phase mapping stimulus. We also hypothesized that the data collection methods influence the polar angle distribution of voxels when using temporal phase mapping [6]. The data collection methods studied are the mode of MR signal detection, MR sampling of the cortex, and definition of cortical regions of interest.

Aim Ib: Determine if the non-uniformity in the polar angle voxel distribution correlates to specific cortical locations in primary visual cortex.

From the data obtained in Aim Ia, we hypothesized that the voxels located along the midline of the primary visual cortex may have a different BOLD response to the temporal phase mapping stimulus than the voxels that lie more lateral to the midline. From literature on human neurophysiology, BOLD fMRI physics, and the data obtained in Aim I, we hypothesized that the voxels along the midline have greater variation in the fMRI response than voxels that lie more lateral to the midline due to noise from physiological sources (draining veins) located near those cortical locations near the midline. The increased variance in fMRI responses is further suspected to contribute additive noise, causing statistical drop out of the voxel, and/or additive delay to the phase estimated for a specific polar angle location. Such additive delay can cause an incorrect assignment of the polar angle location to a region of voxels in the cortex.

Aim II: Determine if random stimulus presentation eliminates non-neuronal biasing effects in the polar angle voxel distribution as compared to temporal phase mapping.

Aim IIa: Develop a method to present and analyze random stimulus presentation fMRI data.

The method for detecting responsive voxels during temporal phase mapping relies on the ability to detect the time delay (or phase) from the start of a stimulus to the onset of the individual fMRI response. With temporal phase mapping the higher correlation between input sequences restricts the voxel to only respond to one stimulus location. Even if the voxel could respond to multiple stimulus locations, the high correlation

between input sequences makes the ability to detect more than one stimulus location very difficult. Studies have shown that neurons in the primary visual cortex have orientation tuning curves [66] that show preference toward specific stimulus locations and sometimes more than one stimulus location [67]. It was hypothesized in the current study that a random stimulus presentation, referred to as code based mapping, where each stimulus location is stimulated with an on and off time sequence that is linearly independent of the stimulus time sequences used to excite any and all other stimulus locations, will be able to elicit detectable responses in a voxel responding to each visual field stimulus. The analysis method used to detect the code-based mapping input sequences will create a voxel "tuning response function" for the stimulus locations excited. We refer to the vector of normalized linear coefficients (goodness of fit) of a voxel's fMRI response to each stimulus location's input sequence as a tuning response function because the vector shows the visual field representation for a voxel given a set of stimulus locations presented to the subject.

Aim IIb: Compare code-based mapping to temporal phase mapping.

Due to the spatio-temporal correlation between temporal phase mapping and V1 during fMRI visual field mapping, it was hypothesized that the high linear correlation between stimulus time series of neighboring visual areas used in temporal phase mapping combined with localized fMRI susceptibility influences on voxel signals due to draining veins reduces the accuracy of the visual field maps produced from temporal phase mapping. We hypothesized that code-based mapping of the visual field onto the visual cortex would eliminate the intrinsic spatio-temporal-hemodynamic confounds that exist

in the temporal phase mapping method, thereby producing a more uniform voxel representation across the polar angle distribution. Along with polar angle assignment for each voxel, further comparison of the mapping methods is performed with respect to noise susceptibility of the mapping methods to stimulus location assignment and qualitative retinotopic organization.

Aim I: Determine if the voxel representations of polar angle, using temporal phase mapping, is biased by non-neuronal sources

Introduction

Blood oxygenation level dependent (BOLD) functional magnetic resonance imaging (fMRI) has been used extensively for mapping the representation of the visual field within the human brain [23, 74-75]. One potential clinical application of visual field mapping using fMRI is in the assessment of patients with pre-existing field deficits, specifically patients with visual field deficits originating from cortical or sub-cortical pathology. For fMRI brain mapping to transition successfully from academic use into clinical practice, the spatial accuracy of the brain maps needs to be characterized better. One key issue is whether fMRI mapping techniques completely and accurately represent the underlying neural organization, especially in the absence of smoothing or other interpolation procedures that may be inappropriate in clinical applications where the detection of pathology-induced distortions or deletions is paramount. This can be particularly important for presurgical mapping of brain function near a tumor resection site since inaccurate rendition of the underlying neural function could potentially lead to inappropriate resection of viable brain tissue. Such concerns are also important for academic neuroscience since undetected distortions in fMRI-based brain maps could lead to inaccurate theories and models of neural organization. In this dissertation, we examined fMRI maps of visual cortex in healthy individuals in order to characterize potential distortions/omissions due to stimulation and to identify their cause.

Temporal phase mapping is a time-efficient method for fMRI-based mapping of the topographical representation of the visual field in human visual cortex [6, 59, 79]. This technique successively activates locations within the visual field using a traveling wave of activation evoked by a slowly expanding, checkered annulus or a rotating checkered wedge [23, 72,, 73, 74]. With temporal phase mapping, the stimulation parameter of interest (eg. preferred polar angle) is encoded in the time delay of the fMRI response relative to the stimulation sequence (Figure 9). When the complete stimulus sequence consists of multiple repetitions (eg. 5 repeated rotations of a checkered wedge), the time delay is typically expressed as the temporal phase delay of the fMRI waveform (approximately sinusoidal) relative to the stimulation timecourse.

Many studies have used this technique to produce human retinotopic maps and to identify the boundaries of multiple, distinct visual areas within the occipital lobe and other brain regions[6, 23, , 22, 73, 75]. However, in preliminary fMRI experiments we observed that there can be significant over- or under-representations of visual field locations near the vertical meridian [5]. Such non-uniformities are noteworthy because macaque monkey data based on microelectrode recordings or other techniques do not appear to indicate major non-uniformities, at least in V1.

In a 2-deoxyglucose (2-DG) study, Tootell showed that the representation of the visual field within primary visual cortex of macaque monkeys has a complete representation of polar angle with approximately equal areas of cortex from one polar angle to the next[1]. Tootell also documented the well known distortion of visual field eccentricity referred to as “cortical magnification” whereby foveal eccentricities are overrepresented within V1 and other visual areas. Other reported non-uniformities

include an asymmetry in ocular dominance column representation [77] and a representation of a strip of the ipsilateral field near the V1/V2 boundary [2,85] that is thought to be associated with callosal connections between the hemispheres [86]. However, there is little evidence that the neural representation of polar angle is distorted by significant over- or under-representation.

Previous fMRI-based studies of human V1 topography in which theoretical models have been fit to the empirical data also have not typically noted major distortions of the polar angle representation. Shira et al. [87] did note a topographic "shear" distortion that is a function of polar angle but this does not appear to constitute a major over- or under-representation of particular polar angles. Winaver et al. [65] do show a significant shift in the B_o field in cortical tissue due to the proximity to the transverse sinus and its nosie distortion of the fMRI response in V4h. This effect may play a role in the distortion of the V1 polar angle map; however, the study does not show that this effect would be as significant in the superior sagittal sinus (due to the superior sagittal sinus's orientation to the B_o field), which is the major sinus that runs along V1.

Given the small amount of evidence for major inhomogenities in the neural representation of visual field polar angle in V1, it follows that apparent over/under representations in the fMRI data may reflect methodological artifacts [2]. A variety of factors could potentially produce artifacts in the temporal phase encoding of preferred polar angle. These include the temporal and spatial characteristics of sequential visual stimulation or of the BOLD hemodynamic response itself. This may include nonlinear spatio-temporal interactions between cortical locations or between hemodynamic elements (eg. blood vessels). Such spatio-temporal interactions might be especially

important for visual stimulation that involves sequential activation of nearby cortical locations, as is the case for temporal phase mapping. Spatial sampling of the convoluted cortex with a uniform fMRI grid can cause some voxels to sample multiple cortical surfaces (e.g. across a sulcus) with significantly different visual field representations. Such voxels could have a BOLD signal reflecting contributions from multiple cortical responses with different stimulus onset times not accurately reflected in the average response. Furthermore, it is not clear if a regular rectangular voxel grid will produce a uniform spatial sampling of the 3-dimensionally convoluted cortical gray matter.

Virtually all of these factors may apply to fMRI mapping of function in other brain areas besides visual cortex. However, the ability to uniformly and completely stimulate all locations within the visual field using video/graphic stimuli provides a unique opportunity to investigate these factors in detail within the human visual cortex. Consequently, the goal of this study was to quantitatively assess the ability of fMRI to accurately reflect the functional topography of primary visual cortex and to examine a number of potential causes of distortion in the resulting fMRI-based maps. We specifically focused on the fMRI representation of visual field polar angle since all available evidence indicates that this parameter should be uniformly represented in the neuronal map of human primary visual cortex. Our results indicate that there can be significant under-representation or even omission of visual field locations near the vertical meridian within the fMRI-based map of V1 and that these distortions may reflect hemodynamic effects and/or susceptibility drop out associated with anatomically fixed structures such as the midsagittal sinus and associated draining veins. Preliminary reports of this work have appeared in Janik et al [5].

General Methods

We conducted six experiments to document distortions of the fMRI-based retinotopic map of V1 and to identify or eliminate potential sources of those non-uniformities. The following methods apply to all experiments.

Subjects

Data were collected from 29 participants (21-51 years of age, 10 female) with no history of neurological or visual deficits. Subjects read and signed a detailed consent form describing the experimental procedures in accordance with the human subject Institutional Review Board of the Medical College of Wisconsin and Marquette University. Prior to data collection, subjects were trained in a mock scanner to position their head in a model of the gradient head coil, to adjust the custom optical system for optimal viewing of the video images, and to perform a visual task while constantly fixating on a point in the center of the visual field.

fMRI Experimental Parameters

Brain images were obtained with a 1.5T General Electric Signa scanner equipped with a custom three axis, shielded head coil designed for rapid gradient field switching. A 64 x 64 voxel matrix covering a 24 x 24 cm field of view was used to obtain voxels of 3.75mm x 3.75mm x 4.0mm. fMRI pulse sequences were gradient-recalled EPI and asymmetric spin-echo EPI. For both gradient-recalled EPI and the asymmetric spin echo

EPI the MR parameters were as follows: an initial 90° RF pulse, a TR of 2000 ms, and TE of 40 ms (gradient echo) and 110 ms (spin echo). The first four images of each scan were discarded to allow brain tissue magnetization to achieve steady state. At the end of the scanning session a high resolution, T1-weighted, spoiled GRASS anatomical image was also collected. The anatomical data set covered the whole brain with a voxel resolution of 1 x 1 x 1.1 mm (flip angle = 30°, TR = 25 ms, FOV = 24 cm).

Visual Stimulation - Retinotopic Mapping

High-quality visual stimulation was achieved using a custom optical system designed to project images directly onto the retina of subjects, thereby providing a high-luminance, 60° field of view, and minimizing the effects of changes in pupillary size [74]. Custom computer graphical images were generated using a Cambridge Instruments VSG 2/3 video card and displayed via a Sharp XG2000U color LCD video projector. A variable, neutral density, polarizing filter was used to adjust the average luminance of the images to a comfortable photopic range (~20 cd/m^2) for each subject. All experiments used an 8 Hz flickering checkerboard design. All subjects were asked to fixate on a green marker located in the center of the visual stimulus.

Figure 9 outlines the temporal phase mapping stimulus paradigm used to chart retinotopy in the visual cortex. A counterphase flickering (8 HZ), checkered 180º wedge slowly rotated (18°/2 sec) clockwise (CW) or counter clockwise (CCW) from 0° to 360° over a period of 40 seconds. The sequence was repeated 5 times during the fMRI scan for a total of 200 seconds. The scans were typically repeated 3 times and averaged to increase contrast-to-noise. The space averaged luminance of the checkerboard matched

the mean luminance of the gray background. Voxels in visual cortex that received visual input from a restricted area on the retina (indicated by one of the colored spots at the left of Fig. 9) were activated each time the wedge passed over that position in the visual field. For retinal locations successively farther from the starting position of the wedge (purple, yellow and blue spots in Fig. 9), the time delay between onset of the stimulation sequence and activation of the voxel increased proportionally. Consequently the delay (equivalently the temporal phase) of the fMRI signal for each responsive voxel encoded the polar angle location of the stimulus that evoked the strongest activation (plus an additional hemodynamic delay that was corrected in post-processing – see below). To help control visual attention, a small checkered circle appeared near the center of the stimulus wedge but was displaced randomly inward or outward every 2 seconds. While maintaining fixation, the subject reported whether the circle moved closer or farther from the fixation point on each successive presentation.

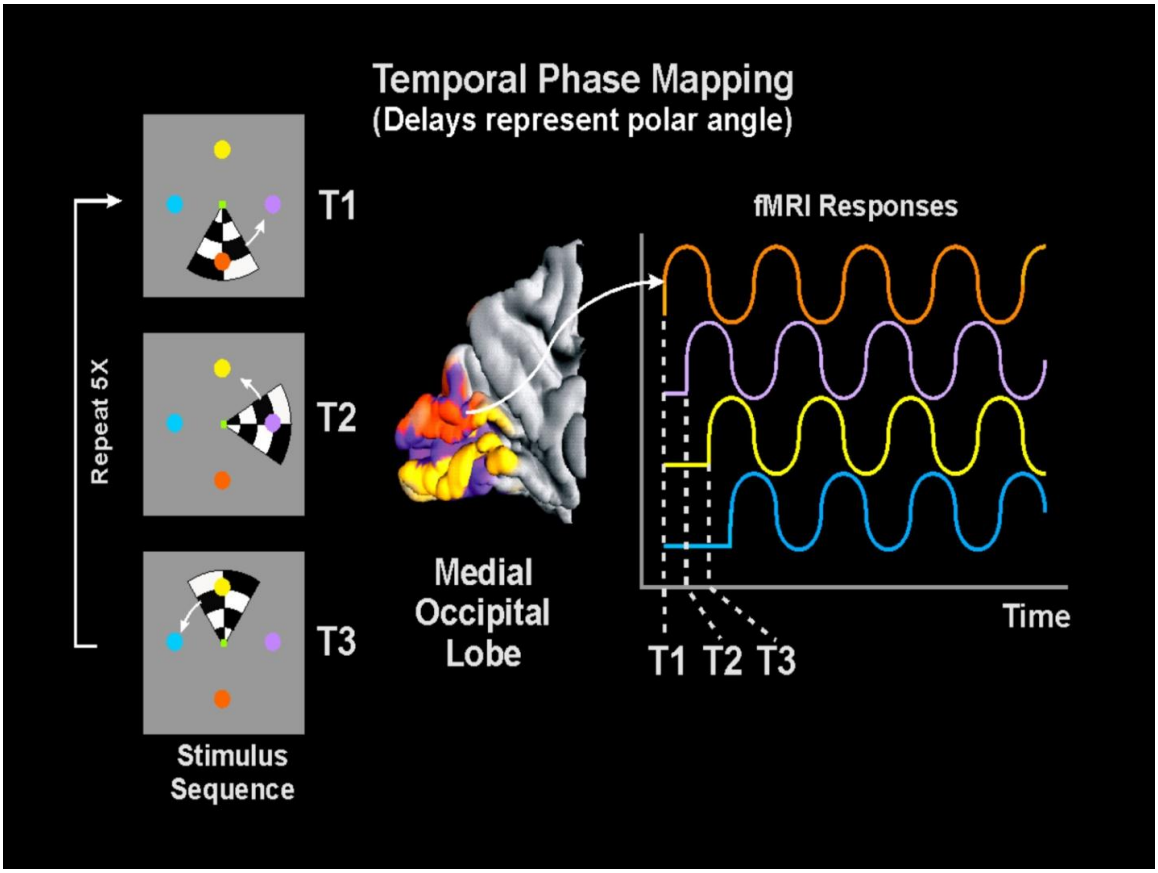

Figure 9: Temporal Phase Mapping. The temporal phase mapping process for retinotopic data acquisition in an fMRI study.

We also mapped preferred eccentricity, using an analogous stimulation sequence involving an expanding checkered annulus whose size, expansion rate and check density were varied in proportion to mean eccentricity. For four experiments, we also used a stimulus consisting of a flickering full-field checkerboard presented in five cycles of twenty seconds ON and twenty seconds OFF, also typically repeated 3 times.

Post-processing

Raw fMRI signals were converted into image format using GE Signa software and assembled into time series of volumetric imaging data using the AFNI analysis package [79]. Each time sequence of collected brain volumes was corrected for head

motion using 3dvolreg in AFNI [79]. Temporal phase mapping data were analyzed using the Hilbert Delay plugin of the AFNI package. The Hilbert Delay calculates the temporal delay of each voxel's fMRI time series to a reference sinusoidal waveform and estimates the correlation coefficient of the fit [76, 79]. For other experiments using a block stimulation paradigm, the data were subjected to conventional cross-correlation analysis [81] with a sinusoidal model of the stimulation sequence using AFNI's 3dFim. AFNI was also used to display the resulting fMRI activation patterns (both magnitude and temporal phase delay maps) as pseudocolored overlays superimposed on the T1 anatomical images.

Functional Field Maps

As described previously [91], a Functional Field Map (FFMap) is a graphical representation of the subject's visual field showing the complete distribution of visual field locations that maximally activated voxels in the primary visual cortex (Figure 10) [91]. The FFMap is created by using the wedge and annulus retinotopic mapping data to identify the preferred stimulus position (angle and eccentricity) that maximally activated each voxel in primary visual cortex. For each activated voxel, a circle symbol is placed on a diagram of the visual field at the preferred location and is pseudocolored to indicate the fMRI response magnitude. The radius of the circles indicates the 70% confidence interval for the preferred location and is based on a separate analysis of the variance of the temporal delay of the BOLD signal [78].

As mentioned above, the temporal phase delay of a voxel's BOLD response is determined by its preferred location in the visual field plus an additional delay caused by

the sluggish BOLD hemodynamic response. To accurately determine a voxel's preferred visual field location, the phase delay was corrected for this latter component. For each visual field direction (eccentricity and polar angle), an ROI is created for each hemisphere including the primary medial cortex. An FFMap is constructed for each of the hemispheres. For the polar angle correction, each hemisphere's FFMap is adjusted with a constant phase delay till each FFMap represents the correct visual hemifield associated with the corresponding cortical hemisphere. Each occipital hemisphere primarily represents the contra-lateral visual field (plus a small strip of ipsilateral field close to the vertical meridian). For eccentricity, the entire FFMap is used for the phase delay correction. The FFMap is examined for a "gap" in the delay distribution corresponding to the point in the stimulus sequence when the ring disappears outside of the display radius. The data points central (closer to the fovea) should than be positions at the maximum eccentricity of the display. This is cross checked by examining the positions of a sample of individual voxels at the occipital pole versus the anterior portions of the calcarine sulcus. This is done to ensure that there is no "wrap around" effect of the most outer eccentricities to the occipital pole or vice versa.

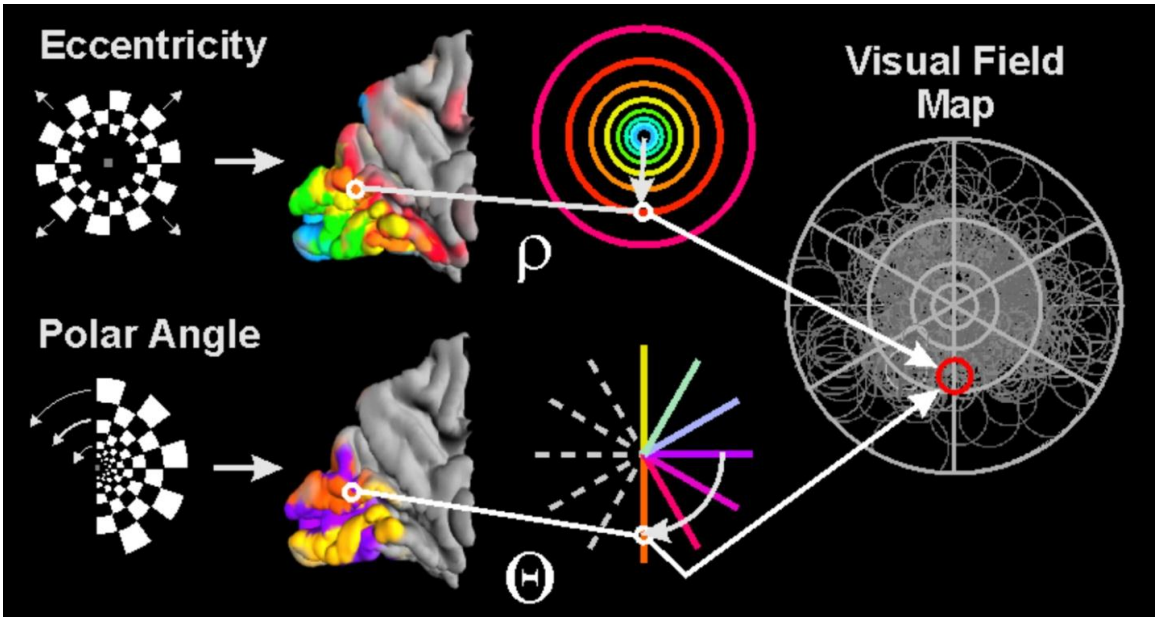

Figure 10: Functional Field Mapping. Functional Field Mapping illustrating how eccentricity and polar angle visual stimuli are analyzed using signal processing techniques and fMRI data from a human subject's primary visual cortex. The fMRI data are then combined

ROI Selection

Flat map brain models were created from the anatomical data using SureFit and Caret v5[80]. Regions of interest for V1 were created by identifying the V1/V2 boundaries from flat maps of the retinotopic data. ROIs were manually drawn in Caret v5 [80] or AFNI/SUMA [79].

Histogram Construction and Analysis

Histograms of the temporal phase delays for all experiments were constructed and analyzed as described here unless otherwise stated in the *Results* section. To construct the histogram of preferred polar angles, we used a correlation coefficient threshold of 0.35

($p<0.02$ whole brain) for detecting activated voxels [104]. Phase delays from voxels in the V1 ROI were sorted into twenty, 2 second bins and the voxel count for each bin displayed graphically as a histogram.

The experiments involved comparisons of histograms obtained under different experimental conditions. The null hypothesis was that there was no change in shape of the histogram across conditions. To test this hypothesis, histogram bin counts were first normalized to the total number of voxels contained in all bins. Any shift offset between the two histograms was then estimated using the Hilbert Delay plugin of AFNI [7] but using the bin values of one histogram as the "standard" waveform and the second histogram as the "test" waveform. If the correlation of the two waveforms was statistically significant ($r>0.3$, $p<0.05$) and the delay offset was non-zero, the bins of one histogram were then shifted by this offset value to align the two histograms (unless the offset itself was of specific interest for a given experiment). Finally, a chi square goodness of fit test was performed in Matlab to detect differences on a bin-by-bin basis at a statistical significance level of 0.05.

Results

Six separate experiments and two computational simulations were performed to document non-uniformities in the cortical representation of preferred polar angle and then to identify or eliminate potential sources of those non-uniformities. We focus here on the representation of preferred polar angle rather than eccentricity to avoid complications that would be introduced by cortical magnification effects on the eccentricity representation. For the purposes of documenting distortions and identifying their causes, either

representation could be used so we have chosen to focus on the most straight-forward analysis. (In Appendix I, Figure S1, we document non-uniformities in the eccentricity representation.)

Experiment 1: Non-uniformity in the polar angle representation: The goal of the first experiment was to document non-uniformities in the polar angle representation measured with phase mapped fMRI employing a rotating checkered hemifield (See Methods). Histograms of preferred polar angle were obtained from 29 subjects (ages 21-51, 10 female) using 3-5 repetitions of the phase mapping scans per subject.

Figure 11A illustrates the range of shapes of the voxel-count histograms obtained from our sample of 29 subjects. Each histogram illustrates the proportion of voxels representing different preferred polar angles in the visual field. The shapes ranged from bimodal, to unimodal, to uniform though the non-uniform shapes accounted for approximately 65% of the subjects tested (Figure 11B) . The bimodal and unimodal types in this figure exhibit more than a 3 fold difference from trough to peak. The small icons on the graphs mark the bins associated with the vertical and horizontal meridian representations. Note that the representations of one or both vertical meridia tend to be under-represented relative to other field positions. The overall shapes of these distributions did not change significantly as the correlation coefficient threshold criterion was increased or decreased over a range of 0.3-0.5. Figure 11C illustrates the data from one subject as the correlation coefficient threshold varies from 0.3 to 0.5. Thresholds above 0.5 are not illustrated since the number of voxels became too small to adequately represent the shape of the histograms.

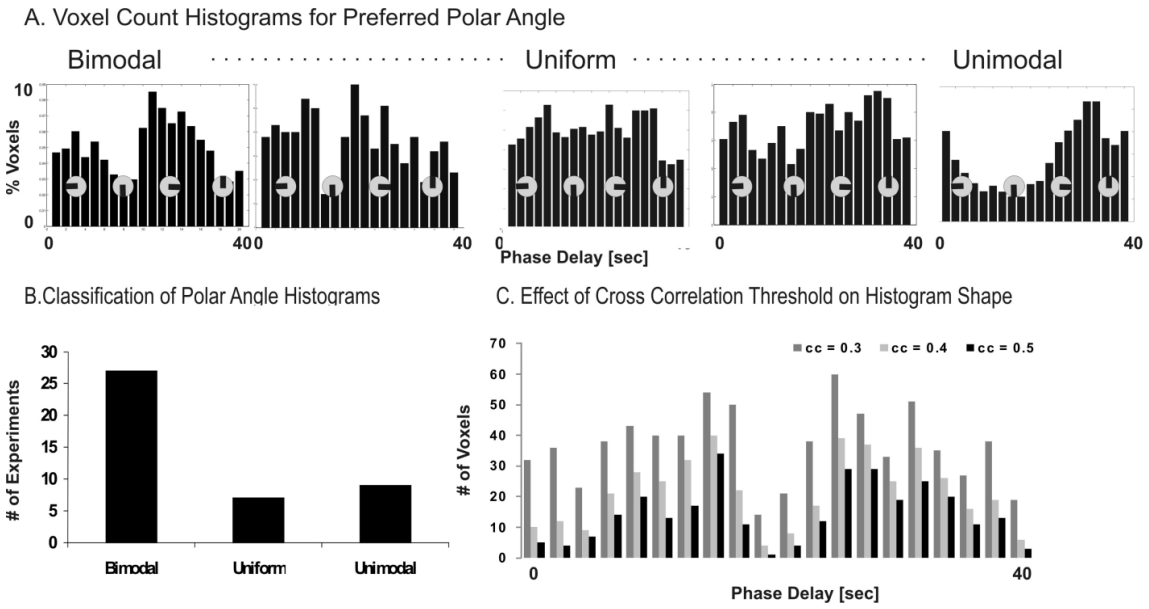

Figure 11: Characterization of the polar angle voxel distributions. (A) The observed range of histogram shapes of polar angle. Circles in the histograms represent the visual field. The location of the black hash represents the visual field location associated with the superimposed bin. (B) The assessment of 43 subjects' polar angle voxel distributions. Each subject was placed into one of three categories. (c) Effects of cross correlation thresholding on the phase delay data.

Voxel histograms for the 29 subjects were classified into the three categories: bimodal (two peaks), unimodal (one peak), or uniform (no discernable peak). Overall 80% (23 out of 29 data sets) revealed a histogram that was not uniform (Figure 11B). Bimodal histograms accounted for the majority (18 out of 29 -- 62%). For this sample, there was an average of a 3.5-fold difference in voxel count from the lowest trough (local minimum) and the highest peak (local maximum) in the histogram.

Using the polar angle data in conjunction with eccentricity mapping data allows construction of a Functional Field Map (FFMap) for each case. As illustrated in Figure 12B, the FFMap permits inspection of the complete visual field representation and can be used to help identify specific visual field locations associated with under-representations in the polar angle histogram (see Methods for additional details of FFMap correction and interpolation). The FFMap fills in valid visual field locations as black circles. A black

area on the FFMap represents a valid visual field area; likewise, an area with color represents a visual field location that the fMRI data did not represent. The FFMap shown in Figure 12B is associated with the histogram shown in Figure 12A. The 0/360 degree (x-axis) bin position of the voxel histogram (Figure 12A) is associated with the upper vertical meridian in the FFMap (Figure 12B). Notice the region of low symbol density in the superior portion of the FFMap near the superior vertical meridian (visible green color in the FFMap in figure 12B). This depression is associated with a broad trough in the associated polar angle histogram. However, the FFMap also shows that certain combinations of polar angle and eccentricity are completely lacking, thus appearing as a "hole" in the FFMap. One can see that polar angles of 324-0° are associated with the superior vertical meridian. In addition, another under-representation can be seen around the inferior vertical meridian. This second under-representation of voxels is associated with polar angles of 162-198°, which represent the inferior vertical meridian. When the delay data is projected onto the primary visual cortex (Figure 12C – dash out line), one can see that the "holes" in the FFMap are not due to a lack of data but a reassignment of data along the vertical meridia to another delay value, thus assignment to another polar angle visual field location. Unimodal histograms from other subjects are associated with a single region of low density symbols in the FFMap, again typically associated with the superior vertical meridian. In contrast, uniform histograms tend to be associated with a more uniform density of symbols throughout the FFMap.

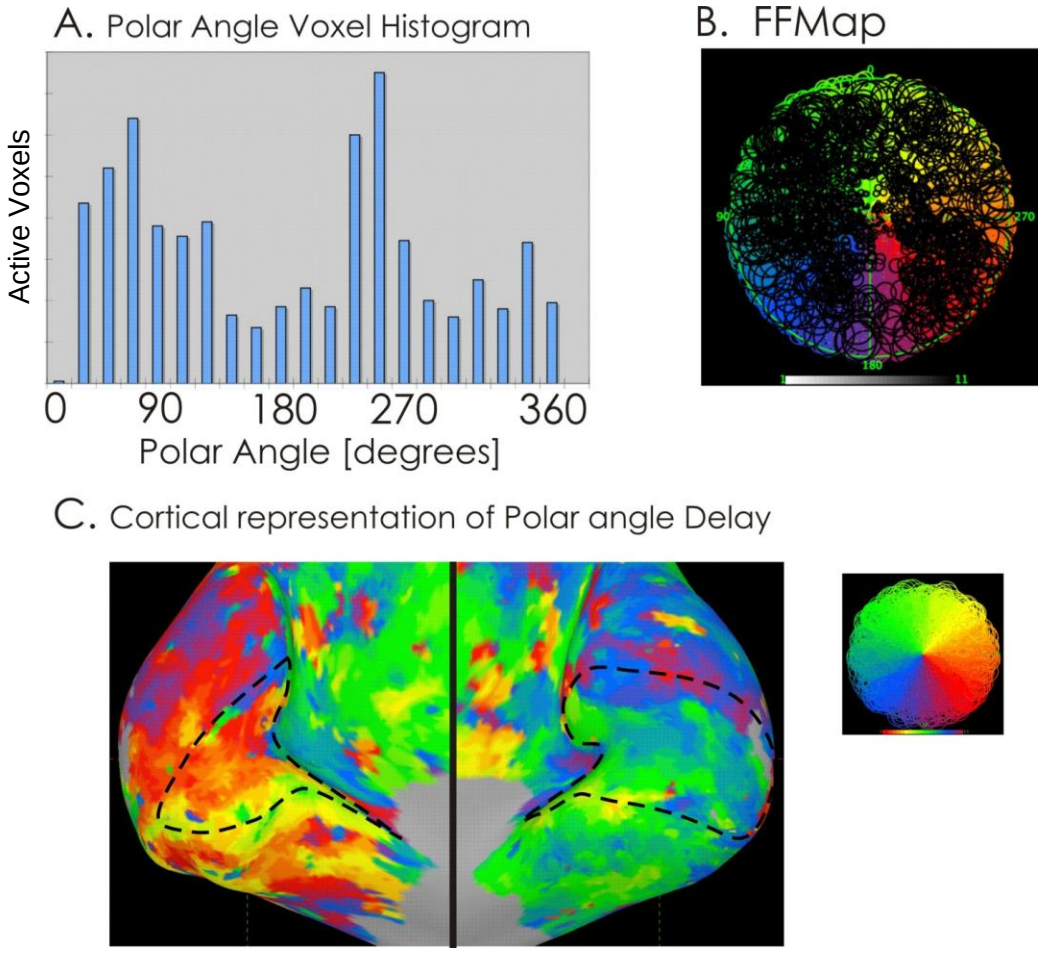

Figure 12: Polar Angle Maps. (A) A typical bimodal polar angle voxel histogram illustrating the under-representations at the vertical meridia. (B) A typical functional field map that corresponds to the polar angle voxel histogram in (A). (C) An inflated brain map with V1 ROI in dashed lines. The pinwheel of colors (right) represents the phase delays associated with each polar angle location in the visual field.

One concern with the preceding analysis was that errors in defining the ROI for V1 could potentially affect the number of voxels representing the vertical meridia which demarcate the cortical boundaries between V1 and V2. More specifically, an overly conservative definition of the V1 ROI could preferentially assign voxels representing the vertical meridian to V2 rather than V1, thus leading to an apparent under-representation in V1. To eliminate this possibility, we performed a careful reconstruction of the cortical retinotopy using cortical surface maps and identified the most likely location of the V1/V2 border based on anatomy and phase mapping representation of the vertical

meridian. We then tested the effects of systematically displacing that border. As illustrated in Figure 13, spatially over- (blue) or under- extending (red) the V1 ROI did not materially alter the bimodal shape of the polar angle histogram. The under-representation associated with the vertical meridian persisted despite the variation in the ROI placement. The only noticeable difference across histograms was in the total number of voxels assigned to V1 (453, 359, and 227 respectively). Thus, a 2 fold change in total number of voxels in the ROI did not eliminate the under-representation of vertical meridian; it only increases the number of voxels in each ROI and thus in the polar angle delay histogram.

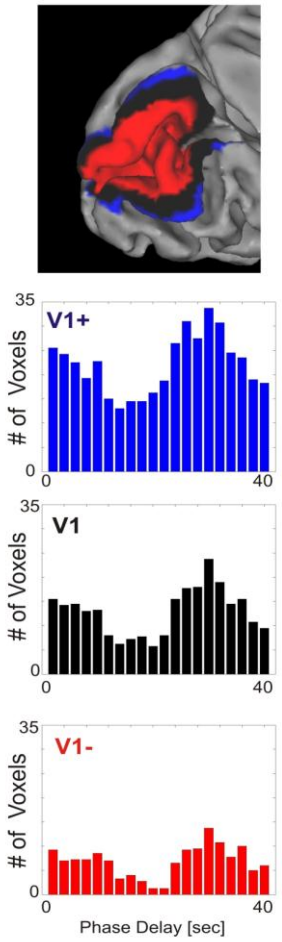

Figure 13: V1 ROI. The different polar angle voxel distributions for three different V1 ROIs: Conservative ROI (red), Moderate ROI (black), and Liberal ROI (blue).

In sum, fMRI retinotopic maps based on temporal phase mapping for the majority of subjects are significantly non-uniform in the representation of visual field polar angle. For V1, these non-uniformities typically manifest as an under-representation of locations near the vertical meridian sometimes with "holes" at certain eccentricities. Given these non-uniformities, we next sought to identify potential causes of the distortions in a series of subsequent experiments.

Expt 2: Anatomically Fixed Noise Source Causing Phase Delay Distortion. One possible cause of distortions in the brain map of polar angle is that there are anatomically

fixed features within the brain, such as the midsagittal sinus, that distort the fMRI signals and associated phase delays of voxels in their vicinity or that cause susceptibility induced drop out. If true, then the peaks and troughs in the phase delay distribution should be associated with voxels at anatomically fixed locations. This can be detected if the rotating wedge stimulus is started at different visual field positions in different fMRI scans. In such case, the phase delay of peaks and troughs should shift in time depending on the start position. Figure 14 illustrates voxel histograms for two stimulus conditions in which the leading edge of the checkered hemi wedge started at the right horizontal meridian (Fig. 14, top) or at the superior vertical meridian (Fig. 14, bottom). These two stimulus sequences should produce roughly the same polar angle histograms but shifted relative to each other by about 10 seconds for a 40 second period. In fact, the histogram for the superior vertical meridian start location (Fig. 14, bottom) was shifted to the left (earlier delay) by approximately 10 seconds (~5 bins) with respect to the histogram for the right horizontal meridian start position. The histograms showed no significant differences in shape on a bin-by-bin basis (Chi-square test, p-value = 0.002) after shifting the histograms to account for the delay induced by the different starting positions. Furthermore, the functional field maps and histograms, which are color coded by polar angle phase delay, show that the depressions in the histograms are associated with the vertical meridian representations regardless of stimulus starting position, consistent with a fixed anatomical location of the under-represented voxels.

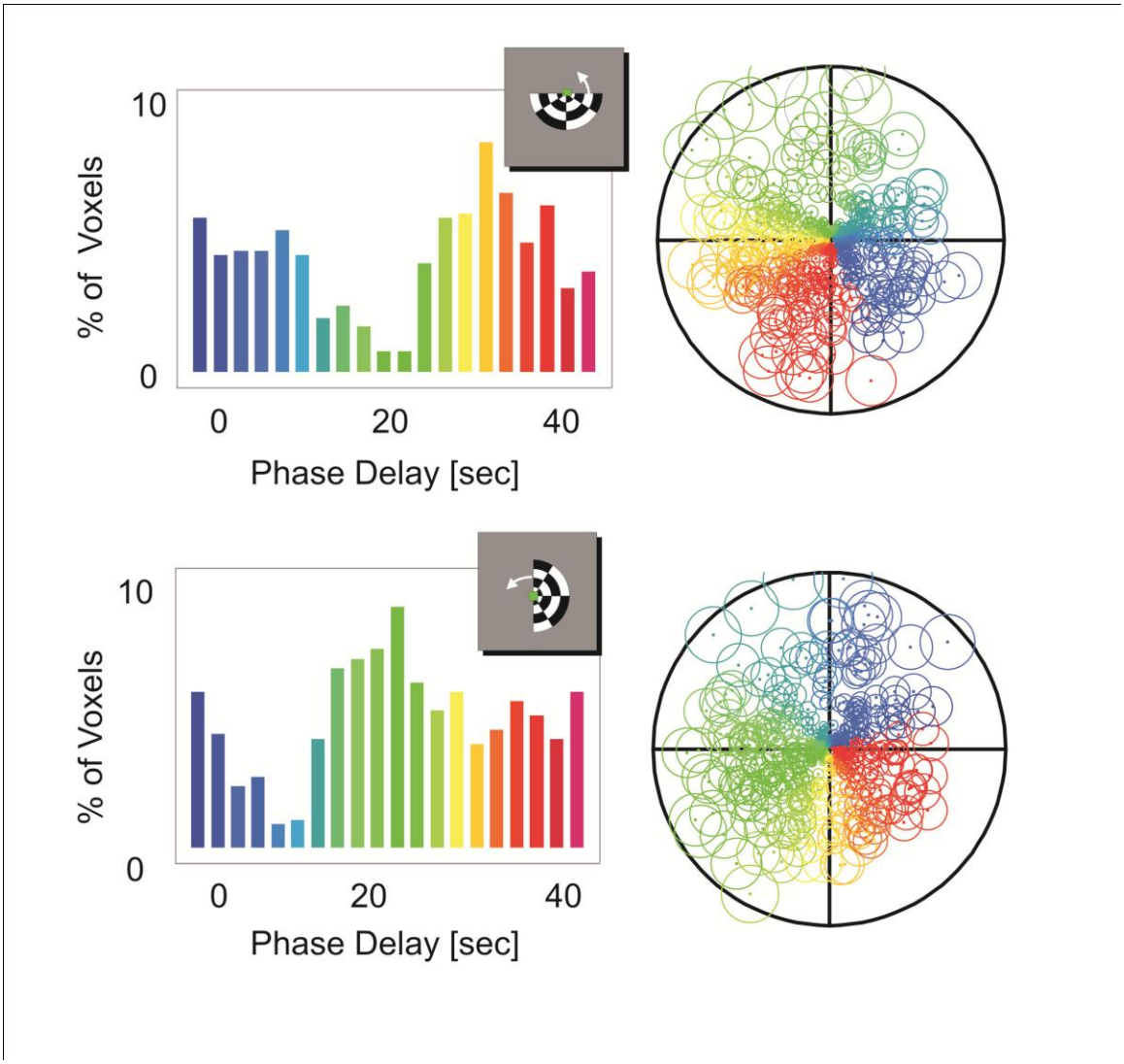

Figure 14: Anatomically fixed voxel under-representations. Voxel Distribution's relationship to the starting position of the stimulus. The original starting position of the hemi-wedge (top) produces a typical bimodal distribution. A change in the starting position of the hemi-wedge (bottom) shifts the bimodality of the phase delay distribution.

The anatomically fixed locations of the under-represented voxels suggest that some process associated with those locations is distorting the BOLD signal. These locations tend to be associated with the vertical meridian representations which, for human V1, are located medially along the lips of the calcarine sulcus. These locations are close to the midsagittal sinus and its associated draining veins. Plausibly, such vascular features might cause distortions of the BOLD hemodynamic signals. It is typical of

voxels along the occipital midline to exhibit noisy BOLD fluctuations that could reduce signal quality in that region. Consequently, we performed a selective analysis of fMRI signals from voxels in this region to assess this possibility.

For 5 subjects, we used retinotopic maps displayed on cortical surface models to define a separate anatomical ROI within V1 that included the lips of the calcarine fissure but omitted the depths of the sulcus (cf. Figure 15b, red shaded zone). We then compared the polar angle histograms for (1) all of V1 (Fig. 15A1 and B yellow dotted line), (2) for all voxels in the midline ROI (Fig. 15A2), and (3) for a "high-noise" (voxels with at NSR > 0.1) subset of voxels in the midline ROI (Fig. 15A3). To make this comparison, we first used a liberal correlation coefficient threshold (0.25). We wanted to allow voxels in all of V1 that had at least some minimal stimulus-induced activation to be counted in the analysis.

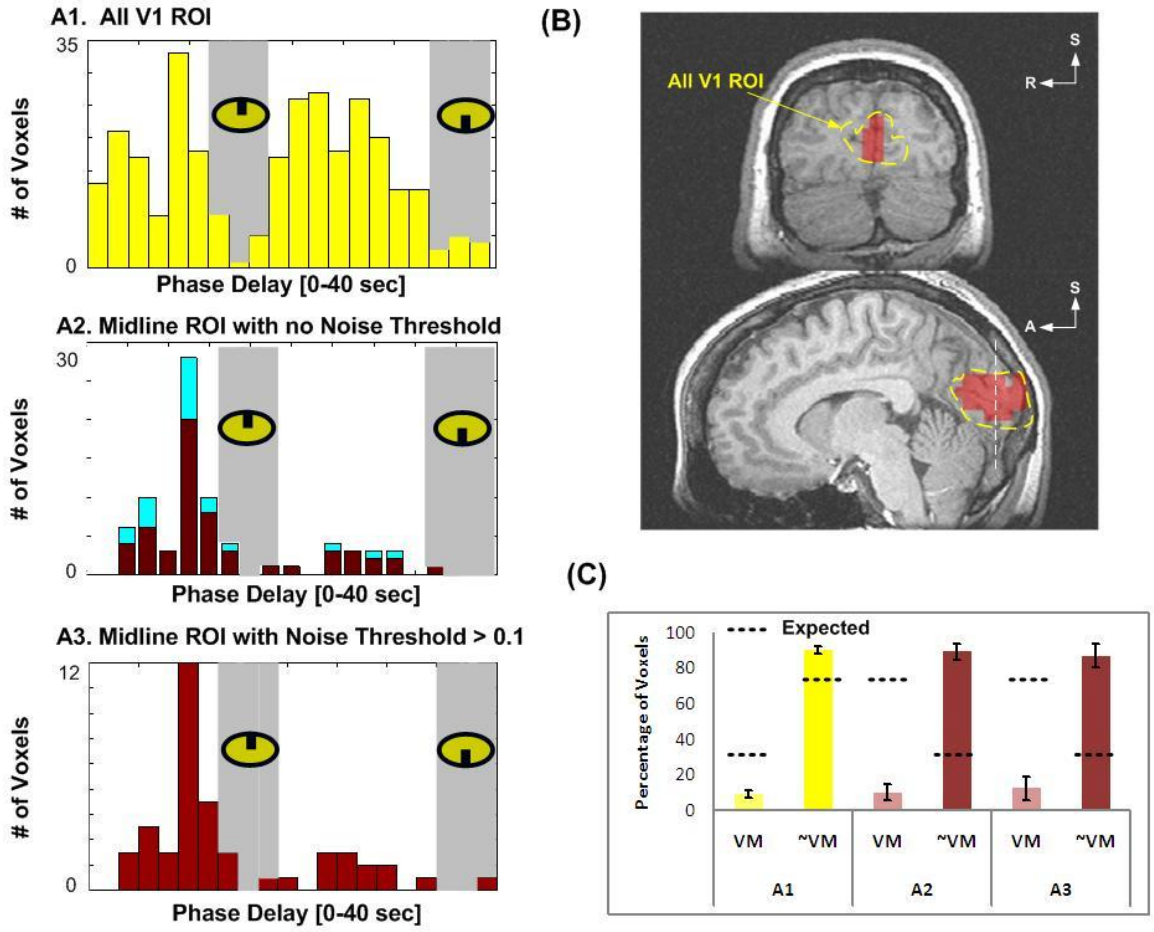

Figure 15: Noise effects in V1. (A1-3) Polar angle voxel histograms of: (1) the entire V1 ROI, (2) Midline ROI with no noise threshold, and (3) Midline ROI with a noise threshold > 0.1. (B) Anatomical representation of the entire V1 ROI (dashed line) and Midline ROI (shaded region). (C) Percentage of voxels for each ROI condition (A1-A3) showing the actual percentage of voxels representing vertical meridian, VM (faded bar), actual percentage of voxels not representing VM (solid bar), and the expected percentage for each of the previous two categories (VM and ~VM, dashed line).

For these voxels, we then calculated the contrast-to-noise ratio (CNR) of the fMRI signals using the power spectrum method of Boynton et al 1999 [98]. To identify voxels that were visually responsive but with relatively high levels of noise, we used a modification of the power spectrum approach to compute an index of the relative noise amplitude, we call Noise to Signal Ratio (NSR):

$$\mathrm{NSR} = \frac{P_{noise}}{P_{\max}}$$

Figure 16 illustrates graphically how the NSR is calculated. The power spectrum of the BOLD signal is analyzed over 100 points. The power spectrum of the noise (P_{noise}) is the average of the shaded red areas on the power spectrum. The fundamental frequency of the stimulus (P_{max}) is represented in the yellow shaded area. The NSR is the ratio of the estimated power of the noise (P_{noise}) to power of the fundamental frequency (P_{max}). Finally, we used this index to select a "high-noise" sub-set of voxels in the midline ROI with NSR > 0.1. (Colors of bar graphs in Figure 15 indicate the corresponding ROI in 15B from which they are computed. The gray shaded bins represent the vertical meridia. Figure 15 shows results for one subject, case APO.)

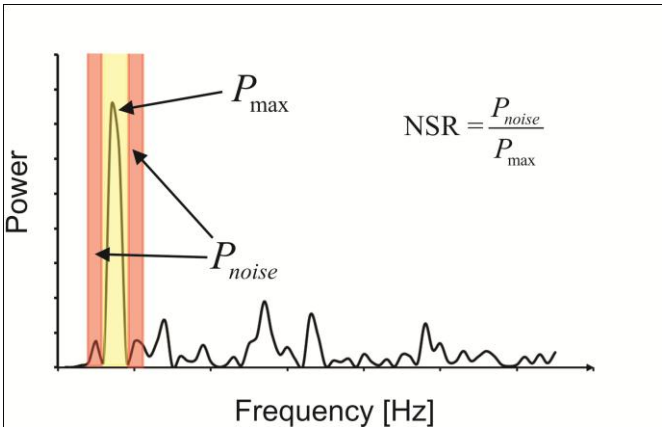

Figure 16: NSR Method. P_{max} is estimated by taking the power spectrum value at the fundamental frequency (shaded yellow) of the stimulus. P_{noise} is estimated by averaging the power spectrum value at the neighboring frequencies surrounding the fundamental frequency.

Figure 15C highlights key differences among the distributions shown in A1-A3 relative to expected values computed from an ideal uniform distribution in which all polar angles are represented equally (dashed lines). Specifically, Figure 15C depicts the percentage of voxels in the vertical meridian (VM, gray) versus non-vertical meridian (~VM, non-gray) bins in each of the distributions of Figure 15A. The expected values (dashed lines) were computed for each distribution (A1-A3) by taking the relative

proportion of the complete V1 ROI represented by the midline ROI and assigning to it the ideal voxel counts for the corresponding number of bins in a uniform distribution. Thus, for the bars labeled A1 in Figure 15C, the expected values represent the proportion of voxels that would have fallen in the 6 bins representing the vertical meridian of a uniform distribution (6 bins out of 20 = 30%). This re-iterates our finding that, for all of V1, there is a relative under-representation of the vertical meridian (with other locations appearing to be correspondingly overrepresented). Additionally however, we see that voxels in the midline ROI do not preferentially represent the vertical meridian (A2), as might have been expected (dashed lines). Moreover, this bias is reflected in the noisiest voxels in the midline ROI (A3) which account for 43 of the total 48 voxels contained in this ROI.

Figure 17, shows the NSR in V1 for the same subject in Figure 15. The occipital pole and lips of the calcarine (V1/V2 boundaries) show the areas of highest noise content in the fMRI BOLD signal (yellow intensity). These areas of higher noise are confirmed by computing the power spectrum (Red box, inset) for the voxels in the corresponding region on the lips of the calcarine (red ROI). The power spectrums of the BOLD signals along the lips of the calcarine are noisy and predominately do not show a dominant spectral peak as expected with a periodic stimulus. The areas along the depths of the calcarine (orange intensity) have lower noise content. Corresponding power spectrums of the fMRI BOLD signals (green box) along the depths of the calcarine (green ROI) confirm that the fMRI BOLD signals are lower in noise compared to the occipital lobe and lips of the calcarine. In fact, the power spectrums in the depth of the calcarine sulcus predominantly show the dominant spectral peak associated with presenting a periodic

visual stimulus. These results suggest that midline voxels in V1 that should preferentially represent the vertical meridian, instead represent other visual field locations far more often than expected, thus potentially accounting for the empirically observed under-representation.

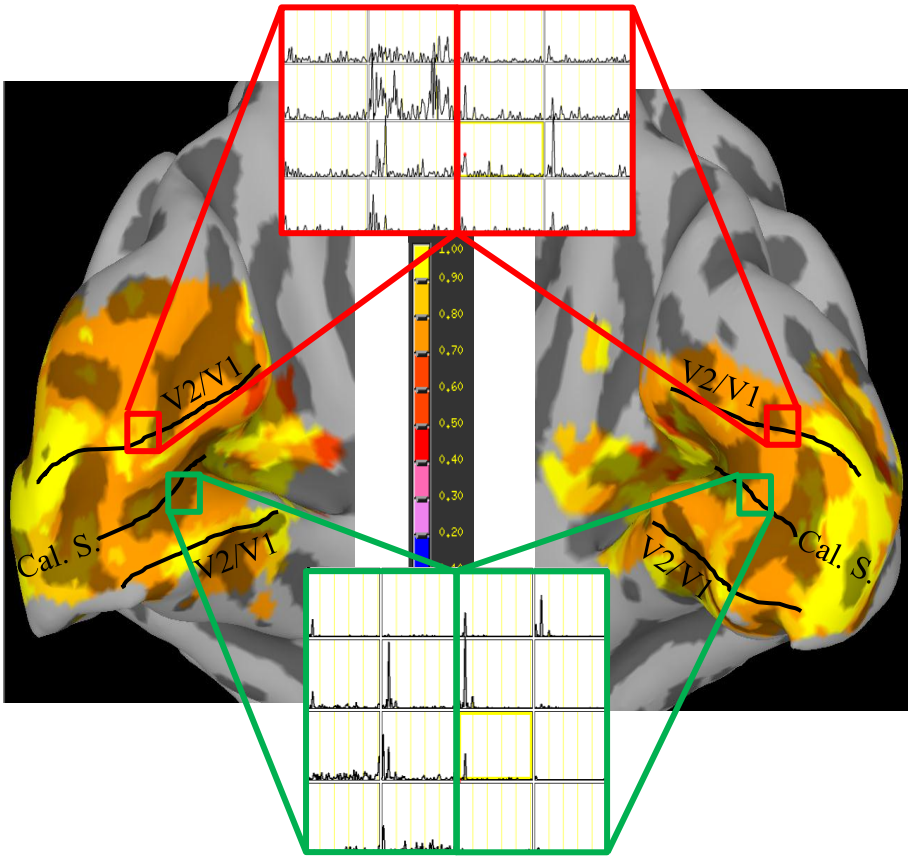

Figure 17: Distribution of Noise in V1. Distribution of noise to signal ratio for a single subject due to the rotating hemi wedge. The color bar in the middle shows the levels of noise to signal. The power spectrum (Red Box) of the fMRI signals along superior V1/V2 boundary in both hemispheres. The power spectrum (Green Box) of the fMRI signals along Calcarine sulcus boundary in both hemispheres.

Expt 3: Gradient Echo vs. Spin Echo. Another possible cause of non-uniformities in the polar angle representation is the pulse sequence by which the fMRI data were collected. It is possible that the BOLD fMRI response is overly sensitive to signals from large blood vessels, or conversely, insensitive to signals from the parenchyma since gradient echo pulse sequences are thought to preferentially reflect signals associated with

larger vessels [82]. This might make the resulting data especially susceptible to hemodynamic-based distortions. To assess this possibility, we used a combined gradient echo / spin echo pulse sequence that acquires both types of images simultaneously. Spin echo images are thought to reflect a more equal contribution from large vessels and parenchyma, so the spin echo sequence should be less likely to show large vessel distortions[82]. Figure 18 shows polar angle histograms for a subsample of 4 subjects. Both the histograms for gradient echo (Fig. 18 - left) and spin echo (Fig 18 - right) show a relative under-representation of the vertical meridian. The peak to trough ratio is approximately 3:1 for spin echo and 3.5:1 for gradient echo. This difference was not statistically significant (t-test, $p>0.05$). Spin-echo EPI yielded significantly fewer activated voxels then gradient echo (mean of 30 vs 175 voxels per bin, t-test, $p<0.001$) consistent with previous reports [5]. But, the shapes of the two histograms were not statistically different on a bin-by-bin basis (chi square, $p>0.05$). Thus, the MRI pulse sequence does not appear to be a contributing factor.

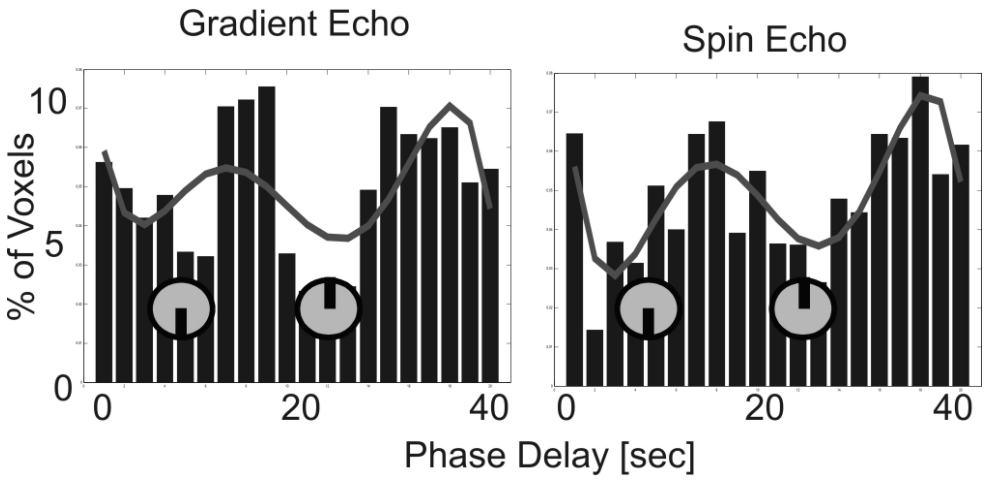

Figure 18: Echo Sequences. Illustrates average phase delay histogram for gradient echo (left) and asymmetric spin echo (right). For most of the subjects, the bimodal characteristic is present in both imaging techniques.

Expt 4: Visual Stimulation Sequence and Contrast. The direction of wedge rotation for polar angle mapping was varied to determine if the non-uniformities in the phase delay distribution might reflect an asymmetric directional facilitation of sequentially activated cortical loci that is interrupted as the activation passes from one hemisphere to the other. The hemifield containing this under-representation would then switch if the direction of stimulus rotation was reversed. To test this possibility, the hemi-wedge stimulus was rotated in counter-clockwise and clockwise directions in separate fMRI scans. Figure 19 compares the mean voxel histograms for a subset of 3 subjects using counterclockwise (CCW) and clockwise (CW) stimulus rotations. Both histograms show under-representations in similar areas with no apparent offset related to direction of rotation. Indeed, the histograms are not significantly different on a bin-by-bin basis (chi square test, $p>0.05$).

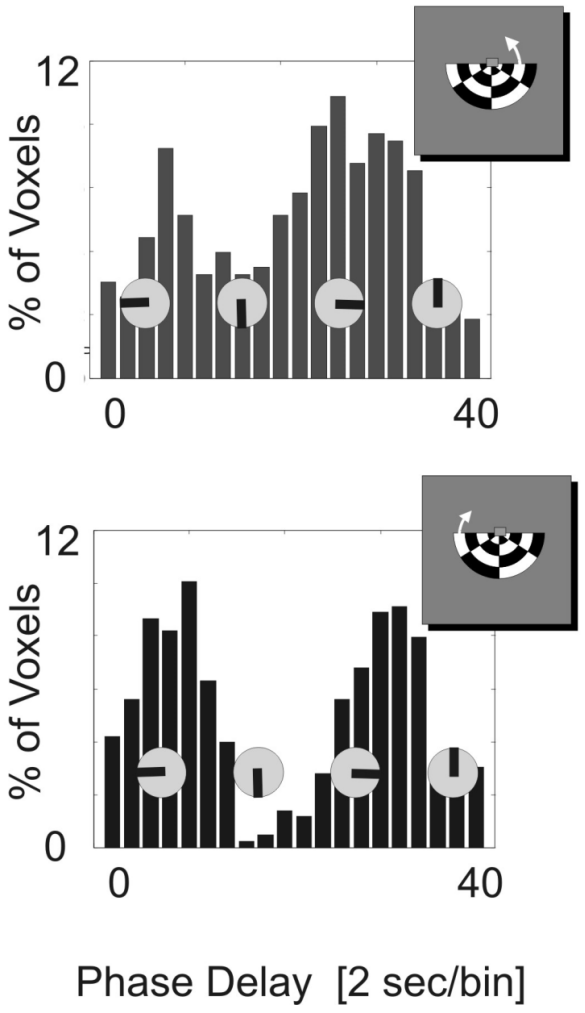

Figure 19: Stimulus rotation. The polar angle voxel distributions for the counter clock-wise rotating hemi-wedge (light) and the clock-wise rotating hemi-wedge (dark).

Another concern was that high stimulus contrast might cause excessively strong BOLD responses with large changes in blood flow, thereby increasing the likelihood of hemodynamic abnormalities distorting the phase delay data. Consequently, we compared polar angle delay histograms for 3 subjects using stimuli with 25% and 99% luminance contrast for the check pattern. Figure 20 shows the average preferred polar angle histograms for the two stimuli. Both histograms are nonuniform and there was no significant difference between the shapes of the two histograms on a bin-by-bin basis (Chi square test, $p>0.05$).

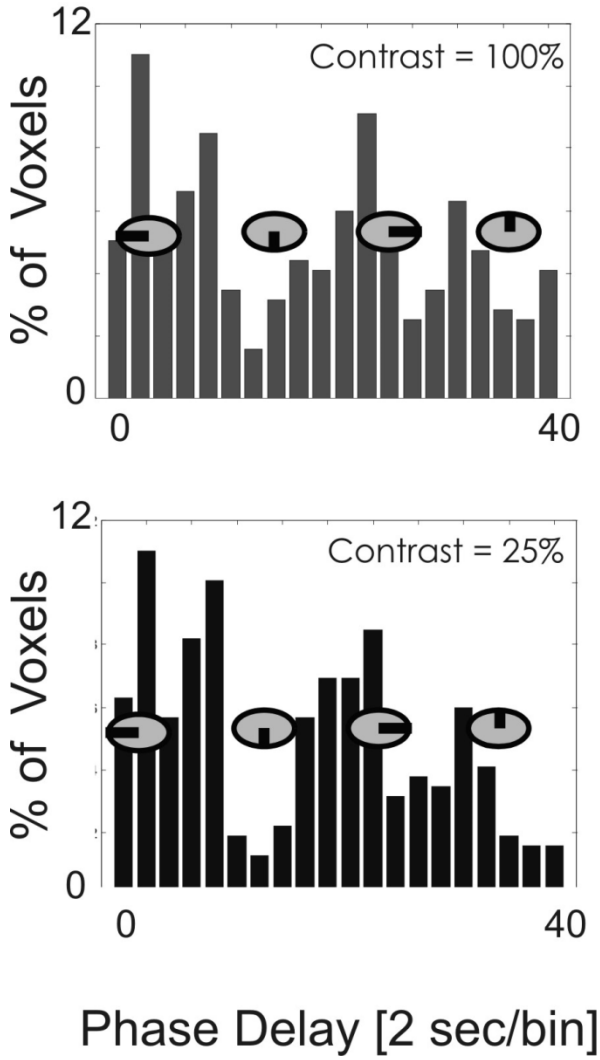

Figure 20: Stimulus Contrast. The distribution of # of voxels versus polar angle was plotted for all activated voxels in V1 and examined for uniformity (Top –100% contrast, Bottom – 25% constrast). For both contrast sensitivities, the distributions were nonuniform and had a bimodal shape with a 3 fold or greater difference from peak to trough.

Expt 5: Stimulus Size and Extent of Cortical Activation. Long-duration, wide-spread, stimulation of one visual hemifield might cause a significant asymmetry in blood flow within, or between, hemispheres. In turn, such a massive lateralized change in blood flow might increase the possibility of a BOLD artifact that is spatially non-uniform in visual cortex and, consequently, within the representation(s) of the visual field. If under-representations in the visual field are related to BOLD artifacts caused by stimulation of

excessive areas of cortex, then these artifacts might be reduced by using a smaller stimulus. To test this hypothesis, we tested 4 subjects with two different wedge sizes 36° and 180° covering 10% and 50% of the visual field respectively. The different stimulus sizes should activate very different areas of V1 visual cortex at any given moment.

We tested 4 subjects with the two stimulus sizes and obtained the average polar angle histograms illustrated in Figure 21. For both stimulus sizes, the histograms were nonuniform with a peak:trough ratio of 3:1. (As mentioned earlier, not all subjects show under-representations for both vertical meridia and this was the case for this subsample of subjects.) There was no significant difference between the shapes of the two histograms on a bin-by-bin basis (Chi square test, $p>0.05$). In sum, we found that stimulus size and associated differences in extent of cortical activation did not account for our observed distortions of the visual field representation.

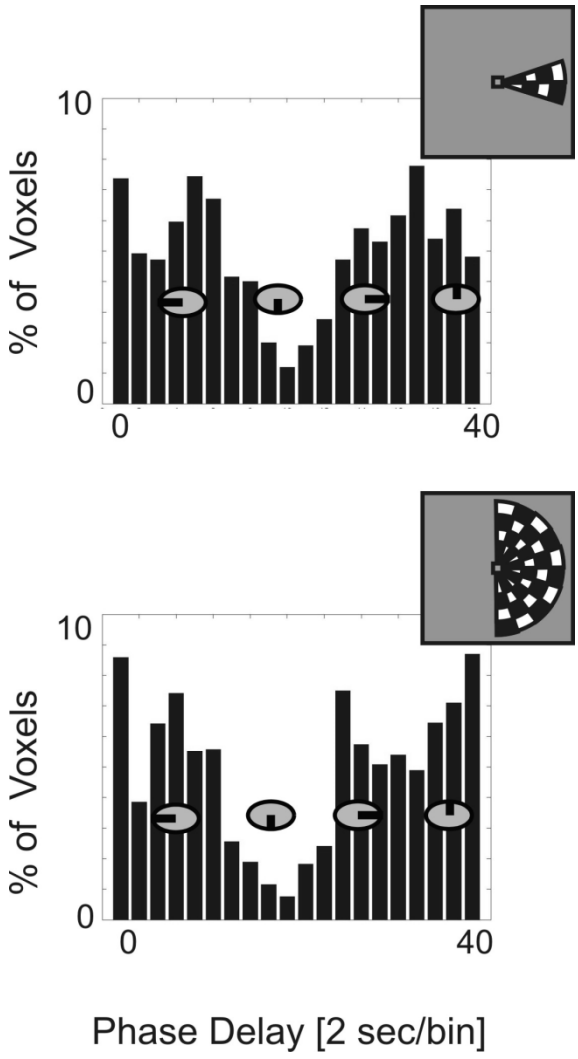

Figure 21: Stimulus Size. The distribution of # of voxels versus polar angle was plotted for all activated voxels in V1 and examined for uniformity (Top – 36° wedge, Bottom – 180° wedge). For both wedge sizes, the distributions were nonuniform and had a bimodal shape with a 3 fold or greater difference from peak to trough. The minimum number of voxels was typically associated with the superior vertical meridian.

Simulation 1: Sampling with large voxels. Using a uniform grid of relatively large voxels to sample fMRI signals along a tortuous surface such as the primary visual cortex might cause unexpected distortions in the apparent representation of the cortical map. Using a simulation created in AFNI/SUMA, we were able to examine the potential sampling distortion of different size voxels. First we constructed a cortical surface model for one of our subjects using Caret software [80]. Each node within primary visual cortex

of the flattened surface model was assigned a simulated fMRI signal approximating a typical sinusoidal response to the temporal phase mapping stimulus. Each sinusoid was assigned one of twenty different temporal phase delays representing the range of possible preferred polar angles. However, each of the 20 phase delayed signals was assigned to an equal number of nodes and hence to roughly equal areas of the flat map in order to simulate an ideal, uniform retinotopic map of preferred polar angle. The flat map was then transformed back to its original folded 3D configuration and sampled using 3 different fMRI voxel grids. We then computed the preferred phase delay for each voxel [7] using the Hilbert delay plugin in AFNI and constructed histograms of preferred polar angle as we had done previously for our empirical data. We ran the simulation using three voxel sizes: 4 mm^3, 3 mm^3, and 2 mm^3 and compared the preferred polar angle histograms with each other and with the empirical data (voxel size 3.75 mm^3 - same data as shown in Figure 15). As illustrated in Figure 22, the voxel histograms for the 3 simulations are effectively uniform and markedly different from the empirical histogram (Chi square test, $p<0.002$ for each simulated data set). (Data for only one hemisphere are show in the figure since the simulation was time consuming and the results are unequivocal.) This simulation indicates that sampling the folded cortical surface with a regularly spaced grid of voxels does not account for the distortions in the visual field representation measured empirically.

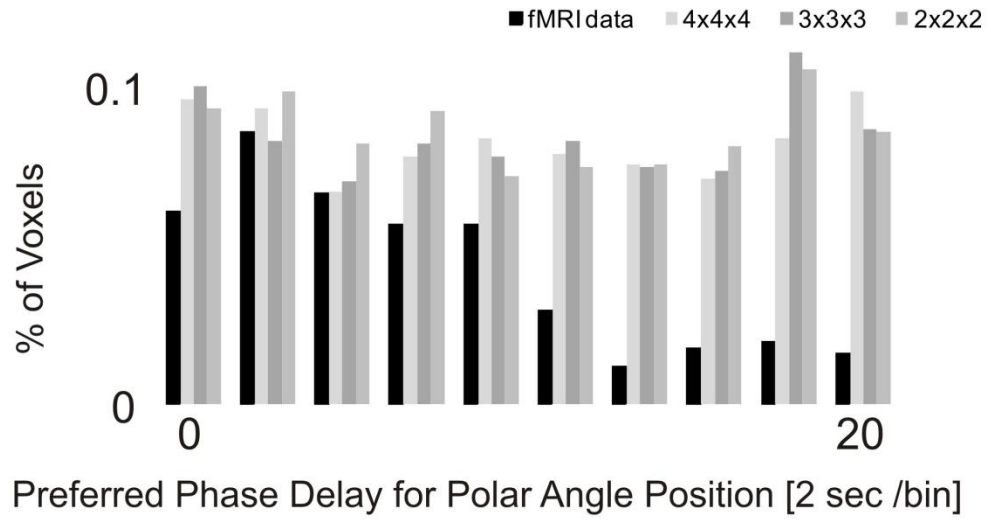

Figure 22: Voxel Size Simulation. Simulation of Grid Sample Sizes versus actual data from Figure 7 single subject (only one hemisphere, half the visual field was simulated).

Simulation 2: Anatomically Specific Noise Effects on Temporal Stimulus. Given that larger veins and draining sinuses are anatomically situated near the midline of the occipital lobe [17, 57, 84], these venous structures could cause a change in the cortical BOLD signals that lie on or near these venous structures. This hypothesis suggests that voxels at the midline (and hence fMRI signals that will represent the vertical meridia) may be adversely affected by noise associated with midline structures. There are two ways that noise can affect a signal and cause distortion. First, the noise can cause the fMRI signal to drop below a statistical threshold. This would eliminate the signal from any type of analysis. Second, the noise could distort the phase information in the fMRI signal. This would cause the fMRI signal to misrepresent the phase information and associated visual field location. To test this, we created a simulation in which we selectively increased the noise associated with the phase delays representing the vertical

meridian. The selective noise was added to a voxel histogram representing twenty (20) phase delays that correspond to polar angle locations of a subject's visual field. 100 simulated fMRI signals were created to represent each phase delay. The noise associated with the specific phase delays representing the vertical meridian was selectively increased to simulate noise associated with midline voxels in the occipital midline. As noise increased and the CNR decreased, troughs appear in the histogram (Figure 23 – left column). To produce the 3:1 difference in peak to trough voxel count observed in the empirical data, the CNR would have to be approximately 0.1 in the troughs and a CNR = 10 dB at the peaks of the voxel histogram (translating to a 1:100 difference in CNR). However, at a CNR = 1 dB we see the beginnings of the troughs at the phase delays that represent the vertical meridia. The right column of Figure 14 shows that starting at a CNR = 1 dB the phase delays not only start to be eliminated by the correlation coefficient threshold but also the voxels start to assign to different phases. The incorrect assignment of phase delay to a voxel is seen in Figure 23 as an increasing peak in specific phase delay bins (right column). This simulation suggests that a predominance of lower CNR values in specific anatomical location may influence the assignment of phase delays in the fMRI signal, and thus distort the voxel histogram representation of polar angle visual space.

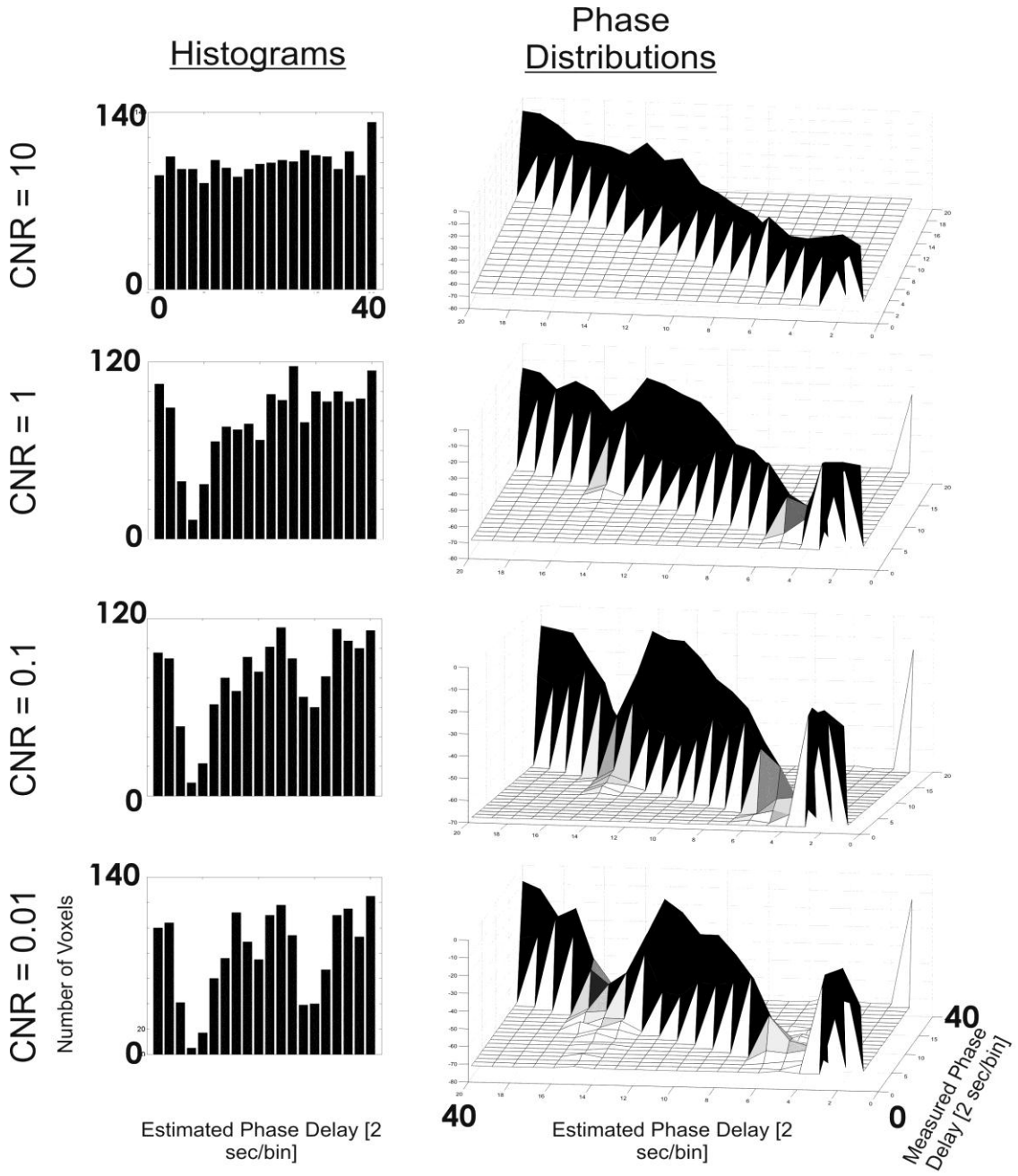

Figure 23: Noise Simulation I. CNR distortion of phase delays that represent preferred polar angle. The CNR decreases for the simulated vertical meridian regions from the top figure to the bottom figure. For each CNR value the left column shows the phase delay histogram and the right column shows the phase distribution illustrating the known phase delay of the simulated signal (y-axis) vs. the estimated phase delay in the presence of noise (x-axis).

Discussion

There can be significant non-uniformities in the cortical representation of the visual field obtained with fMRI-based temporal phase mapping of human primary visual cortex. Though this is not necessarily true for every subject, the majority do exhibit significant under-representations of restricted portions of the visual field typically at, or close to, the vertical meridian. These non-uniformities often appear in the histogram of preferred polar angle as peaks (horizontal meridian representation) and troughs (vertical meridian representation) which, on average, have a 3:1 ratio in number of voxels, respectively. The under-representations are associated with anatomically fixed locations in the cortex typically near the occipital midline where the vertical meridian is usually represented. Indeed a close examination of the polar angle preference of V1 sites near the midline indicated that significantly fewer voxels had a vertical meridian preference than expected given an ideal uniform distribution. Such distortions do not appear to be related to the fMRI pulse sequence, the definition of the V1 region of interest or to stimulus features such as size, contrast or the spatiotemporal order of presentation. Simulations indicated that potential spatial sampling biases due to voxel size and the rectangular fMRI voxel grid also do not account for the empirically observed distortions. In other studies from our lab, we have used checkered stimulus segments that were flashed at fixed locations in a random sequence and obtained similar non-uniform representations of polar angle (See Appendix A: Figure S2). This alternate technique is much less sensitive to the temporal properties of the fMRI signal to encode visual field preference. This further corroborates the findings that our observations are robust with respect to specific stimulation or analysis techniques.

Could our results reflect a true neuronal bias in the human representation of polar angle? This seems unlikely. As outlined in the introduction, there is little evidence for a major non-uniformity in the neuronal retinotopic representation in V1, though a slight over-representation of the vertical meridia might be expected due to the known presence of a thin strip of ipsilateral field representation near the vertical meridian that is associated with callosal connections between the hemispheres [10, 86]. Electrode and 2-DG studies of V1 in non-human primates [1, 2 , 77, 85] do not show major retinotopic non-uniformities of the neuronal representation of the vertical meridian. By homology, this would be expected to be true for humans as well. Functional considerations also argue against a true neuronal bias. If a consistent neural under-representation was the norm, this would be expected to have corresponding sensory effects such as reduced acuity along the vertical meridian. To our knowledge, no such sensory deficits have been reported for healthy human observers [36, 37]. This is also consistent with a study by Boynton et al. [89] in which fMRI-based measurements of cortical magnification (mm of cortex per degree of visual field) revealed significant differences among subjects that correlated with differences in acuity. They did not report any obvious reduction in magnification or acuity associated with the vertical meridian.

It is important to point out that our results could appear to be at odds with several previous fMRI studies of human visual cortex that failed to note major distortions of V1 retinotopy [e.g. 60, 23, 75, 85, 87, 90]. One clue to this potential discrepancy is that for most of these studies the retinotopic data were examined in the form of a cortical surface map to which a topographic grid was “fit” through some optimization procedure either manual or computational. In addition, the retinotopic data themselves often were

"smoothed" to reduce local heterogeneities that were assumed to represent noise or measurement variance. In contrast, our voxel count histograms, cortical representation of the data, and FFMaps (Figs 11 and 12) are computed directly from the retinotopic phase delay data without smoothing and thus may be more sensitive indicators of "holes" and local distortions of the retinotopic map. Also our data may not be as disparate as it might seem. A careful examination of one previous study, Engel et al. [23], does reveal non-uniformities in polar angle data on flat maps (Engel, Figure 7A) that may be consistent with those reported here. Finally, it is important to note that there remains some controversy over the exact nature of the topographic mapping between the visual field and primary visual cortex. Schira et al. [87], argue that there is more "shear" distortion in the retinotopic map than may have been appreciated previously, especially near the vertical meridian. While such shear distortion does not necessarily imply an under-representation of the vertical meridian, the study does highlight the fact that our ability to precisely measure and quantify the human retinotopic map is still evolving and that important details can be overlooked. Thus, our results may not necessarily contradict previous studies. Rather, our explicit focus on the completeness and uniformity of the cortical map may have allowed us to highlight the fMRI distortions more dramatically and precisely than previous studies.

A Vascular Explanation: The battery of tests described in this study effectively eliminated many potential methodological artifacts that might have accounted for our results and we have argued above that our results are unlikely to reflect a true neuronal effect. One explanation that we have not been able to reject, however, is that the observed distortions of the cortical maps arise from anatomically fixed vascular elements, such as

the mid-sagittal sinus and its associated draining veins. These structures may have hemodynamic properties that differ from those of blood vessels in other areas of the brain [42, 57].

Winawer et al [65] reported shifts in B_o field in tissue that caused distortions in fMRI data for visual stimulus exciting V4h along the transverse sinuses. The transverse sinuses run along the inferior portion of the occipital pole and portions of V1, which may induce some of the distortions that have been reported here but not all of the distortions. So, it is plausible that the draining veins could alter the temporal properties of BOLD signals in certain physiological locations. These effects may include the introduction of excessive noise or changes in the speed/latency of the BOLD response. For V1 and V2, the retinotopic representation of the vertical meridian tends to be located along the medial lips of the calcarine sulcus and thus the sagittal sinus. According to Winawer et al, the sagittal sinus has less distortion of the B_o field than areas such as the transverse sinus. Tissue in the medial lips of the calcarine still could be preferentially affected by midline vascular structures thereby causing a locally restricted degradation or delay of BOLD responses.

We propose that the potential effects of midline vasculature structures on the BOLD response may be adding a systematic and/or random delay to the conventional hemodynamic delay of the undistorted, phase mapped, fMRI signal (Equation 1).

$$\theta_{measured} = \theta_{stimulus} + \theta_{hemodynamic} + \theta_{systematic} + \theta_{random}$$

Equation 1: Factors potentially contributing to measured temporal phase of BOLD fMRI signals.

Normally, the measured temporal phase delay, $\theta_{measured}$, is composed of the delay due to the timing of the visual stimulus, $\theta_{stimulus}$, plus a delay due to the BOLD hemodynamic

mechanism, $\theta_{hemodynamic}$. This latter component is relatively constant across voxels and is taken into account during analysis of the temporal phase mapping data [76, 78].

However, we propose that for voxels near the occipital midline, the mid-sagittal sinus or associated large veins may introduce an additional systematic delay, $\theta_{systematic}$, and/or a random component, θ_{random}. The random shift would arise from noise added to the BOLD signal. However, noise also would reduce the quality of response and, if large enough, would cause a voxel to fall below the threshold for acceptance, thus dropping out of any subsequent analysis. Both systematic and random changes in the measured delay would shift the apparent preferred polar angle away from its true value, thereby leading to an apparent under-representation of the true polar angle preference. Voxels inside the calcarine sulcus that are farther from the midline would be less affected, so that their phase delays would encode the correct polar angle preference.

In this respect, it is important to point out that the analysis of temporal phase mapping data typically incorporates an implicit "winner-take-all" effect in that each voxel is assigned a single, unique temporal phase associated with the stimulus location that produced the best activation. However, a given voxel may actually respond well to a range of stimulus locations. Indeed, as pointed out by Dumoulin et al. [88] a voxel's complete response is determined by the convolution of the stimulus sequence with the voxel's population receptive field (the area of the visual field to which the voxel is responsive). Consequently, a relatively minor distortion of the BOLD response could

shift the preferred retinotopic locus over a significant range of stimulus locations, especially if the BOLD signal is relatively noisy for the reasons proposed above[1].

Conclusions

If fMRI brain mapping is to be used clinically to guide tumor surgery or other invasive treatments, then it is essential to understand its ability to accurately and completely represent the underlying neuronal signals. Errors in this respect could compromise the physician's ability to maximize treatment success while minimizing neurological side effects. For academic neuroscience, errors in fMRI brain maps may have less severe consequences, but still could lead to inaccurate conclusions about brain function and theory. Here we have used the retinotopic organization of human visual cortex as a model system for assessing the accuracy of fMRI-based brain mapping by documenting distortions and identifying their likely cause. While it has long been appreciated that BOLD fMRI signals could be distorted by so called "draining vein" effects [42, 57], it has not always been apparent exactly how these effects might play out with respect to any particular brain map. A critical, but rarely addressed issue in this respect is whether fMRI-based maps are "functionally complete" in the sense of containing a reasonably equivalent representation of all neurons that contribute to the underlying neuronal map, albeit not individually. The answer is "no", at least for cortical areas in the vicinity of midline vascular structures such as the mid-sagittal sinus and its

[1] Dumoulin et al, [35] point out that the preferred retinotopic locus assigned to a particular voxel can be improperly computed if the size (and shape) of the population receptive field is not modeled accurately. Though true in general, the error is minor for small pRF's as found in V1, and is more significant for eccentricity mapping with rings than for polar angle mapping with rotating wedges. This is another reason for our focus in this paper on the polar angle representation in human V1 for which these factors are insignificant.

draining veins [65]. While this has been demonstrated here for visual cortex, it is likely to be true for other midline systems such as sensorimotor cortex, parietal areas involved in attention and midline frontal areas associated with executive functions. Whether non-midline vasculature structures can exert similar influences is unclear but should be considered when interpreting BOLD-based mapping data. FMRI techniques that are less dependent on the temporal precision of BOLD signals may be less susceptible to these distortions but are unlikely to be completely immune unless based on some alternate non-vascular mechanism.

Aim II: Determine if random stimulus presentation eliminates non-neuronal biasing effects in the polar angle voxel distribution as compared to temporal phase mapping

Introduction

Blood oxygenation level dependent (BOLD) functional magnetic resonance imaging (fMRI) has been used extensively for mapping the representation of the visual field within the human brain [6, 23, 71]. Visual field mapping using fMRI has been used clinically to assess patients with cortical or sub-cortical pathology and to plan surgical treatment impacting the visual system. For use as a clinical tool, the accuracy of fMRI-based visual field mapping methods needs to be better understood. This accuracy can be particularly important for presurgical mapping of brain function near a tumor resection site since inaccurate rendition of the underlying neural function could potentially lead to inappropriate resection of viable brain tissue. As shown previously (Aim 1), the most widely used method for visual field mapping, temporal phase mapping, is susceptible to hemodynamic distortions that lead to missassignment of visual field locations in the functional field maps (FFMaps). These missassignments are commonly seen as virtual holes in the FFMaps. Further analysis of the visual field mapping data indicates that the frequency distribution of voxels representing different angular position within the visual field is markedly non-uniform, with under-representations of locations near the vertical meridia in V1 being most common. These results are also consistent with data reported in other published studies [92]. In this study, we explore an alternate visual field mapping

method using a random rather than sequential stimulus presentation sequence. This alternative mapping method can reduce spatial inaccuracies induced by hemodynamic distortions on or near the primary visual cortex [5, 66].

In previous experiments using fMRI retinotopy and temporal phase mapping, we have shown that the number of voxels responding to equivalent regions of visual space is not uniform [5]. Based on previous animal studies where retinotopy has been performed using 2-DG [8], we expect that the number of voxels responding to equally sized and distributed regions of visual space will be uniform throughout the visual cortex. We have evidence to suggest that the source of the non-uniform distribution of voxels is hemodynamic in nature and lies along the midline of the occipital lobe, at or near the cortical representation of the vertical meridian.

Based on voxel time series simulations and empirical evidence of the effects of the major sinuses that lie near the occipital midline [5], it has been shown that fMRI time series along the occipital midline have lower contrast-to-noise ratios relative to more lateral aspects of the primary visual cortex (Aim 1). A high concentration of veins rests along the occipital midline contributing to the high noise content of the local fMRI signals [66, 103]. From this physiological phenomenon, two possible factors affect the response of the voxel to sequentially presented stimulus locations. First, in the cortical regions of high noise (i.e. hemodynamic noise), the sequentially presented stimulus locations, distinguished by phase only, have a high probability of being assigned to other visual field locations [5]. Previous simulations have shown that the probability of detecting the correct sequentially presented stimulus location decreases significantly as the noise content increases [5]. Second, the level of noise present along the occipital

midline can also lower the statistical correlation coefficient of an active voxel below the statistical threshold set for validly active voxels.

Given a sequentially independent set of input stimulus functions, poor signal to noise contrast in the fMRI time series could be less significant in mapping the polar angle visual field location to a voxel location in the brain. Moreover, the probability of detecting multiple stimulus locations in a single voxel is increased due to the reduced linear correlation between the input stimulus functions. To reduce the error in assigning a voxel to a specific location of visual space that may stem from the linear correlation of the stimulus sequences used in temporal phase retinotopic mapping, we have examined the use of a more randomized presentation of stimuli in the visual field when performing retinotopic mapping. In using this random presentation of stimuli, wedges of visual field vary randomly in polar angle over time.

Using a more randomized presentation of visual stimuli; we sought to eliminate systemic distortions due to the temporally correlated nature of the input stimuli produced in temporal phase mapping. Previous work has been done on using psuedo-random sequences to elicit fMRI responses in the visual cortex [68, 102]. Gallant et al. used polar angle sectors displayed in a psuedo-random sequence to examine the spatial linearity in the BOLD response in V1 [92]. Linearity of the fMRI response by spatial summation of visual sectors was assessed directly by comparing responses to wedges and rings with sums of responses to sub-component sectors [92]. Others have previously investigated using pseudo-random sequence approaches to visual field mapping [68, 102]. These studies did not focus on the accuracy of mapping the visual field or producing functional field maps for the analysis of a subject's visual field [68, 102].

In this study, we investigate whether a code-based (random stimulus) mapping technique is more accurate than temporal phase mapping in identifying those stimulus locations that activate each voxel in the primary visual cortex, V1, of human subjects. We hypothesize that the random code-based technique will be less susceptible to hemodynamic distortions and will be less susceptible to errors as fMRI signal quality degrades. We further hypothesize that the code-based technique can determine if single voxels are activated by multiple stimulus locations. If true, we predict that the frequency distribution of voxels responding to different angular locations within the visual field will be uniform.

Experimental Methods

Subjects

Data were collected from ten subjects (21-36 years old, 4 female) with no history of neurological or visual deficits. Subjects read and signed a detailed consent form describing the experimental procedures in accordance with the human subject Institutional Review Boards at the Medical College of Wisconsin and Marquette University. Prior to data collection in the MRI environment, subjects were trained in a mock MR scanner to position their head in a model of the gradient head coil, adjust the optical system to allow optimal viewing of the video images, and perform the visual task while constantly fixating on a central fixation marker.

Visual Stimulus

High-quality visual stimulation was achieved using an Avotec optical system (Avotec Inc., Stuart, FL) designed to project images directly onto the retina of subjects, thereby providing a high-luminance, 16-20° (diameter) field of view, and minimizing the effects of changes in pupillary size. Custom computer graphical images were generated using a Cambridge Research Systems (Cambridge Research Systems, Rochester, Kent, UK) VSG 2/3 video card and displayed via the Avotec optical system.

Retinotopic Mapping Methods

Temporal Phase Mapping

For temporal phase mapping [81], the visual stimulus consists of a single black and white checkered, 8 Hz flickering, wedge of 180° that is slowly rotated (18° every 2 seconds) counter clockwise throughout the 360° of visual field over a period of 40 seconds. The rotation is repeated 5 times, so that any wedge of the visual field can be presented by an activation sequence that alternates between OFF and ON every 20 seconds (50% duty cycle). Subjects were asked to fixate on a green marker (<1 degree dia.) located in the center of the visual stimulus. The activated voxels were detected using the Hilbert Delay plugin of the AFNI analysis package [30] to estimate the phase delay relative to a sinusoidal reference waveform [78, 76]. The input sequences for temporal phase mapping are identical across all wedges of the visual field, except for a time delay between ON and OFF periods between neighboring regions (Figure 24A). Therefore,

assigning a voxel to a specific location (visual polar angle sector) of the visual field simply translates to finding the estimated delay between the fMRI response to an input sequence and a reference waveform. To determine whether a voxel is significantly activated ($p < 0.05$) using the Hilbert Delay plugin, a minimum threshold value of 0.35 (correlation coefficient, $p < 0.05$) is used. A number of techniques have been previously reported for determining the maximum correlation value [, 76, 81].

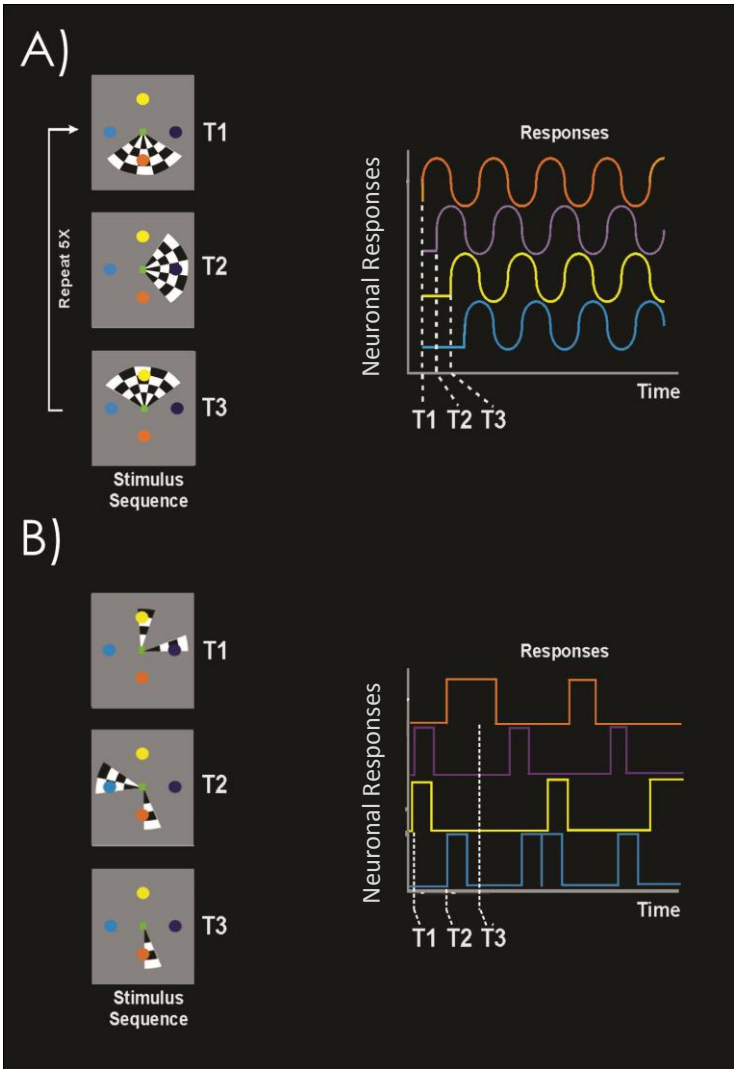

Figure 24: Retinotopic mapping methods for fMRI visual field mapping. (A) Temporal phase mapping of polar angle visual field locations moving in a sequential fashion counter clockwise. (B) Code-based mapping of the polar angle visual field location which is in a random presentation mode.

Code-Based Mapping

The term “code-based” is derived from information theory [93] and refers to a protocol in which different sources (e.g. stimulus locations) are represented by unique binary sequences (codes) when transmitted through a noisy channel. In the code-based retinotopic mapping experiments, the stimulus consisted of twenty distinct, 18° non-overlapping, 8Hz flickering black and white checkered wedges that together covered the entire visual field (Figure 24B). Each wedge was randomly presented in five distinct 10-second epochs, with each epoch randomly distributed within the 240 second scan run. The on-off (or activation) sequence for a particular wedge was uncorrelated with the activation time sequences of any of the other wedge presentations. On average, at any given moment, 50% of the visual field was stimulated by a combination of wedges. All subjects were asked to fixate on a green fixation point located in the center of the visual stimulus, thereby establishing a fixed center point for the code base mapping.

In a defined set of visual field sectors, we can define a fixed sector of visual space, G. We can further identify G in time with a binary sequence representing visual presentations of G. If we let one (1) represent the time that G is displayed (in our example G is a wedge) and zero (0) represent the time that G is not displayed (ie. no wedge), then each G_i where i is a unique sector number, can be identified with a binary sequence through time. In order for each G_i to be uniquely identifiable with respect to time, each binary sequence must be uncorrelated to all other sequences, and preferably orthogonal with respect to all binary sequences in the set. Each unique sequence can then be used to identify which voxels of the visual cortex are associated with a specific region of visual

space. When each unique sequence, Σ_i, is detected via the fMRI signal; Σ_i is convolved with a hemodynamic response function (HRF), typically estimated as a gamma variate function [95]. This convolution with the HRF distorts the orthogonality of the set of input sequences. However, each G_i in the code-based mapping method is less correlated to all other G_j (where $i \neq j$). In temporal phase mapping, each voxel in the code-based method has a greater probability to uniquely respond to G_i. Figure 25 shows the correlation matrices for the input sequences of the code-based (left) and temporal phase mapping methods (right), where the x and y axes represent the input sequences (1-20 input sequences) and the color represents the Pearson's correlation coefficient, +1 (hot, red) and -1 (cool, blue). Below each correlation matrix is the distribution of correlation coefficients, where the y-axis is the number of counts for each correlation coefficient bin and the x-axis is the correlation coefficient range, +1 to -1, broken down into ten bins. The main mode for the code-based correlation matrix is a correlation coefficient of 0.1 and +/- 1 for the temporal phase method. Therefore, the code-based stimuli are not systematically correlated with each other whereas temporal phase stimuli are highly correlated with each other.

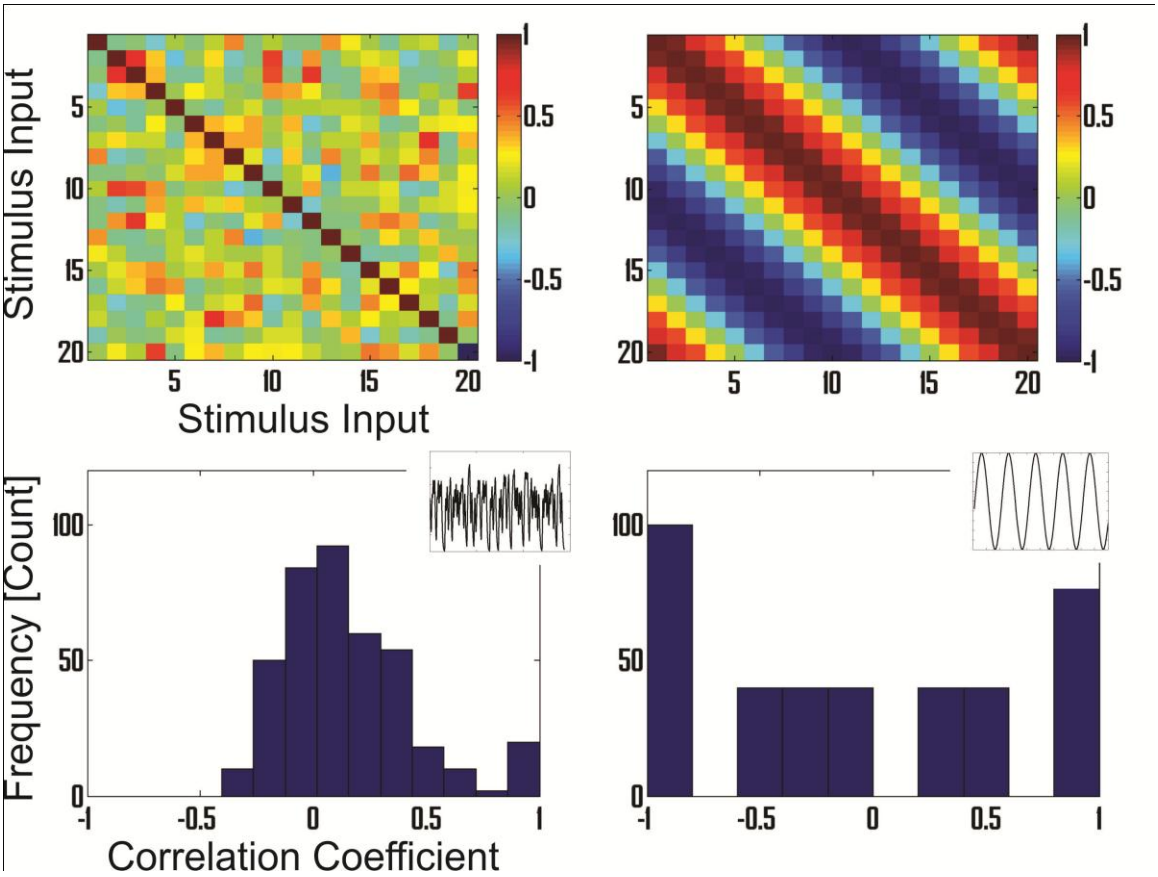

Figure 25: Input Stimuli Comparison. The correlation matrices (top) for the input stimulus sequences for the code-base (left) and temporal phase (right) mapping techniques. The distribution of the correlation coefficients (bottom) between the input stimulus sequences for the code-based (left) and temporal phase (right) mapping techniques.

Mathematically, multiple linear regression analysis is used to detect active voxels and, for each voxel, to identify which stimulus locations evoke a statistically reliable response. The code-based analysis contains four steps (Figure 26). For the code-based method, we assume that the twenty input excitation sequences are binary and uncorrelated to each other. The following steps explain the code-based retinotopic analysis [94]:

(1) *Creation of the Modeled fMRI responses.* A gamma variate function, which represents the hemodynamic impulse response (H(t)), is convolved with the input excitation sequence to yield the "modeled" response for a voxel responding to the input

excitation sequence. After the convolution, fMRI noise, approximated with the pink noise spectrum, was added to the modeled response.

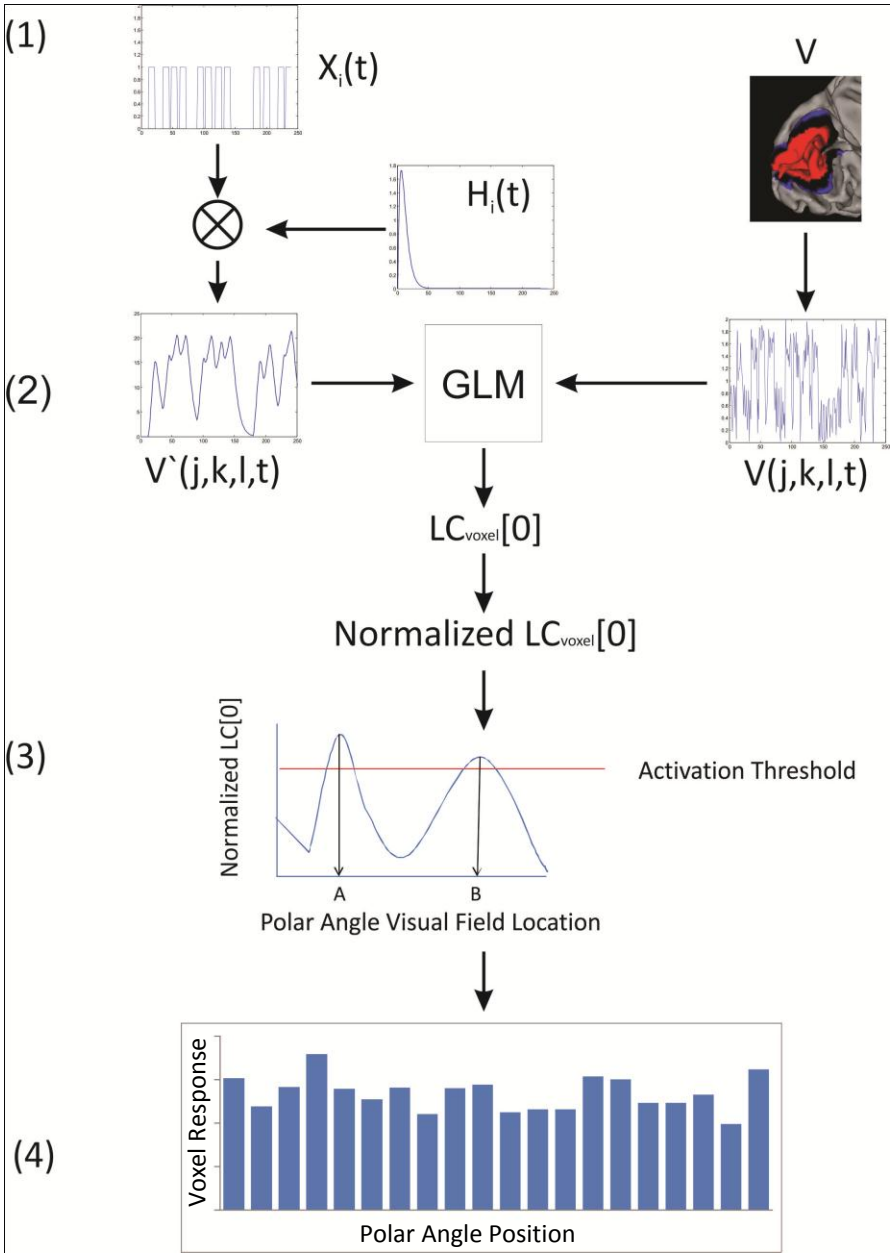

Figure 26: Code-based Mapping Signal Detection. Graphical representation of the signal detection method and histogram generation of the code-based mapping method.

(2) *Computation of the General Linear Model (GLM) coefficients for each input stimulus per voxel.* For each input stimulus the GLM coefficient was calculated. This

was accomplished by first defining a null hypothesis that includes the twenty stimulus locations as linear constraints on the model parameters.

$$Ho: C\beta = 0 \qquad (1)$$

Where C is an 20 X B matrix, B is the total number of parameters in the full model (20 polar angle locations + noise + constant + linear trend). The least squares estimate for β that satisfies the linear constraints for the model is given by:

$$b_R = b_F - (X^tX)^{-1}C^t(C(X^tX)^{-1}C^t)^{-1}Cb_F \quad (2)$$

Where b_F = the least squares estimate of β under the full model, b_R = the least squares estimate of β under the reduced model, and X is the input matrix. The error sum of squares for this reduced model is given by:

$$SSE(R) = (Z - Xb_R)^t(Z - Xb_R) \qquad (3)$$

Where Z is the model of the measured fMRI response to the presented stimulus. The test statistic for each general linear test is defined as the F-test:

$$F^* = \frac{\frac{SSE(X) - SSE(F)}{df_B - df_F}}{\frac{SSE(F)}{df_F}} \qquad (4)$$

Where $df_X - df_F = s$. Now *20 X B* can be written in terms of C. We can estimate Cβ by:

$$C\ b_F = \begin{pmatrix} C_1^t b_F \\ C_2^t b_F \\ \vdots \\ C_{20}^t b_F \end{pmatrix} = \begin{pmatrix} LC[0]_1 \\ LC[0]_2 \\ \vdots \\ LC[0]_{20} \end{pmatrix} \qquad (5)$$

Where $LC[0]_1$, $LC[0]_2$ … $LC[0]_{20}$ are the twenty linear combinations of the vector b_F specified by the GLM.

Repeat steps (1) and (2) for every modeled input signal (in this case, twenty inputs), this will produce a vector (LC[0]) of linear coefficient values, $LC[0]_i$, showing the strength of the fit of each modeled input signal to the voxel's actual fMRI response.

(3) *Stimulus selectivity tuning curve for each voxel*. To assign the visual field location(s) to a voxel using the $LC[0]_i$, a Z-score is estimated by the following:

$$\hat{L}_{voxel} = \frac{L_i - \mu_L}{\sigma_L} \quad (4)$$

where, $LC[0]_i$ is the linear coefficient for a voxel when modeled by a specific input signal, x_i, μ_L is the average linear coefficient for all voxels across all inputs, and σ_L is the standard deviation of linear coefficients for all voxels across all inputs. All statistically valid $\hat{L}_{voxel}$ scores ($p<0.05$) for input signals are assigned to a voxel. In the assignment to the visual field, each voxel can now have multiple visual field locations to which each voxel responds.

(4) Histogram of responses to all stimulus locations. We wish to summarize the response of all voxels to the different stimulus locations while allowing that each voxel may respond to more than one location. Consequently, each voxel's response tuning curve is normalized so that the sum of its significant responses to each stimulus location is unity. For example, if a voxel has statistically significant responses to two stimulus locations, then its normalized response to each location is 0.5. We then sum the normalized responses of all voxels to each stimulus location to produce a composite histogram (Fig 26, panel 4). This approach also has the advantage that it permits a direct comparison of the histograms for code-based and temporal phase mapping, since the latter typically employs a winner-take-all computation that assigns each voxel's response to a single (best) stimulus location.

Code-based vs. temporal-phase based mapping

If the code-based approach is to be accepted as a valid method for mapping of visual fields with quantitative certainty, we need know how the two mapping methods addressed in this paper compare to each other. The following are a series of comparisons that will allow us to determine if the code-based mapping technique is at least as accurate as temporal phase mapping with respect to assigning visual field stimulus locations.

- Assess the physiological organization of the retinotopic mapping techniques. Do the mapping techniques produce similar representations of retinotopy in the primary visual area, V1?
- Assess the mapping techniques ability to produce the known polar angle visual field representation as stated by different subjects and known neurophysiology in research literature [21, 73, 92]. Statistically comparing the voxel distributions between the mapping methods to determine irregularities in voxel responses for the polar angle visual field representation. Further assess the performance of the mapping techniques by statistically compare the voxel-by-voxel stimulus location assignment given the full signal detection capability of each mapping technique.
- Assess the performance of highly correlated input sequences versus highly uncorrelated input sequences in the presence of noise. More specifically, use simulations to compare the effects of noise on the ability of the mapping techniques to properly detect the correct stimulus location.

Results

Code-based and temporal-phase based paradigms were both used to map the occipital visual cortex in 10 subjects. As described below, the results of the two methods were then compared in several ways designed to quantify the sensitivity of the methods to the presence of hemodynamic noise in the fMRI measurement in voxels residing in V1.

Retinotopic Maps of Occipital Visual Cortex. Qualitative comparison of the code-based and temporal phase techniques is illustrated in Figure 27, which shows the retinotopic organization of the medial occipital lobe as displayed on a smoothed representation of the cortical surface. Use of a surface model permits better appreciation of the functional retinotopic organization without the complications introduced by the 3-dimensional folding of the cortical sheet. Figures 27A and B show results from the code-based and temporal-phase based mapping respectively. Before mapping onto the cortical surface model, each voxel was colored according to the single visual field location (polar angle 18° wedge) that produced the highest normalized linear coefficient ($\hat{L}$, equation 4) for the code-based mapping and the delay value for temporal phase mapping. The color coding of preferred stimulus location is depicted by the small inset of Figure 27A. The progression of colors is seen to extend from the lower vertical meridian (purple colors in upper right cortex) down through the depths of the right calcarine sulcus (blue-green colors) to the superior vertical meridian (green) across to the upper vertical meridian in the left hemisphere. It then continues dorsally into the left calcarine sulcus (oranges) and ending at the inferior vertical meridian representation in the upper left cortex (magentas/purples). In other words, the left visual field is represented in the right

hemisphere of V1 and the right visual field is represented in the left hemisphere of V1. Likewise, the superior vertical meridian is represented in ventral V1 while the inferior vertical meridian is represented dorsally. Moreover, there appears to be qualitative agreement between the two mapping techniques though with some differences in local details.

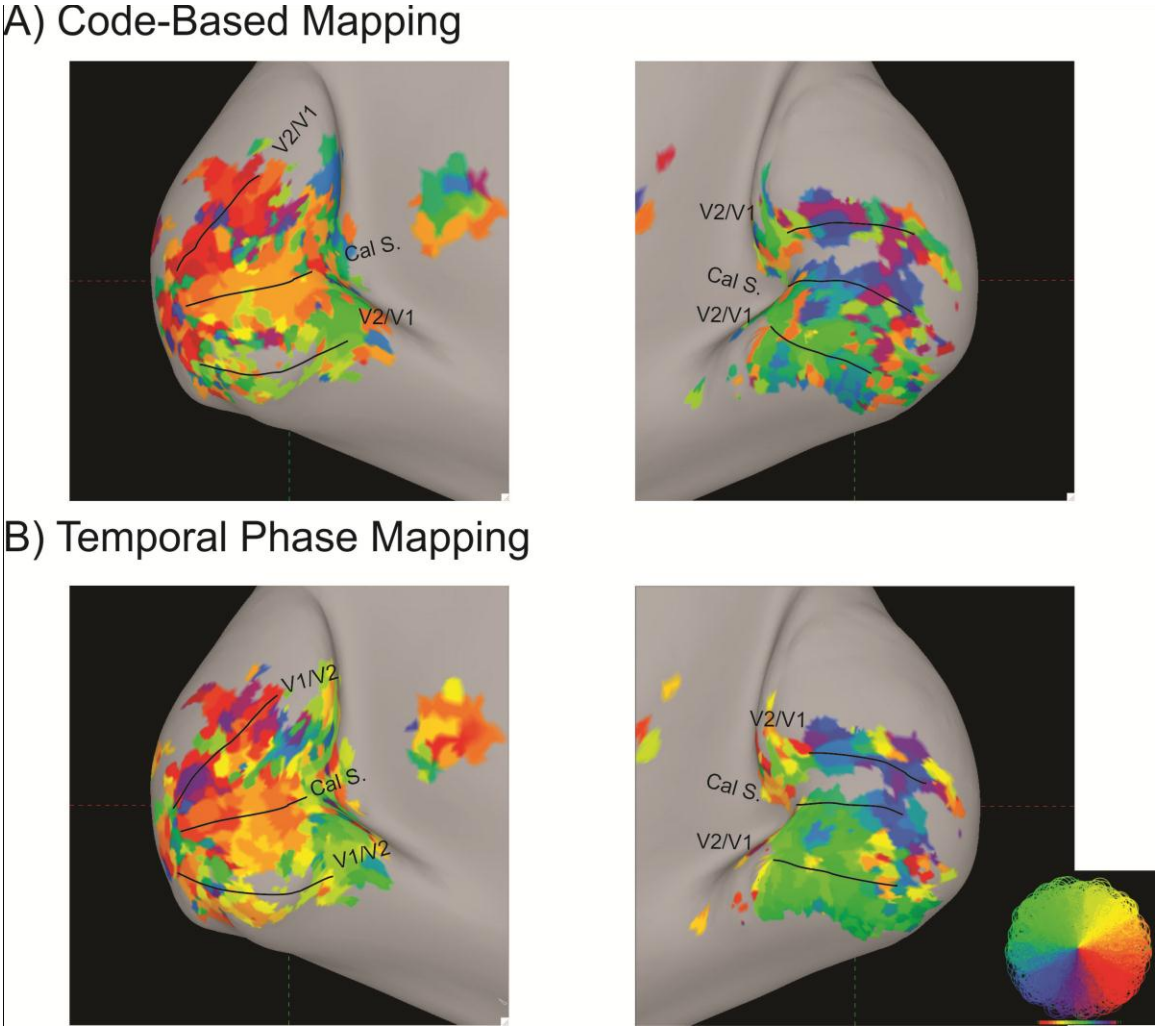

Figure 27: Polar Angle Maps. (A) The "best-fit" polar angle location for the random presentation of wedges as detected by code-based mapping technique. (B) The polar angle location for the rotating wedge stimulus as detected by temporal phase mapping.

Individual voxel tuning curves. The foregoing analysis assigned a single preferred stimulus location to each voxel. However, as mentioned above, the code-based technique

can determine if individual voxels are responsive to multiple stimulus locations. To highlight this aspect of the data, Figure 28A color codes the cortical map of one subject to voxels that respond to any number of wedge stimuli (1 through 20 wedges). The colors that code for a voxel that responds to greater than 5 wedges lie primarily on the lips of the calcarine sulcus and on the pole of the occipital lobe. Figure 28C shows two examples of voxel tuning curves from the data generated in the V1 ROI. The voxel tuning curves show the normalized GLM coefficients (y-axis) for each polar angle location in the visual field (x-axis). For a given voxel, a stimulus location is considered valid if the GLM coefficient is greater than 3.0 (regression analysis, $p< 0.05$). The majority of voxels respond to more than one stimulus location. The voxels that respond to only one stimulus location tend to reside on the occipital pole and the most distal portion of V1 with respect to the calcarine sulcus. Figure 28B illustrates the frequency distribution of voxels for one subject responding to one or more stimulus locations in the V1 ROI. The V1 ROI was determined by the V1/V2 boundaries created by the temporal phase mapping. Over 70% of voxels respond to five stimulus locations or fewer and over 95% of the voxels respond to fewer than 10 stimulus locations (i.e. half of the visual field).

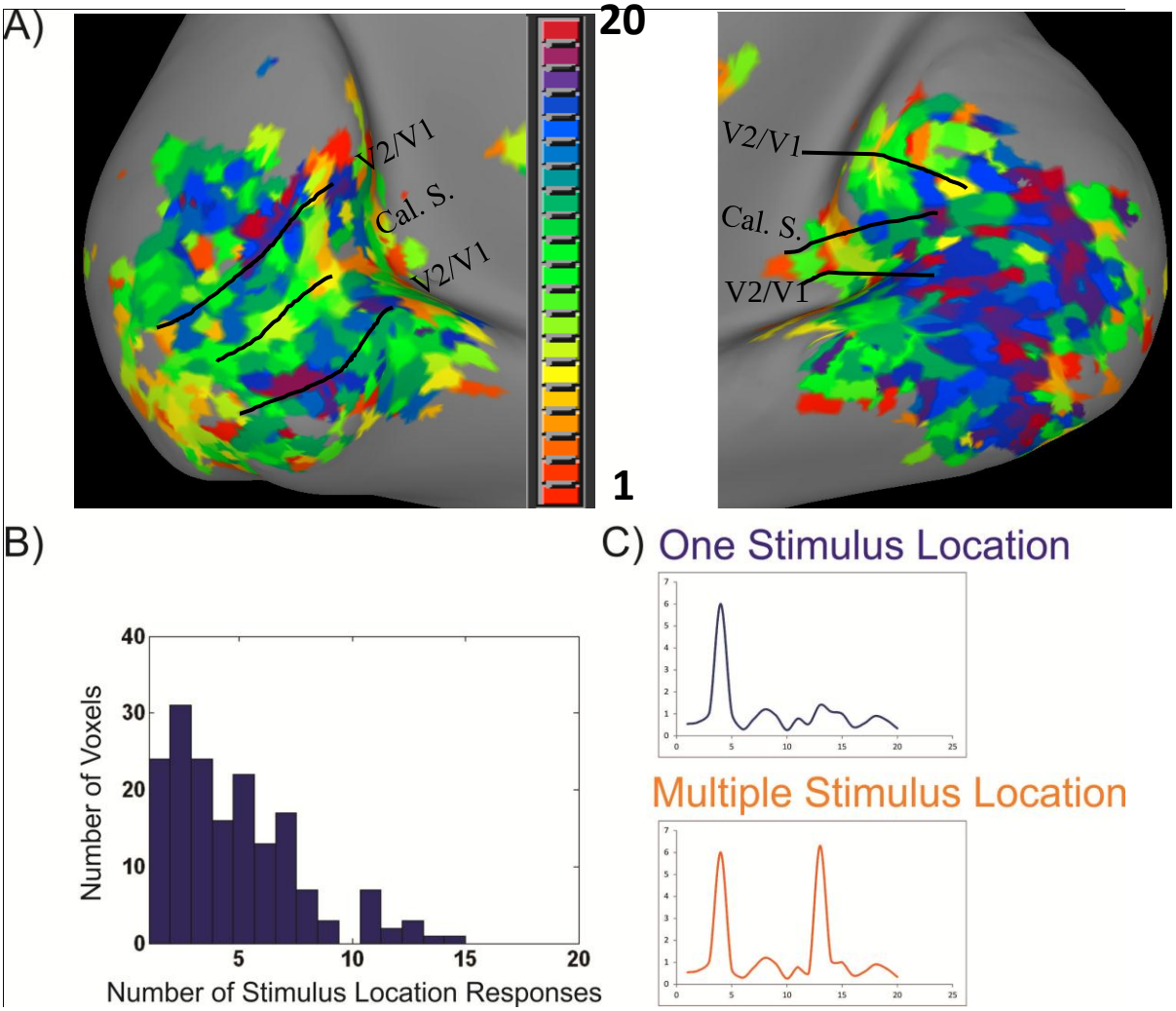

Figure 28: Number of Stimulus Location Maps. (A) The distribution of cortical locations that elicit a response from any number of stimuli, ranging from one polar angle location to all 20 polar angle locations using code-based mapping method. (B) The frequency histogram for the number of voxels that respond to any stimulus location. (C) Representations of the voxel tuning curves for a voxel that responds to one stimulus location (blue) and multiple stimulus locations (orange).

Population representation of polar angle location. According to animal studies [8, 10], the area of cortex representing different polar angles within V1 is essentially uniform. As demonstrated previously [5], however, the cortical representation of polar angle in human cortical mappings using fMRI is distinctly non-uniform. Figure 29 illustrates this effect. The average frequency histograms, for ten subjects, for the code-based (top) and temporal phase (bottom) methods are distinctly different. The error bars

on each histogram represent the standard error of the number of voxels representing each polar angle location. The temporal phase method (lower graph) yields a non-uniform histogram with a bimodal characteristic. In contrast, the code-based method yields a more uniform distribution. The temporal phase and code-based methods yielded a total of 393 and 395 responsive voxels respectively for the same V1 ROI in each subject. Even though there was no difference in the number of activated voxels ($p<0.6$, Wilcoxon rank sum), the uniform (code-based) versus bimodal (temporal phase) were statistically different on a bin-by-bin comparison (Chi-square test XI = 31.6, $p< 0.03$). Moreover, the code-based histogram was not significantly different from an ideal, uniform distribution (Chi-square XI = 6.07, $p<0.99$), whereas the temporal phase histogram was significantly different (Chi-square XI = 45.1, $p<6.6e-4$). In contrast, when tested for similarity to a bimodal distribution, the code-based histogram was different (Chi-square XI = 50.4, $p<1.1e-4$), but the temporal phase histogram was not (Chi-square XI = 11.5, $p<0.9$).

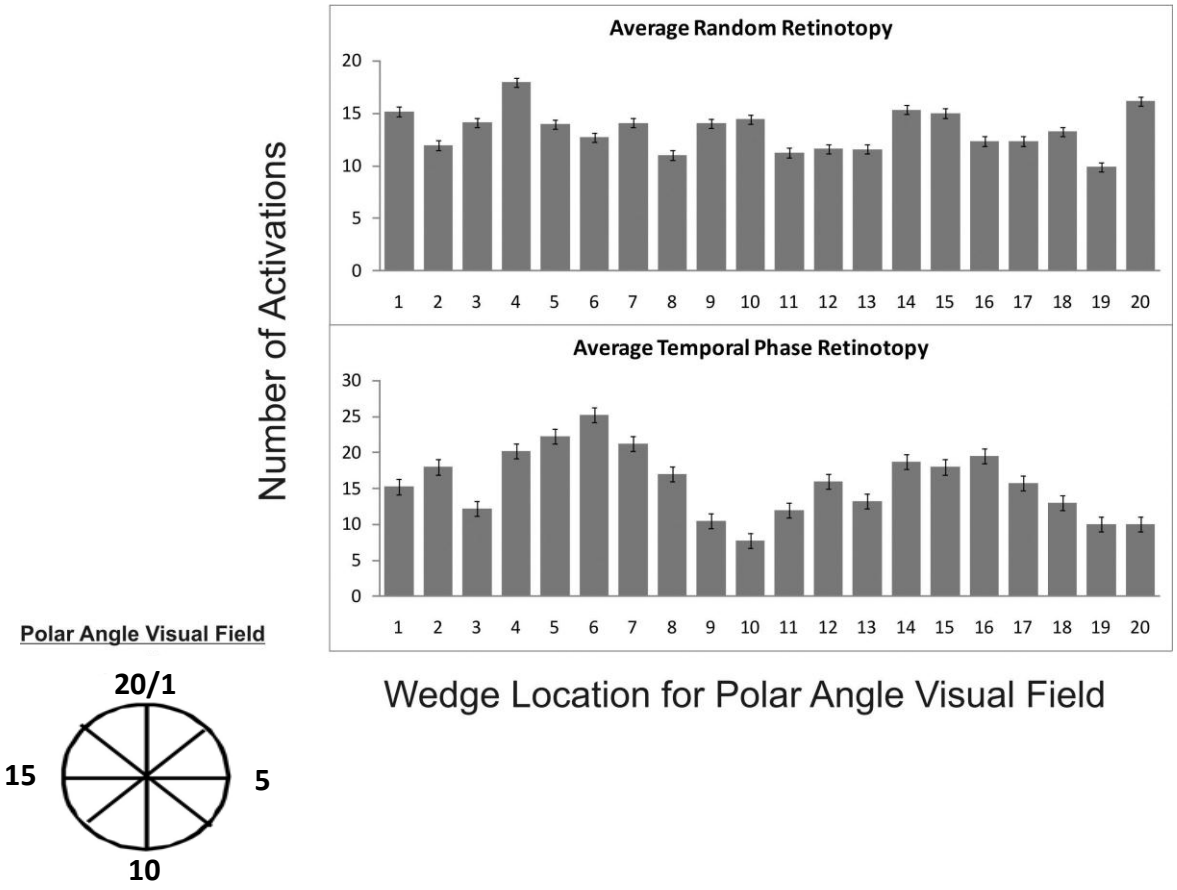

Figure 29: Polar Angle Voxel Distributions. The average (n = 10) voxel distributions for the polar angle stimulus locations (visual field positions described in lower left corner) for the code-based (top) and temporal phase (bottom) mapping.

Effects of Noise on the Visual Stimulus (Input) Signals via Simulation. The effects of applying higher, but physiologic, noise levels to simulated voxels representing specific visual field locations were investigated. In a previous study, we showed that the ability of the temporal phase mapping technique to produce a uniform distribution across all polar angle locations is highly susceptible to noise [5]. It was hypothesized that the temporal phase mapping method would result in a depression of detected voxels in the visual field locations where the increased levels of noise are located. It was further hypothesized that the code-based method would be considerably less susceptible to the increase in noise. One hundred voxel time series were created for each of the twenty visual field locations.

Each set of voxels was assigned either a unique code-based input stimulus function or temporal phase delay. The baseline CNR for all-time series was 10 dB. The two visual field locations chosen for increasing level of noise was the superior vertical meridian (90°) and inferior vertical meridian (270°). These two visual field locations were decremented in CNR to 1dB. Figure 30 shows the code-base method's (bottom) and temporal phase method's (top) ability to code for the true visual field location (x-axis) relative to all other visual field locations with the CNR for the simulated voxels representing inferior and superior vertical meridia at a CNR level of 1dB. The black dots on each plot only represent the locations where voxels respond to visual field locations, not the number of voxels responding to each location. With the inferior and superior vertical meridia at 1 dB the code-base method correctly assigns every voxel to the correct visual field location, thus creating a uniform distribution of voxels across the visual field representation. The temporal phase mapping method begins to incorrectly assign voxel visual field locations at a CNR = 1 dB. Not only does a depression in the correct visual field locations start to occur but the voxels that should have been in the superior and inferior vertical meridian locations are assigned to different (incorrect) visual field locations.

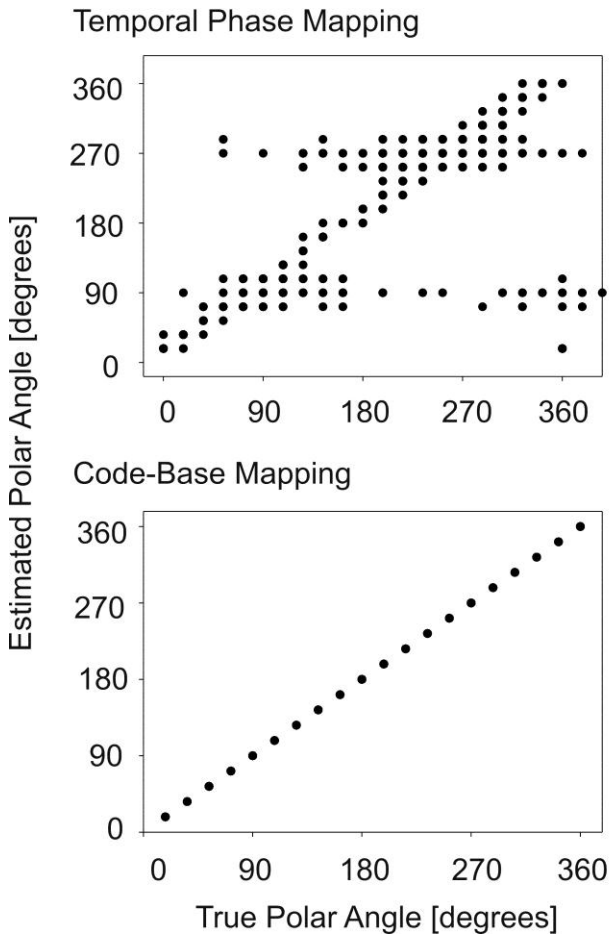

Figure 30: Noise Simulation II. CNR distortion of phase delays that represent preferred polar angle at a CNR = 1 dB. The known phase delay of the simulated signal (x-axis) vs. the estimated phase delay in the presence of noise (y-axis) is shown for the temporal phase (top) and code-based (bottom) mapping.

The simulation above illustrates the effects of noise on the mapping methods when trying to detect signals in a defined space (ie polar angle visual field assessment). A simpler approach to the above study is to examine the ability of each mapping method to correctly assign one polar angle location to a group of voxels undergoing increased levels of noise. We hypothesized that the code-based mapping method will be less susceptible to noise with respect to assigning the true polar angle of a group of voxels. This hypothesis is primarily based on the random design of the code-based mapping input stimulus functions, which are more linearly independent than the temporal phase

mapping input stimulus functions. We created two groups of 100 simulated voxel time series. In Group 1, all the voxels contained times series that consisted of a sinusoid with a constant phase (temporal phase). In Group 2, all the voxels contained the same random presentation of the input stimulus (code-based). Each group of simulated voxel time series underwent cross correlation analysis to a respective reference signal with varying levels of white noise added to the voxel time series. Five simulated trials were run with increasing levels of additive white noise for each trial. The degree of noise was measured by controlling the contrast to noise level of each group of simulated voxels. The CNR for each trial increased by decades, ranging from 0.01 dB to 100 dB. Figure 31 shows the percentage of simulated voxels that were correctly assigned by each mapping method given greater levels of noise (ie. lower value of CNR). At CNR > 10 dB, both methods will assign the voxel's visual field position correctly > 95% of the time. The percentage of correct assignment using temporal phase mapping decreases to ~20% at 1 dB, whereas, the code-base mapping assignment only slightly decreases in accuracy as the CNR decreases. Also, note that the temporal phase method incorrectly assigns the voxels to other visual field locations. The code-base method neglects the voxels with low CNR, and thus does not assign it to a visual field location, therefore, limiting the error in assigning voxels to incorrect visual field locations.

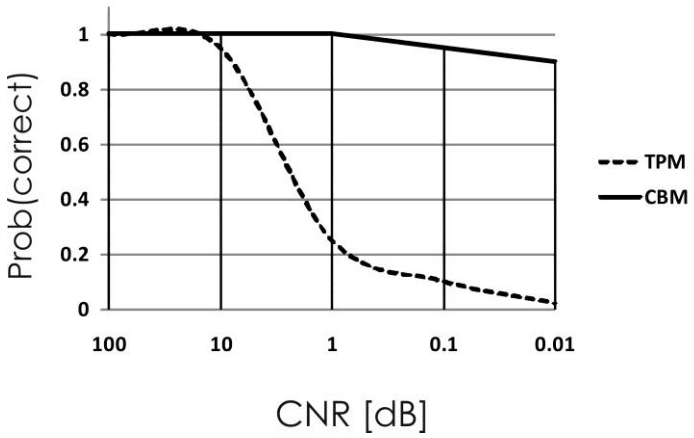

Figure 31: Mapping Method Detection Sensitivity. Illustrates the percentage of simulated voxels that were correctly assigned by each mapping method given greater levels of noise (ie. lower value of CNR). CBM = Code-based Mapping, TPM = Temporal Phase Mapping

Discussion

In this study, we investigated whether a code-based (random stimulus) retinotopic mapping technique can more accurately assign regions of cortex to the polar angle visual field than temporal phase mapping. The techniques were compared on cortical retinotopic topography, single and multiple voxel responses, and on noise immunity. Topographically, the methods showed little difference with respect to the overall pattern of retinotopic organization. However, the code-based technique produced a more uniform representation of polar angle compared to temporal phase mapping. In regards to the immunity of the mapping techniques to anatomical specific noise, temporal phase mapping is highly susceptible to noise with respect to the inaccuracy of the assignment of a voxel's visual field location. This anatomically specific susceptibility leads to two effects. First, the increase in local noise causes a displacement of the assignment of the voxel location at CNR levels as high as 1dB. The code based technique, on the other hand, was not influenced by the presence of noise as low as CNR = 0.1 dB. Second, the

increase in noise causes statistical drop out of the validly responding voxels to visual stimuli, which ultimately affects both mapping techniques.

The results indicate that the code-based technique produces a relatively uniform representation of angular position within the visual field. This is in agreement with 2-DG studies that suggest primary visual cortex is equally distributed with respect to polar angle [23]. In contrast, the voxel distribution from the temporal phase mapping technique produced a non-uniform (bimodal) distribution, consistent with previously reported fMRI data [5]. We speculate that the major difference between the techniques is the interaction of how the stimulus is presented and how the stimulus presentation interacts with the cortical tissue when sampled by fMRI. This difference can be seen in the anatomical layout of the stimulus location responses to the mapping techniques (Figure 27). Even though the mapping techniques globally have a similar pinwheel representation on V1, a closer examination of the noisier areas (on the lips of the calcarine and the occipital pole) shows that the mapping techniques differ in these areas with respect to the stimulus location assignment. In fact, these anatomical regions are where the code-based method responds to the most wedges. Possible sources of this difference related to the anatomy and physiology of V1 are that cortical surface in these areas are highly convoluted responding to multiple stimulus locations or the underlying hemodynamics in the region is producing high noise content. An examination of the differences between the stimulus presentation, the signal integrity, and visual field mapping implications is warranted.

Stimulus Presentation and Information Content in the fMRI Signal. Temporal phase mapping's high correlation within the input stimulus set representing visual field locations and between the input stimulus set and reference causes complications with

respect to assigning visual field locations to voxels. As it has been shown in this work and previous [23], the assignment of a specific voxel's fMRI response to a specific visual field location is highly sensitive to increased levels of noise in the voxel response. The number of voxels correctly assigned to the correct stimulus location decreased by a factor of 4 when the CNR dropped from 10 dB to 1 dB. Also due to this high correlation between input sequences, the ability to detect multiple stimulus locations in a voxel becomes highly improbable. Code-based mapping codes visual field polar angles with input stimulus functions (pseudo-random binary sequences) that are more linearly uncorrelated than temporal phase mapping. The input sequence describing each polar angle location of the visual field is independent of each other [93, 95]. The low correlation coefficient between input stimulus sequences used in code-based mapping allows a unique fMRI response to be assigned to an equally unique input signal. Thus, the assignment of a specific voxel's fMRI response to a specific visual field location is less sensitive to increased levels of noise in the voxel response. The number of voxels assigned to the correct stimulus location did not decrease when the CNR dropped from 10 dB to 1 dB. Even when the CNR was dropped to 0.01 dB, the percent of correctly assigned stimulus locations for the fMRI responses was >85%. Of course, both mapping methods are still susceptible to statistical drop out at very low CNR levels.

The low correlation coefficient between input sequences in code-based mapping also provides the opportunity for the technique to detect multiple stimulus locations in one voxel. The code-based method allows clarification of the neuron's action in the voxels to respond to multiple locations, essentially treating the voxels as if they have orientation tuning curves [96-101]. The ability to create stimulus location response tuning curves

allows the code-base technique to be insensitive to the possibility that the voxel possibly contains a cortical surface that may be highly convoluted, containing two cortical surfaces that respond to two distinct visual field locations [99-101]. This allows the voxel to add more information to the assessment of a patient/subject's visual field.

Let us examine how each mapping technique would respond to a voxel that can code from more than one location. Assume a voxel, v, responds to three visual field sectors (vf_1, vf_2, and vf_3). Voxel, v, using the temporal phase mapping will respond to all three locations but due to the phasic relationship between the input sequences and the winner-take-all algorithm, the response will be a composite of all three locations. On the other hand, using code-based mapping, voxel, v, will "tune" to all three possible visual field sectors. Translating this result to the voxel histogram or visual field map, there will be two visual field locations that will not be counted as a positive visual field location for the subject using temporal phase mapping. However, using code-base mapping all three visual field locations will be counted.

Signal Integrity Effects on Mapping Primary Visual Cortex using fMRI. The main finding in this study is that the two mapping techniques correlate with respect to polar angle visual field assignment when the contrast-to-noise ratio (CNR) is relatively high (>= 5 dB). When the CNR is relatively low (<= 5 dB), the agreement between the two mapping techniques is inconsistent. In this study, we showed, through simulation, that the code-based mapping technique is significantly less sensitive to the noise in the fMRI signal than the temporal phase mapping technique. In fact, the majority of the time the code-based mapping technique assigns a voxel to the correct polar angle if the voxel continues to have a statistically significant response. The only effect of the noise on the

assignment of voxels by the code-based technique is “drop-out” of voxels due to the statistical threshold set. Temporal phase mapping is susceptible to not only statistical drop out but also the incorrect assignment of stimulus locations due to high noise content. Most of this noise can be attributed to hemodynamic-related fMRI noise [23, 66]. The code based technique provides a higher probability of mapping the correct polar angle visual field location to a voxel due to a decrease in sensitivity to noise content.

In previous reports [5], we have shown that temporal phase mapping can be systematically biased by an increase in the noise of BOLD signals within restricted spatial regions of visual cortex, particularly in the vicinity of draining veins. In such cases, the increased noise can cause selective misassignment of a voxel’s preferred location to nearby locations. This is due to the relative similarity of the response waveforms representing neighboring locations, which differ by only a small shift in temporal phase (Figure 24A). In effect, the variance of the phase estimate depends on the contrast to noise ratio (CNR). Though a reduced CNR lowers the probability that the response will be statistically significant, it simultaneously raises the likelihood that the true preferred location will be miss-assigned to a nearby location before statistical significance is lost altogether. This effect is ameliorated in code-based mapping because stimuli at nearby locations are presented with markedly different (uncorrelated) time sequences (Figure 24B). So, a key advantage of code-based mapping is the decreased sensitivity of the method to changes in signal-to-noise relative to temporal phase mapping.

Visual Field Mapping Implications. One major issue with temporal phase mapping in regards to visual field mapping is the need to correct for the hemodynamic

delay. Before each phase delay is mapped to the FFMap, the phase delay must be "calibrated" to the static hemodynamic delay present in every fMRI response. The calibration is typically accomplished heuristically or by using oppositely sequenced stimuli. The first approach is time intensive on the post processing side of creating an FFMap. The second approach doubles the acquisition time of the scan. In code-based mapping, the hemodynamic delay is either accounted for in the regression model or the optimal delay can be found from the cross correlation function.

Conclusion

The main reason for developing a new retinotopic mapping technique is to reduce the biases posed by using temporal phase mapping when assigning a stimulus location to a voxel. The main source of biasing that effects temporal phase mapping is the underlying hemodynamics in the occipital midline region which produces high noise content voxels. For research applications, these issues can be tolerated. However, in a clinical setting, it is important to have a high statistical confidence that voxels will code for the correct stimulus location(s). We have demonstrated the following:

- Code-base mapping offers the ability to detect a voxel's response to all of the presented stimulus locations.
- When using code-base mapping, polar angle visual field locations across V1 have a more uniform distribution compared to temporal phase mapping.
- Both mapping techniques elicit a similar global polar angle retinotopic response in the primary visual cortex.

- The visual stimulus inputs used in code-based mapping are less spatio-temporally correlated than temporal phase mapping and thus less susceptible to fMRI noise effects.
- On a per voxel basis, the two techniques have a high probability to assign stimulus locations at high CNR levels. As CNR decreases, probability of correct assignment for temporal phase mapping decreases but code-based mapping does not decrease.

Analyzing all of these findings, suggests that the code-based mapping technique is a valid technique for mapping polar angle retinotopic locations in the primary visual cortex and provides promise for mapping visual fields in the clinical fMRI setting.

Conclusion

Relevance of Thesis to the Body of Research

This thesis illustrates that using temporal phase mapping for coding the polar angle visual field locations in V1 does not accurately represent the distribution of polar angle as the research literature suggests. This leads to an irregular representation of a subject's visual field map. The irregularity presents itself as false negative depressions in the visual field.

This thesis suggests that the depressions in the visual field in V1 are due to the interaction of the sequential nature of temporal phase mapping with the anatomically fixed noise sources (i.e. draining vein effects) local to specific polar angle visual field locations. The visual field locations that are affected reside on or near the lips of the calcarine sulcus and typically represent the visual field areas on or near the vertical meridia. Examining these inherent limitations in temporal phase mapping turned the focus of this thesis towards an alternative method to mapping stimulus locations that was less susceptible to the aforementioned issues.

The code-based method developed was a pseudo random presentation of the stimulus locations representing polar angles in the visual field. This method decreases the correlation between the input stimuli sequences associated with the set of stimulus locations being mapped onto the cortex. Code-based mapping allows a voxel to respond to multiple stimulus locations regardless of the voxel content. We suggest that voxels could respond to multiple locations because the cortex being sampled in a voxel actually

represents different physical locations and/or the effective receptive field of the voxel is more broadly tuned. The code-base technique also provides a more robust method for detecting a voxel's response to a stimulus location in the presence of noise. It turns out that utilizing the above mentioned features of code-based mapping provides a uniform voxel distribution of the polar angle visual field assignments in V1 unlike temporal phase mapping.

Code-based mapping as explored in this thesis sets a foundation for mapping visual cortex in a clinic setting to presurgically assess visual function that lies near tissue malformations such as tumors. Code-based mapping gives the physician a more confident statistical measure of a voxel's response to a set of stimulus locations presented visually to a patient. Code-based mapping also provides more information than temporal phase mapping about the function of the tissue in a sampled voxel as the voxel responds to the set of visual stimulus locations.

Future of Code-based Mapping

The research from this thesis can evolve into clinical applications that require detailed assessment of a patient's visual field and provide presurgical information for surgeons to make a better decision regarding the course of action. More specifically the concentration of future research for code-based mapping can be understood by the following mission statement:

Characterize the dynamics of the visual field map of patients as they recover from surgery that involves removal of neural tissue affecting the patient's visual field.

When dealing with presurgical planning of tissue removal (in our case visually specific tissue) around any viable, functional neural tissue, the code-based mapping method can assist in addressing two of the surgeon's main tasks:

1. Weigh the risks associated with removing the malformation and boundary areas of tissue and trying to maximize the functional tissue around the risk area that the patient will have after surgery.
2. Consulting with (or predicting for) the patient on how much visual field the patient will have after the surgery.

In regards to the first task, the risk assessment in the presurgical planning stage typically leads to an area of tissue classified as the boundary area. The boundary area is the tissue that lies between what is classified as viable tissue and non-viable tissue. Surgeons must decide how much of this boundary area to remove. Ultimately, surgeons would prefer to collect functional data prior to the surgery that would allow them to describe the boundary area more clearly. Currently temporal phase mapping is being used to provide visual field information in some medical institutions but unfortunately as in the research described above, temporal phase mapping has limitations in the assignment of voxels that reside in tissue areas that contain a high content of noise. Some of the tissue in the boundary areas contains viable areas of tissue but have noise laden fMRI signals due to the presence of the malformation and therefore go undetected. The tissue responding to visual field locations in the boundary areas go undetected due to the interactions of temporal phase mapping with the different noise sources in fMRI signals and the insensitivity of temporal phase mapping to detect a voxel's multiple stimulus locations. Code-based mapping provides an opportunity to map the boundary areas by

reducing the effects of noise on the detection method. Adding the code-based mapping's ability to be highly sensitive to the geometry in a voxel and the opportunity to respond to multiple stimulus locations, code-based mapping seems to be a good fit for visual field mapping in patients with neural malformations affecting the visual field.

The first set of experiments could be focused on developing the fully optimized code-based mapping stimulus set. First one would need to show that code-based mapping can be used on normal subjects and clinical patients to map the visual field. The experiment could be ran with two separate stimulus sets, polar angle and eccentricity, mimicking the temporal phase mapping method. Although this is not an optimal format, this would prove the effectiveness of code-based mapping in two populations. Also evolving out of this experiment would be the need to develop a new method for creating functional field maps (FFmaps) from the data. The approach would consist of building individual voxel functional field maps (VFFMaps), since a voxel has the ability to respond to all visual field locations. To construct the global FFmap, a statistically valid method for combining each of the VFFMaps needs to be constructed. The next step would be to determine the effectiveness of showing polar angle and eccentricity stimulus sets simultaneously. There are two feasible approaches: (1) show traditional eccentricity and polar angle stimulus simultaneously or (2) present two dimensional chords as visual field sectors. The traditional method of stimulus presentation would provide the ability to determine the entire visual field with only 40 stimulus inputs which will make the number of presentations shorter to run. To prove the concept is feasible, a larger spatial resolution can be ran (i.e. 10 polar angle stimuli and 10 eccentricity stimuli). In order to optimize the stimulus presentation, the next step would be to determine the actual spatial resolution

limitations and the needed spatial resolution in the clinic. Several studies can be executed here determining several aspects of spatial resolution of the visual stimulus.

- What is the smallest size of visual stimulus that can be detected?
- Study the effects of the number of stimulus presentations to stimulus size. This may lead to an unbalanced number of presentations for stimulus locations as they vary in size as scaled by cortical magnification.
- How small can two neighboring stimulus locations be before they can no longer be detected as separate stimulus locations?
- Is there a degree a complexity of geometry in the cortical surface that the code-based mapping method cannot detect? This outcome could lead to not having to use higher resolution fMRI scans which trade-off lower SNR per voxel for finer anatomical resolution.
- Determine if spatial linearity of stimulus locations affects the voxel response to the point that detectability is compromised. This outcome could lead to design constraints around the level of acceptable correlation between stimulus locations.

Once the optimal set of stimuli has been created the next step will be to start mapping other visual areas of the brain. This is very important if code-based mapping is to be used to determine the effects of neural malformations on the visual field. Not all neural malformations will affect only the primary visual cortex, so code-based mapping must be able to map the visual field in the higher order visual areas. With this specification in mind, the code-based mapping method would also integrate the ability to test the visual features of contrast sensitivity, color sensitivity, and enable the ability to test visual neglect. All of the experiments mentioned would provide a robust foundation for code-

based mapping to be used in the clinic to assess visual fields that are compromised by neural malformations. The final study of this section of research would be to have patients that undergo both an fMRI-based retinotopic mapping using code-based mapping and during their surgery have a cortical-based visual field mapping especially around the tumor location. This study would illustrate that the code-based mapping technique is accurately mapping data to the physiological response on the cortex, and that the visual function around the boundary area in the cortical tissue is mapping similar to the fMRI collected data.

The second task builds on top of the optimization of the code-based mapping method and the clinical evidence showing the utility of visual field mapping in patients with malformations affecting the visual field. The main goal of the long term research would be to gain insight into reorganization of the visual field in the viable cortex after tissue removal. More specifically, the aim would be to develop a prediction model based on the study of visual field functional reorganization/recovery after a patient's surgery. The model would ideally provide the surgeon the ability to remove tissue in a virtual setting and show the degradation of the visual field as more tissue was removed. For this model, one could focus only on patients that have a tumor that directly affects the visual cortex and thus the patient's visual field. The first major study in this aim would be to collect visual field maps using fMRI prior to surgery and after surgery at days 5, 10, 15, 20, 25, and 50. The first patient population of 20 patients would be used to determine if there are predictable indicators using fMRI in visual field reorganization after tissue removal. Some of the first observations would be to determine how the visual field is dynamically

changing in the first two months post-surgery. The changes would include but not limited to the following:

- Global organizational changes in the functional topology of the visual field map both on the cortex and expressed in the VFFMaps.
- Voxel-by-voxel analysis of changes over time
- Changes in blood volume over time as measured with rCBF maps
- Changes in magnetic field susceptibility as measured with a Bo map

Other factors would also be documented such as tumor location, volume of tumor, volume of tissue removed, additional treatments the patient is undergoing (ie radiation, chemotherapy), and general medical history. The patients would then be followed on a monthly basis for six months. Once indicators have been identified, the next step is to run a larger test sample of 50-100 patients and follow the same protocol. This set of data would be used to verify that the indicators in the first study are consistently present and the relationships of these indicators could then be investigated.

The final evolution of this research would be to extend the mapping method to investigate functional connectivity between the LGN and V1. Clinically, the ability to determine if the tumors located at or near the white matter fiber tracks involving visual processing affect the visual field if removed would add another level of value to presurgical planning. This would be beneficial for tumors that involve the white matter fibers (optic radiations) related to visual field processing. The first step would be to retinotopically map the LGN and V1 in normal subjects and functionally correlate specific locations in the LGN to specific cortical locations in V1 using fMRI and DTI. Code-based mapping would be a good tool again for retinotopic mapping in the LGN due

to the level of noise in the anatomical area. Once the method to retinotopically map the LGN/V1 system is understood, the next step would be to complete a study of patients with a before and after surgery retintopic map using fMRI. The ideal outcome of this study would be to show that the LGN is processing the visual information without defect and that V1 is mapping either incorrectly or is rewired. From this point the reorganization study can be repeated for tumors affecting visual processing location in or near the white matter fibers.

Appendix A: Supplementary Figures for Aim I

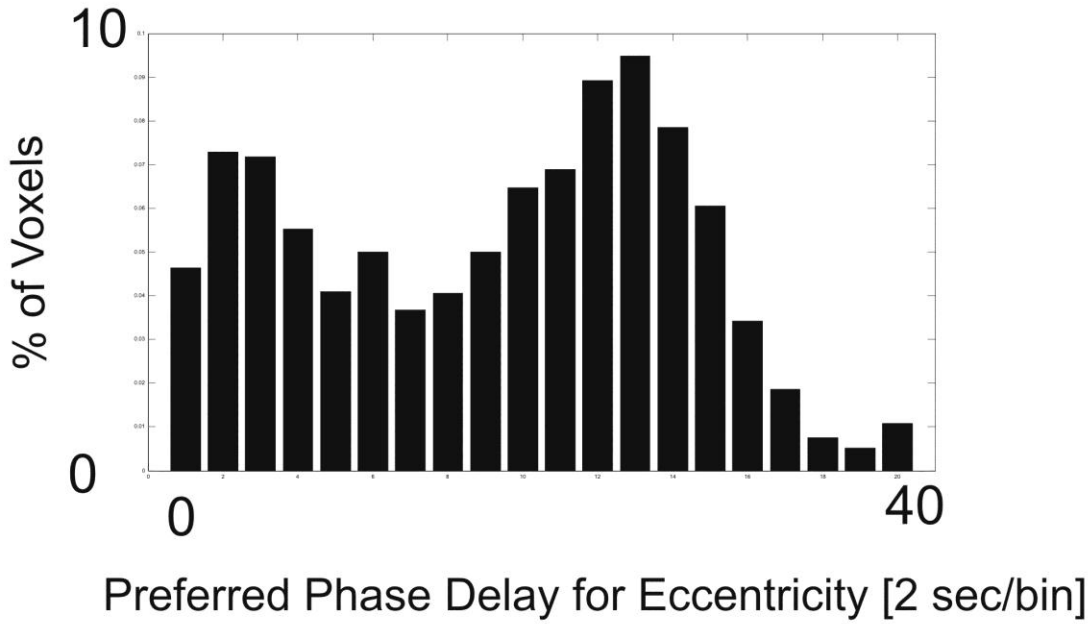

Figure S1: Eccentricity Histogram. The preferred phase delay for the visual field eccentricity. The under-representation of voxels beyond 34 seconds of phase delay is a stimulus anomaly and not the true subject's visual field representation. It is noted that the subject's typically did show a slight under-representation in the peri-foveal eccentricities.

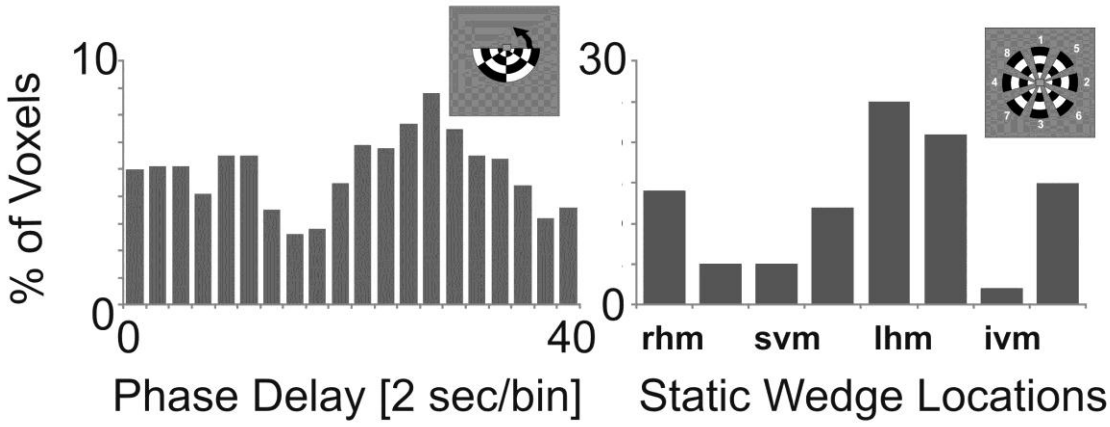

Fig S2: Static Wedge Analysis. The voxel histograms for the counter-clockwise rotating hemi wedge (left) and the statically-presented eight polar angle wedge locations (right). Both voxel histograms have under-representations at the vertical meridia representations using the two visual stimuli.

REFERENCES

1. Tootell, R.B., et al., *Deoxyglucose analysis of retinotopic organization in primate striate cortex.* Science, 1982. **218**(4575): p. 902-4.

2. White, L.E., et al., *Maps of central visual space in ferret V1 and V2 lack matching inputs from the two eyes.* J Neurosci, 1999. **19**(16): p. 7089-99.

3. Bosking, W.H., J.C. Crowley, and D. Fitzpatrick, *Spatial coding of position and orientation in primary visual cortex.* Nat Neurosci, 2002. **5**(9): p. 874-82.

4. Van Essen, D.C., et al., *The projections from striate cortex (V1) to areas V2 and V3 in the macaque monkey: asymmetries, areal boundaries, and patchy connections.* J Comp Neurol, 1986. **244**(4): p. 451-80.

5. Janik, J.J., Ropella, K. M., DeYoe, E. A. *Distortions of Human Retinotopy Obtained with Temporal Phase Mapped fMRI*. in *Society for Neuroscience*. 2003. New Orleans, LA USA.

6. DeYoe, E.A., et al., *Mapping striate and extrastriate visual areas in human cerebral cortex.* Proc Natl Acad Sci U S A, 1996. **93**(6): p. 2382-6.

7. Saad, Z.S., E.A. DeYoe, and K.M. Ropella. *Time delay estimates of FMRI Signals: Efficient algorithm & estimate variance*. in *Proceedings of the 19th International Conference - IEEE.EMBS*. 1997. Chicago, IL USA.

8. Tootell, R.B., et al., *Functional anatomy of macaque striate cortex. II. Retinotopic organization.* J Neurosci, 1988. **8**(5): p. 1531-68.

9. Hubel, D.H. and T.N. Wiesel, *Ferrier lecture. Functional architecture of macaque monkey visual cortex.* Proc R Soc Lond B Biol Sci, 1977. **198**(1130): p. 1-59.

10. Gattass, R., A.P. Sousa, and M.G. Rosa, *Visual topography of V1 in the Cebus monkey.* J Comp Neurol, 1987. **259**(4): p. 529-48.

11. Kandell, E., Schwartz, JH, Jessell TM, *Principles of Neuroscience*. 4th edition ed. 1991, New York: McGraw-Hill. 1414.

12. Hubel, D.H.W., T. N., *Sequence regularity and geometry of orientation columsn in monkey striate cortex.* J Comp Neurol, 1974. **158**: p. 267-294.

13. Hubel, D.H.W., T. N., *Receptive fields and functional architecture of monkey striate cortex.* J. Physiol., 1968. **195**: p. 215-243.

14. Hubel, D.H., Wiesel, T. N., *Functional architecture of macaque visual cortex. Ferrier Lecture.* Proc. R. Soc. Lond [Biol], 1977. **198**: p. 1-59.

15. Hubel, D.H., *Cortical unit responses to visual stimuli in nonanesthetized cats.* Am J Ophthalmol, 1958. **46**(3 Part 2): p. 110-21; discussion 121-2.

16. Hubel, D.H., *Integrative processes in central visual pathways of the cat.* J Opt Soc Am, 1963. **53**: p. 58-66.

17. Hubel, D.H., *The Visual Cortex of the Brain.* Sci Am, 1963. **209**: p. 54-62.

18. Hubel, D.H. and T.N. Wiesel, *Uniformity of monkey striate cortex: a parallel relationship between field size, scatter, and magnification factor.* J Comp Neurol, 1974. **158**(3): p. 295-305.

19. White, L.E., W.H. Bosking, and D. Fitzpatrick, *Consistent mapping of orientation preference across irregular functional domains in ferret visual cortex.* Vis Neurosci, 2001. **18**(1): p. 65-76.

20. Felleman, D.J., and Van Essen, D. C., *Distributed hierarchical processing in the primate cerebral cortex.* Cereb Cortex, 1991. **1**: p. 1-47.

21. Connolly, M. and D. Van Essen, *The representation of the visual field in parvicellular and magnocellular layers of the lateral geniculate nucleus in the macaque monkey.* J Comp Neurol, 1984. **226**(4): p. 544-64.

22. Sereno, M.I., et al., *Borders of multiple visual areas in humans revealed by functional magnetic resonance imaging.* Science, 1995. **268**(5212): p. 889-93.

23. Engel, S.A., G.H. Glover, and B.A. Wandell, *Retinotopic organization in human visual cortex and the spatial precision of functional MRI.* Cereb Cortex, 1997. **7**(2): p. 181-92.

24. Galetta, S.L., *A stimulating view of human visual cortex.* Neurology, 2000. **54**: p. 785-786.

25. Ojemann, G.A., I. Fried, and E. Lettich, *Electrocorticographic (ECoG) correlates of language. I. Desynchronization in temporal language cortex during object naming.* Electroencephalogr Clin Neurophysiol, 1989. **73**(5): p. 453-63.

26. Ojemann, G.A., *Functional mapping of cortical language areas in adults. Intraoperative approaches.* Adv Neurol, 1993. **63**: p. 155-63.

27. Ojemann, J.G., J.W. Miller, and D.L. Silbergeld, *Preserved function in brain invaded by tumor.* Neurosurgery, 1996. **39**(2): p. 253-8; discussion 258-9.

28. Ojemann, J.G., G.A. Ojemann, and E. Lettich, *Cortical stimulation mapping of language cortex by using a verb generation task: effects of learning and comparison to mapping based on object naming.* J Neurosurg, 2002. **97**(1): p. 33-8.

29. Penfield, W., *The supplementary motor area in the cerebral cortex of man.* Arch Psychiatr Nervenkr Z Gesamte Neurol Psychiatr, 1950. **185**(6-7): p. 670-4.

30. Penfield, W. and M. Baldwin, *Temporal lobe seizures and the technic of subtotal temporal lobectomy.* Ann Surg, 1952. **136**(4): p. 625-34.

31. Penfield, W., *Combined regional and general anesthesia for craniotomy and cortical exploration. I. Neurosurgical considerations.* Curr Res Anesth Analg, 1954. **33**(3): p. 145-55.

32. Penfield, W., *Functional localization in temporal and deep sylvian areas.* Res Publ Assoc Res Nerv Ment Dis, 1958. **36**: p. 210-26.

33. Birchmeier-Nussbaumer, A.K., *[The Penfield temporal lobe brain stimulation experiments in the light of speech analysis of pertinent patients' statements]*. Schweiz Arch Neurol Neurochir Psychiatr, 1974. **114**(1): p. 37-56.

34. Black, P., et al., *Minimalist approach: functional mapping.* Clin Neurosurg, 2002. **49**: p. 90-102.

35. Duffau, H.V., S.; Capelle, L., *Intra-operative mapping of the subcortical visua pathways using direct electrical stimulations.* Acta Neurochirurgica, 2004. **146**: p. 265-270.

36. Brenton, R.S. and C.D. Phelps, *The normal visual field on the Humphrey field analyzer.* Ophthalmologica, 1986. **193**(1-2): p. 56-74.

37. Barton, J.S., Benatar, M., *Field of Vision: A Manual and Atlas of Perimetry*, ed. D. Tarsy. 2003, Totowa, NJ: Humana Press Inc. 334.

38. Roux, F.E.I., D et al., *Perimetric visual field and functional MRI correlation: implications for imag-guided surgery in occipital brain tumors.* J Neurol Neurosurg Psychiatry, 2001. **71**: p. 505-514.

39. Black, P.M., et al., *Development and implementation of intraoperative magnetic resonance imaging and its neurosurgical applications.* Neurosurgery, 1997. **41**(4): p. 831-42; discussion 842-5.

40. Haacke, E., *Magnetic Resonance Imaging: Physical Principles and Sequence Design*. 1999, New York City: Wiley-Liss.

41. Ogawa, S., et al., *Intrinsic signal changes accompanying sensory stimulation: functional brain mapping with magnetic resonance imaging.* Proc Natl Acad Sci U S A, 1992. **89**(13): p. 5951-5.

42. Menon, R.S., et al., *Functional brain mapping using magnetic resonance imaging. Signal changes accompanying visual stimulation.* Invest Radiol, 1992. **27 Suppl 2**: p. S47-53.

43. Thompson, J.K., M.R. Peterson, and R.D. Freeman, *Single-neuron activity and tissue oxygenation in the cerebral cortex.* Science, 2003. **299**(5609): p. 1070-2.

44. Devor, A., et al., *Coupling of total hemoglobin concentration, oxygenation, and neural activity in rat somatosensory cortex.* Neuron, 2003. **39**(2): p. 353-9.

45. Mayhew, J.E., *Neuroscience. A measured look at neuronal oxygen consumption.* Science, 2003. **299**(5609): p. 1023-4.

46. Logothetis, N.K., et al., *Functional imaging of the monkey brain.* Nat Neurosci, 1999. **2**(6): p. 555-62.

47. Logothetis, N., *Can current fMRI techniques reveal the micro-architecture of cortex?* Nat Neurosci, 2000. **3**(5): p. 413-4.

48. Logothetis, N.K., et al., *Neurophysiological investigation of the basis of the fMRI signal.* Nature, 2001. **412**(6843): p. 150-7.

49. Logothetis, N.K., *The neural basis of the blood-oxygen-level-dependent functional magnetic resonance imaging signal.* Philos Trans R Soc Lond B Biol Sci, 2002. **357**(1424): p. 1003-37.

50. Logothetis, N.K., *The underpinnings of the BOLD functional magnetic resonance imaging signal.* J Neurosci, 2003. **23**(10): p. 3963-71.

51. Logothetis, N.K. and B.A. Wandell, *Interpreting the BOLD Signal.* Annu Rev Physiol, 2004. **66**: p. 735-69.

52. Smith, A.J., et al., *Cerebral energetics and spiking frequency: the neurophysiological basis of fMRI.* Proc Natl Acad Sci U S A, 2002. **99**(16): p. 10765-70.

53. Attwell, D. and C. Iadecola, *The neural basis of functional brain imaging signals.* Trends Neurosci, 2002. **25**(12): p. 621-5.

54. Rees, G., K. Friston, and C. Koch, *A direct quantitative relationship between the functional properties of human and macaque V5.* Nat Neurosci, 2000. **3**(7): p. 716-23.

55. Heeger, D.J. and D. Ress, *What does fMRI tell us about neuronal activity?* Nat Rev Neurosci, 2002. **3**(2): p. 142-51.

56. Disbrow, E.A., et al., *Functional MRI at 1.5 tesla: a comparison of the blood oxygenation level-dependent signal and electrophysiology.* Proc Natl Acad Sci U S A, 2000. **97**(17): p. 9718-23.

57. Frahm J, M.K., Hanicke W, Kleinschmidt A, Boecker H, *Brain or vein - oxygenation or flow? On signal physiology in functional MRI of human brain activation.* NMR Biomed, 1994. **7**: p. 45-53.

58. Saad, Z.S., et al., *The spatial extent of the BOLD response.* Neuroimage, 2003. **19**(1): p. 132-44.

59. Engel, S.A., et al., *fMRI of human visual cortex.* Nature, 1994. **369**(6481): p. 525.

60. Hansen KA, D.S., Gallant JL, *Parametric revers correlation reveals spatial linearity of retinotopic human V1 BOLD response.* Neuroimage, 2004. **23**(1): p. 233-41.

61. Biswal. *Assumption free analysis of fMRI data*. in *Human Brain Mapping*. 2002. Japan.

62. Szeder, V., J. K. Williams, Wieser, J.A., Maciejewski, M., Janik, J., Hacein-Bey, L., and B.F. Remler, Ulmer, J.L., DeYoe, E.A. *Multifunctonal neuroimaging: A new approach for assessing brain-related vision deficits*. in *American Society of Neuroradiology*. 2004.

63. Dawei W. D. and Atick J.J, *Network - Temporal Decorrelation: A Theory of Lagged and Nonlagged Responses in the Lateral Geniculate Nucleus,* 1995, pp. 159-178.

64**.** Schneider KA, Richter MC, and Kastner S. *Retinotopic Organization and Functional Subdivisions of the Human Lateral Geniculate Nucleus: A High-Resolution Functional Magnetic Resonance Imaging Study*. The Journal of Neuroscience, October 13, 2004, 24(41):8975-8985

65. Winawer J, Horiguchi H, Sayres R, Anamo K, and Wandell B. *Mapping hV4 and ventral occipital cortex: The venous eclipse.* Journal of Vision, 10 (5):1, 1-22, 2010.

66. S. Bisti, R. Clement, L. Maffei and L. Mecacci. *Spatial Frequency and Orientation Tuning Curves of Visual Neurones in the Cat: Effects of Mean Luminance*. Exp. Brain Res. 27, 335-345 (1977).

67. Bradley A., B Skottun, I. Ohzawa, G. Sclar, R. Freeman. *Visual Orientation and Spatial Frequency Discrimination: A Comparison of Single Neurons and Behavior.* J of Neurophys. Vol. 57, No. 3, March 1987.

68. Slotnick S, Klein S, Carney T, Sutter E, and Dastmalchi S. *Using multi-stimulus VEP source localization to obtain a retinotopic map of human primary visual cortex.* Clinical Neurophysiology, 1999, 110: 1793-1800.

69. DeYoe E.A. *MRI System for Measuring Vision Capabilities*. US Patent 6430431 2002.

70. Desu I, Wiggins M, Luther A, Harper R, and Chacko J. *Understanding Visual Fields, Part I: Goldman's Perimetry.* Journal of Ophthalmic Medical Technology, Vol. 2 No. 2. June 2006.

71. Sereno, M.I., *Brain mapping in animals and humans.* Curr Opin Neurobiol, 1998. **8**(2): p. 188-94.

72. Sereno, M.I., C.T. McDonald, and J.M. Allman, *Analysis of retinotopic maps in extrastriate cortex.* Cereb Cortex, 1994. **4**(6): p. 601-20.

73. Tootell, R.B., et al., *Functional analysis of primary visual cortex (V1) in humans.* Proc Natl Acad Sci U S A, 1998. **95**(3): p. 811-7.

74. DeYoe, E.A., et al., *Functional magnetic resonance imaging (FMRI) of the human brain.* J Neurosci Methods, 1994. **54**(2): p. 171-87.

75. Wandell, B.A., *Computational neuroimaging of human visual cortex.* Annu Rev Neurosci, 1999. **22**: p. 145-73.

76. Saad, Z.S., et al., *Analysis and use of FMRI response delays.* Hum Brain Mapp, 2001. **13**(2): p. 74-93.

77. Tootell, R.B., et al., *The representation of the ipsilateral visual field in human cerebral cortex.* Proc Natl Acad Sci U S A, 1998. **95**(3): p. 818-24.

78. Saad, Z.S., E.A. DeYoe, and K.M. Ropella, *Estimation of FMRI response delays.* Neuroimage, 2003. **18**(2): p. 494-504.

79. Cox, R.W., *AFNI: software for analysis and visualization of functional magnetic resonance neuroimages.* Comput Biomed Res, 1996. **29**(3): p. 162-73.

80. Van Essen, D.C., et al., *An integrated software suite for surface-based analyses of cerebral cortex.* J Am Med Inform Assoc, 2001. **8**(5): p. 443-59.

81. Bandettini, P.A., et al., *Time course EPI of human brain function during task activation.* Magn Reson Med, 1992. **25**(2): p. 390-7.

82. Donahue, K.M., et al., *Utility of simultaneously acquired gradient-echo and spin-echo cerebral blood volume and morphology maps in brain tumor patients.* Magnetic Resonance in Medicine, 2000. **43**: p. 845-853.

83. Boynton, G., et al., *Neuronal basis of contrast discrimination.* Vision Research, 1999. **39**: p. 257-269.

84. Gati, J.S., et al., *Experimental determination of the BOLD field strength dependence in vessels and tissue.* Magn Reson Med, 1997. **38**(2): p. 296-302.

85. Swisher, J.D., Halko, M.A., Merabet, L.B., McMains, S. A., Somers, D.C. *Visual Topography of Human Intraparietal Sulcus*. J Neurosci, 2007. 27(20): p. 5327-37.

86. Van Essen DC, Zeki SM. *The topographic organization of rhesus monkey prestriate cortex*. J Physiol, 1978. 277:193-226.

87. Schira MM, Wade AR, and Tyler CW. *Two-dimensional mapping of the central and parafoveal visual field to human visual cortex*. J Neurophysiology, 2007. 97: 4284-4295.

88. Dumoulin SO and Wandell BA. *Population receptive field estimates in human visual cortex*. Neuroimage, 2008. 39(2): p. 647-60.

89. Duncan R, Boynton G. *Cortical Magnification Human Primary Visual Cortex Correlates with Acuity Thresholds*. *Neuron*, 2003. 38 (4): p. 659-671.

90. Tootell, R.B. et al. *The Retinotopy of Visual Spatial Attention*. RNeuron, Vol. 21, 1409–1422, December, 1998.

91. Szeder V, Williams K, Wieser J, Maciejewsk, M J, Janik J J, Hacein-Bey L, Remler B, Ulmer J, DeYoe E A (2004). "Multifunctional Neuroimaging: fMRI assessment fo occipital lobe pathologies with visual field loss."

92. Hansen KA, D S, Gallant JL (2004). *Parametric reverse correlation reveals spatial linearity of retinotopic human V1 BOLD response.* Neuroimage **23**(1): 233-41.

93. Shannon, C E (1948). *A mathematical theory of communication*. Bell System Technical Journal **27**(3): 379-423 and 623-656.

94. Ward, B D (2000). Deconvolution analysis of FMRI time series data. Milwuakee, WI, Medical College of Wisconsin.

95. Wells, R B (1999). Applied Coding and Information Theory for Engineers. Upper Saddle River, NJ, Prentice Hall.

96. Henkrisson L, Nurminen L, Hyvarinen A, and Vanni S. *Spatial frequency tuning in human retinotopic visual areas*. Journal of Vision, vol. 8 no. 10. 2008.

97. Lee H, Jang J, and Lee S. *Direction tuning curves of motion adaption in the visual cortex revealed by event-related fMRI study*. Journal of Vision, vol. 5 no. 8. 2005.

98. Engel S, Zhang X, and Wandell B. *Colour tuning in human visual cortex measured with functional magnetic resonance imaging*. Nature, vol 388, 1997.

99. Mazer J.A, Vinje W, McDermott J, Schiller P, and Gallant J. *Spatial frequency and orientation tuning dynamics in area V1*. PNAS, vol 99, no. 3, 2002.

100. Ringach D, Hawken M, and Shapley R. *Dynamics of orientation tuning in Macaque V1: The role of global and tuned suppression.* J Neurophysiol 90: 342–352, 2003.

101. Celebrini S, Thorpe S, Trotter Y, and Imbert M. *Dynamics of orientation coding in area V1 of the awake primate*. Vis Neurosci 10: 811–825, 1993.

102. Warnking J, Dojat M, Guerin-Dugue A, Delon-Martin C, Olympieff S, Richard N, Chehikian A, and Segebarth C. *fMRI Retinotopic Mapping – Step by Step*. NeuroImage, 17: 1665-1683, 2002.

103. Moonen, C.T.W and Bandettinni P.A. Functional MRI. New York: Springer, 2000. Print.

104. Brefczynski JA and EA DeYoe: A physiological correlate of the spotlight of visual attention. *Nature Neuroscience* 2:370-374, 1999.